2011-01-01

# Combustion Of Lunar Regolith Mixed With Energetic Additives: Thermodynamic Calculations And Experimental Studies

Francisco Alvarez
*University of Texas at El Paso*, falvarez@miners.utep.edu

# COMBUSTION OF LUNAR REGOLITH MIXED WITH ENERGETIC ADDITIVES: THERMODYNAMIC CALCULATIONS AND EXPERIMENTAL STUDIES

FRANCISCO ALVAREZ

Department of Mechanical Engineering

APPROVED:

Evgeny Shafirovich, Ph.D., Chair

Yirong Lin, Ph.D.

Cesar Carrasco, Ph.D.

Benjamin Flores, Ph.D.

Acting Dean of the Graduate School

A mis padres

# COMBUSTION OF LUNAR REGOLITH MIXED WITH ENERGETIC ADDITIVES: THERMODYNAMIC CALCULATIONS AND EXPERIMENTAL STUDIES

by

FRANCISCO ALVAREZ

THESIS

Presented to the Faculty of the Graduate School of

The University of Texas at El Paso

in Partial Fulfillment

of the Requirements

for the Degree of

MASTER OF SCIENCE

Department of Mechanical Engineering

THE UNIVERSITY OF TEXAS AT EL PASO

December 2011

## ACKNOWLEDGMENTS

I would like to first acknowledge and thank my mentor Dr. Evgeny Shafirovich for the support provided while working towards my Master of Science degree. I would also like to thank Ashvin Kumar Narayana-Swamy, Armando Delgado, Jorge Alberto Frías, Mario Rubio and Christopher White as part of the In-Situ Resource Utilization team from the Center for Space Exploration Technology Research for their collaboration during this research project. I would also like to acknowledge Michelle Jones from NASA for all the support and advice provided for the NASA Microgravity Flight Week, as well as to Alan Alvillar and Colin Davis for their collaboration as part of the Space Miners Microgravity Flight Team. Finally, I would like to thank Dr. Ahsan Choudhuri and the Department of Mechanical Engineering, Nathaniel Robinson and Sharon Griffin for their support during my participation as a research assistant in the NASA University Research Center at UTEP.

## ABSTRACT

The future of space exploration will require longer missions in order to better understand the conditions of near-Earth celestial objects, like the Moon or Mars. Future space missions will require the development of goods, such as propulsion fuel and structural materials, produced using the extraterrestrial resources available. The area that develops these technologies is called In-Situ Resource Utilization (ISRU). ISRU allows reducing the payload, and as a consequence reduces the energy consumption and cost of space travel. The production of structural materials on the Moon can be accomplished using Self-Propagating High-Temperature Synthesis (SHS). This work describes the combination of ISRU and SHS for the production of dense and strong structural ceramics by means of the combustion of mixtures of lunar regolith simulant JSC-1A and energetic additives (magnesium, aluminum, calcium, and titanium and boron). The thermodynamic calculations to validate the combustion of these mixtures, experimental studies using magnesium and aluminum additives, the design of a rig to fly onboard Zero-G, and the effect of microgravity on the combustion are presented in this document. The calculation of the adiabatic flame temperature shows that magnesium is the better option for low-additive concentrations. JSC-1A/Mg mixtures combustion was performed for different JSC-1A particle sizes and under different gravity conditions. The temperature and front velocity were measured. The temperature and front velocity increase with decreasing JSC-1A particle size. The front velocity shows a slight increase as the gravity conditions increase. The JSC-1A/Al mixtures do not show propagation for a standard SHS process. The products do not show a high strength. SHS Compaction can be used to increase strength and density.

# TABLE OF CONTENTS

## LIST OF TABLES

## LIST OF FIGURES

# 1. INTRODUCTION

Any future space exploration mission to the Moon, Mars or beyond requires the advancement of technology to guarantee the success and welfare of these projects. One important technology feature that needs to be further researched and assessed is the so-called In-Situ Resource Utilization (ISRU). ISRU is the utilization of the extra-terrestrial resources to produce and fabricate useful materials. Examples of useful materials are: oxygen and hydrogen for propulsion, and ceramics and metals for structure construction. The benefits of ISRU include the reduction of transportation costs from Earth to the mission site due to the reduction of the spaceship payload, the reduction of energy consumption, and the possibility of lengthening the missions' duration.

An important area of ISRU is the production of structural materials on the site, i.e. the mission place. Ceramics are a very important component of structures and can be manufactured from the soil of the different celestial bodies that are target of human exploration, such as the Moon or Mars. The production of ceramics is a very well developed technique and the same procedures used on Earth can be modified to be used elsewhere. However, the techniques typically used on Earth, like sintering, are energy intensive and require a large amount of power. One less energy-consuming option is the so-called self-propagating high-temperature synthesis (SHS). SHS can be used on the Moon to produce hard and dense ceramic products that can be used for construction purposes.

This chapter will explain the advancement on self-propagating high-temperature synthesis (SHS) technologies and in-situ resource utilization (ISRU) in the last decades. Also, the

following sections will introduce the purpose of the theoretical and experimental studies presented in this thesis, which is the use of both technologies to produce structural materials on the Moon.

## 1.1. Self-Propagating High-Temperature Synthesis

Self-propagating high-temperature synthesis (SHS) is a process discovered in the USSR in 1971 by Merzhanov, Borovinskaya and Shkiro [1]. They realized that by using thermite-type reactions (highly exothermic reactions) different refractory inorganic compounds such as carbides, nitrides and borides could be synthesized by profiting from the high heat of formation liberated during the combustion. The reaction needs two components: a fuel (almost always a metal) and an oxidizer (a non-metal). After the reaction is initiated, a small region of the sample undergoes the chemical process and pre-heats the unreacted section. The region where the reaction takes place is called *combustion front.* The heat released in the combustion front must be sufficient to trigger the combustion in the layers adjacent to the front. After a section of the sample has reacted it is left to cool down. Figure 1.1 shows a schematic of the reaction process and the different regions that occur during SHS.

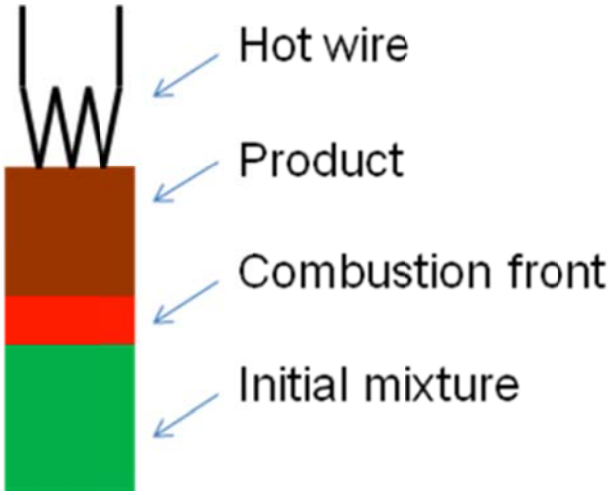


**Figure 1.1. Illustration of self-propagating high-temperature synthesis**

Merzhanov et al. concluded that [1]:

1. The reactions occur in the condensed phase and have a luminescent zone that may propagate steady or unsteadily,
2. The samples sometimes retain their original shape and size, and the physical structure of the products may differ (from sintered to loose powder)
3. The systems in which both fuel and oxidizer are solid belong to *nongaseous combustion,*
4. The degree of conversion is determined by several factors
5. In most cases the products of combustion are homogeneous.

Maksimov, Merzhanov and Shkiro first described the gasless composition. To achieve the gasless reaction, they diluted thermite reaction components (25% Al/ 75% $Fe_2O_3$) with the products of these reactions (in a ratio of 70:30) to reduce the combustion temperature to 2450

K and avoid the production of gas phase of the most volatile component that may be present during the process (Aluminum boiling point= 2600 K) [2]. Although this example of gasless combustion depicts the reaction between the metal and the additive, SHS may also happen because of the reaction between the additive components.

After the observations and findings made by these scientists, SHS (a term coined by Merzhanov) started to attract the eyes of scientists around the world and research efforts started to take place in countries like Japan and the United States to produce refractory materials free of volatile impurities. The interest on this reaction led to the study of the parameters that influence SHS and the reaction mechanisms [3] [4] [5] [6] [7].

SHS has several benefits: relatively simple equipment; large quantities of ceramics can be produced inexpensively; the energy consumption is greatly reduced; low boiling point volatiles are vaporized and give a high purity material; and the duration of the reactions is relatively short [8]. Also, SHS is commercially used and more than 500 compounds have been synthesized by this method [4].

One of the several benefits of SHS is the relatively low energy consumption compared to other ceramic production methods like sintering in which the whole amount of material is heated up. In the case of SHS, the reaction has to be initiated at a point and the chemical condition of the reacting system provide the energy to heat up the products, yield the desired solid and take advantage of the properties of the products. The propagation may be started by several methods, like electrical heating, but one possibility that can further decrease the energy consumption is the initiation of SHS by means of solar concentrators.

## 1.2. Lunar In-Situ Resource Utilization

In-Situ Resource Utilization (ISRU) is the area of space science in charge of finding ways to exploit the resources *on the land* to produce useful goods instead of bringing them from elsewhere (i.e. the Earth or other mission sites). ISRU has been an area largely studied in the last decades given the possibility of long-duration missions on the Moon, Mars and other near-Earth bodies [9]. Due to the big differences between Earth and these bodies, cosmic ray protection, solar panels materials, oxygen, and ceramics are needed to establish mission sites on those places.

Due to the proximity to the Earth, the Moon is a body that has been studied and visited in several occasions to better understand its composition and geological conditions. The Moon will then be a milestone to a new space era of long-term duration missions. However, the necessities on the Moon are numerous and have to be satisfied to ensure the success and duration of these enterprises. Several examples are to be presented next to better understand the necessities for these missions.

Lunar soil is very fine and, when landing and taking off, the dust may start to float and damage the hardware and instrumentation because of the particles sticking to the equipment. Building solid landing pads is important to ensure the well-being of the equipment. These solid materials may be composite ceramics that have the appropriate mechanical properties to withstand the stresses imposed on them. In the same fashion, these ceramics may be used for protection from solar rays, cosmic radiation, and habitat building [10]. Several studies have been performed to assess the feasibility of different processes. Sintering of lunar regolith by

radiant and microwave energy has been proposed [11] [12]. Sintering is the high-temperature process with which the materials weld without reaching the melting point of the materials thanks to molecular diffusion. Lunar soil sintering can be reached from radiation shielding at temperatures of approximately 1100°C. Unfortunately, this method has proven to be difficult to perform due to the high amount of energy required and to the insulation properties of rich-glass regolith [11].

An interesting concept that arose in 2009 to protect the space hardware during the lunar night is the thermal wadis (Figure 1.2). The thermal wadis consists of a thermal mass and a series of radiation collector that accumulates the solar energy through a radiant energy reflector during the day, while the rovers can travel on the lunar surface and do their job. When the night arrives, the rovers go back to the thermal wadis and are kept warm to avoid damage due to the low temperatures of the lunar dark periods. Lunar regolith has a low thermal diffusivity ($6.6 \times 10^{-9}$ $m^2/s$) and is not suitable for the thermal storage of energy. If a solid shape is manufactured from lunar regolith in a given region of the Moon, it will have a higher thermal diffusivity (due to the better contact between the grains in the solid as compared to a loose powder) and, thus become a good thermal storage material (Table 1.1) [13]. The higher diffusivity of the thermal mass (Figure 1.2) is supposed to enhance the heat transfer to the hardware as opposed to the loose regolith around it. The energy reflector will minimize the amount of energy lost to the surroundings.

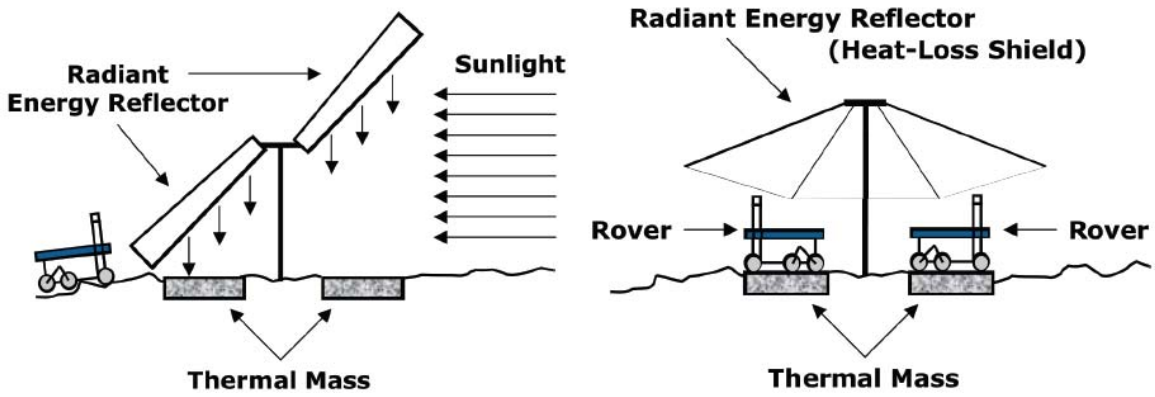


**Figure 1.2. Illustration of the thermal wadis and its functions [13]**

**Table 1.1. Physical Properties of Wadis Materials [13]**

| **Properties** | **Native regolith** | **Basalt rock** |
|---|---|---|
| Thermal diffusivity | $6.6 \times 10^{-9}$ $m^2/s$ | $8.7 \times 10^{-7}$ $m^2/s$ |
| Density | 1800 $kg/m^3$ | 3000 $kg/m^3$ |
| Specific heat | 840 J/(kg K) | 800 J/(kg K) |
| Thermal conductivity | 0.01 W/(m K) | 2.1 W/(m K) |

The radiation shelter has been also studied. As previously mentioned, the conditions on the Moon allow to a great amount of radiation to reach the surface and this represents a big risk for humans and hardware. Studies have shown that a shelter made out of aluminum reduces the radiation dose below the limits established by NASA for astronauts, but a shelter built with aluminum and regolith reduce the exposure below the limits for radiation workers [14]. Building this type of shelter also requires a more solid form of regolith.

Also, for the survival of humans, the production of oxygen is extremely important, because of its use as human life support. Another use of oxygen is fuel for propulsion purposes. Figure 1.3 shows the composition of the lunar regolith. Because the Moon is 42% oxygen [9], methods to extract the oxygen from the mineral form have been studied.

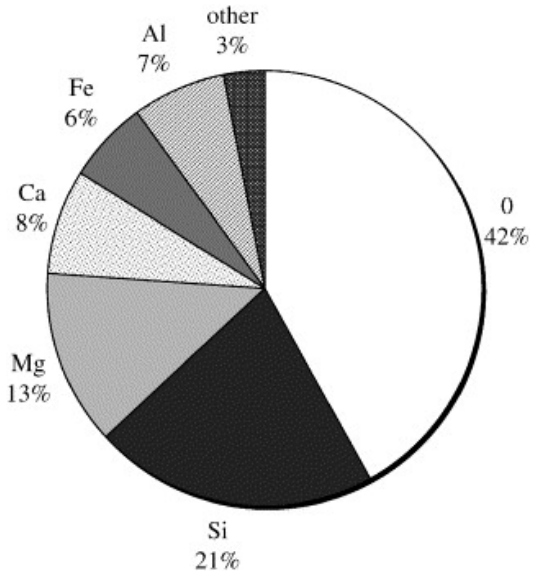


**Figure 1.3. Composition of the lunar regolith [9]**

It is important to note that after oxygen, the main elemental component of lunar regolith is silicon. Silicon is the main component for the production of solar panels, and the extraction of silicon from the regolith is important for the production of photovoltaic components to collect solar energy. Landis has proposed a candidate to extract the main necessary materials to fabricate solar panels by chemically processing lunar regolith with fluorine [9].

Other methods for the extraction of oxygen include carbothermal reduction of regolith by methane and ilmenite reduction by hydrogen. Carbothermal reduction consists on reducing

the metal oxides found in lunar regolith using carbon in any suitable form [15] and has proven feasible although improvements are required to introduce the use of solar energy [16]. Other methods studied include the reduction of ilmenite with carbon monoxide and hydrogen [17] [18].

It is clear that lunar ISRU is under development and needs improvement. NASA and other space agencies around the world are working to advance this area. The greatest problem is still the transportation of the necessary materials from Earth to perform the processes and fabricate the devices and products herein described. The following section describes a different approach to the production of solid materials from lunar regolith for structural purposes using self-propagating high-temperature synthesis and minimizing the amount of material to be brought from Earth.

## 1.3. Self-Propagating High-Temperature Synthesis and In-Situ Resource Utilization: Production of Structural Materials on the Moon

As described previously, the sintering of regolith for the production of structural materials has been studied extensively. A different method including the combustion synthesis of lunar regolith and several additives has been proposed to produce solid ceramics on the Moon. This method takes advantage of the composition of lunar regolith, which is a mixture of oxides of several metals and silicon in the form of glass and minerals (mainly silicates). As explained in Section 1.1, SHS consists of the reduction of metal oxides by a metal additive or the heating of the materials by the reaction between two compounds in the additive.

The reaction between regolith and the highly exothermic titanium/boron mixture has proven to propagate for a 60 weight percent regolith and 40% of a stoichiometric mixture of titanium and boron where the temperature reached about 1400°C [19]. The reaction was started at the top of a cylindrical pellet with an electrically heated coil.

Regolith/aluminum mixtures reactions have been performed for mixtures as low as 19.44%Al [20]. The purpose of this reaction is to fabricate different shapes to build a semi-spherical shelter [21]. The experiments were performed under normal atmospheric and vacuum conditions. The reaction was started embedding a Nichrome wire in the mixtures and heating it up electrically. The results showed to be successful in terms of material strength.

More recently, the SHS reaction between lunar regolith, ilmenite ($FeTiO_3$) additive, and aluminum as reducing agent has been proven [10]. Ilmenite can be found in lunar regolith and, in regions with sufficient of it, does not need to be brought from Earth or from other regions. The combustion reached temperatures in the interval of 1610-1700°C.

The research efforts presented in this section intend to produce ceramic composites suitable for structural purposes. The work presented in this thesis broadens the knowledge presented in this section by studying some of the regolith/additive reactions to ensure its feasibility, their properties, evaluate the effect of some of the parameters of self-propagating high-temperature synthesis on them, and minimize the amount of fuel necessary. These reactions will be studied theoretically (thermodynamically) and experimentally under several conditions. The studies were performed using lunar regolith simulant JSC-1A, which will be explained in further detail in Chapter 2.

# 2. LUNAR REGOLITH SIMULANT JSC-1A

The composition of lunar regolith has been extensively researched in the last decades, primarily after NASA's Apollo missions. The Apollo missions landed and collected lunar soil samples from several regions of the Moon. As happens on Earth, the mineral and chemical composition from the soil in different parts has a different composition. Of course, the number of samples of actual lunar regolith is very limited and is not available for experimentation. To simulate the composition of the lunar regolith, several Earth sites with similar soil compositions to lunar regolith have been mined. Although these soils are chemically and mineralogically similar, they are not exactly the same and, consequently, have different physical properties. Nonetheless, due to the high value and the scarcity of samples of actual lunar regolith, lunar simulants are the best option available for lunar-oriented research conducted on Earth.

Currently, one of the most used regolith simulants is JSC-1A. This simulant comes from an ash deposit located near Flagstaff, Arizona and closely resembles the actual composition of lunar soil [22]. JSC-1A is commercialized by ORBITEC. Table 2.1 shows a comparison between JSC-1A and some samples collected during the Apollo era [23]. Table 2.1 shows clearly that a large amount of the JSC simulants composition and lunar soil is glass, while the mineral composition shows a large interval of values. For the present studies the simulant used was JSC-1A made available by NASA once the JSC-1 simulant reserve was depleted. The difference between the minerals present is large and thus must be carefully used. Table 2.2 shows a comparison of the constituent oxides (the oxides that form the minerals) in one sample of

Apollo 17 and in the JSC simulants [22]. It is shown that the chemical composition is very similar for the simulants and the samples.

**Table 2.1. Comparison of the composition of JSC simulants and some Apollo samples**

| Minerals (wt. %) | Apollo 16:64001/2 | Apollo 11 & 12 | JSC-1 | JSC-1A | JSC-1AF |
|---|---|---|---|---|---|
| Plagioclase | 43-44 | 11-15 | 32.47 | 37.83 | 48.47 |
| Clinopyroxene | 0.6-0.7 | | 14.67 | 18.77 | 21.15 |
| Orthopyroxene | ~2.5 | | 0.65 | 0.66 | 1.62 |
| Total Pyroxene | ~3 | 25-37 | 15.32 | 19.43 | 22.77 |
| Olivine | 0.8-0.9 | 2-10 | 18.29 | 12.44 | 9.22 |
| Glass | 44-46 | 31-45 | 30.86 | 26.67 | 15.68 |

The mineral and chemical composition of simulant JSC-1A is available from different sources [24] [25] [23] and can be summarized in Table 2.3. The main minerals present in JSC-1A are silicates; however, some sulfides, titanates, and carbonates may be found in trace amounts. This simulant composition will be used for these studies and will be called regolith from now on, although some properties are different from the actual lunar regolith.

Table 2.3 shows that the main component of JSC-1A, as well as in lunar soil, is glass. Glass is an amorphous component and does not have a crystalline arrangement that cannot be properly characterized. For this reason, the crystal structure of glass is unknown and a mixture of simple metal and metalloid oxides would be the better representation for it. The glass chemistry of JSC-1A is shown in Table 2.4 [23]. Clearly, most of the glass is made of silica,

followed by alumina, ferrous oxide, and calcia closely following the overall composition of the moon (Figure 1.3).

**Table 2.2. Composition (wt. %) of the major constituents of JSC-1, JSC-1A, JSC-1AF and Apollo 17 Sample 70051**

| Constituent oxides | JSC-1A | Apollo 17 Sample 70051 | JSC-1A/JSC-1AF |
|---|---|---|---|
| $SiO_2$ | 47.4 | 42.2 | 45.7 |
| $Al_2O_3$ | 15.0 | 15.7 | 16.2 |
| CaO | 10.4 | 11.5 | 10.0 |
| MgO | 9.0 | 10.3 | 8.7 |
| FeO | 7.4 | 12.4 | - |
| $Fe_2O_3$ | 3.4 | - | 12.4 |
| $Na_2O$ | 2.7 | 0.2 | 3.2 |
| $K_2O$ | - | 0.1 | 0.8 |
| $TiO_2$ | 1.6 | 5.1 | 1.9 |
| $P_2O_5$ | - | - | 0.7 |
| MnO | - | 0.2 | 0.2 |

**Table 2.3. Mineral Composition of Lunar Simulant JSC-1A**

| Mineral | | Formula | JSC-1A composition, wt% |
|---|---|---|---|
| Plagioclase | Anorthite | $CaAl_2Si_2O_8$ | 26.48 |
| | Albite | $NaAlSi_3O_8$ | 11.35 |
| | Orthoclase (K feldspar) | $KAlSi_3O_8$ | 0.07 |
| Pyroxene | Wollastonite | $CaSiO_3$ | 7.77 |
| | Enstatite | $MgSiO_3$ | 7.38 |
| | Ferrosilite | $FeSiO_3$ | 4.28 |
| Olivine | Forsterite | $Mg_2SiO_4$ | 9.08 |
| | Fayalite | $Fe_2SiO_4$ | 3.36 |
| | Glass | | 26.67 |
| | MgFeAl Silicate | | 3.06 |
| | Troilite | FeS | 0.17 |
| | Ilmenite | $FeTiO_3$ | 0.11 |
| | Calcite | $CaCO_3$ | 0.11 |
| | Magnetite | $Fe_3O_4$ | 0.01 |
| | Quartz | $SiO_2$ | 0.01 |
| | Others | | 0.07 |
| | Total | | 99.98 |

**Table 2.4. Glass chemistry of JSC-1A**

| Oxide | Weight Percentage |
|---|---|
| $SiO_2$ | 46.8 |
| $TiO_2$ | 2.44 |
| $Al_2O_3$ | 13.9 |
| FeO | 12.1 |
| MnO | 0.21 |
| MgO | 5.6 |
| CaO | 10.5 |
| $Na_2O$ | 3.89 |
| $K_2O$ | 1.17 |
| $P_2O_5$ | 1.04 |
| $Cr_2O_3$ | Below detection limit |
| LOI | Not determined |
| Total | 97.65 |

# 3. THERMODYNAMIC CALCULATIONS

## 3.1. Gibbs Free Energy, Spontaneity, and Equilibrium

Self-propagating High-Temperature Synthesis (SHS) relies on the spontaneity and exothermicity of the chemical reactions occurring during the process and the heat transfer to the non-reacted areas. Entropy has the status of the primary source of information to determine whether a process is spontaneous or not. It has been determined that a spontaneous process is accompanied by an increase in the entropy of the system. However, manipulation of the entropy function to determine spontaneity is not simple, and alternate criterions have been established [26]. The most frequently used condition for the spontaneity of a process utilizes the Gibbs free energy (G) defined as:

$$G = U + PV - TS = H - TS \tag{3.1}$$

In this expression G is the Gibbs free energy, H is the enthalpy, T is the temperature and S is the entropy of the system. For a chemical reaction of the form

$$aA + bB = cC + dD \tag{3.2}$$

the Gibbs free energy change can be expressed as the difference between the products and reactants free energies:

$$\Delta G = aG_A + bG_B - cG_C - dG_D. \tag{3.3}$$

Combining expressions for the first and second laws of the thermodynamics, one can obtain the following expression:

$$dU + pdV - TdS = dH - TdS \leq 0 \tag{3.3}$$

At constant temperature and pressure dG=dH-TdS so,

$$dG_{T,P} \leq 0 \tag{3.4}$$

And for a finite process, the latter expression can be written as:

$$\Delta G_{T,P} \leq 0 \tag{3.5}$$

The last expression is frequently used as the criterion for the determination of the spontaneity or the equilibrium of a process [26].

In a heterogeneous system undergoing a chemical reaction as the one shown in Equation 3.2, the system reaches a minimum value for the Gibbs free energy function when stabilized and has reached an equilibrium state. During this chemical reaction, the obtained products will minimize the amount of energy available and, thus will minimize the Gibbs energy function as much as possible. In the case of a known composition of initial mixture compounds, the Gibbs free energy function can be minimized by assuming the product composition and calculating ΔG. This iterative process is known as Gibbs free energy minimization.

As the number of reactants increase, the amount of possible products also increases as well as the number of iterations necessary, making this process cumbersome. This process can be automated with the help of computer software. To perform the minimization of the Gibbs free energy, the THERMO software was used. This software has a database containing thermochemical properties of about 3000 compounds [27] and it will be explained in detail.

## 3.2. Selection of Metal Fuels for Combustion Synthesis

As explained in Chapter 1, the SHS process requires the addition of a metal fuel in order to occur. The selection of the metal fuels can be justified with the help of the free energy-temperature diagram or Ellingham diagram. The Ellingham diagram for some common metals is shown in Figure 3.1. This diagram shows the change in Gibbs free energy of formation as a function of the temperature. The Gibbs free energy of formation is the Gibbs free energy required to produce one mole of compound from its elements. In the case of regolith combustion, the metal fuel reacts with the oxygen present in the mixture and forms metal fuel oxides. Figure 3.1 shows the Gibbs energy of formation as a function of temperature and partial pressure of oxygen. For the case of regolith-metal system case, the oxygen will not be provided in gaseous form, but it will be provided by the minerals and metal oxides present in the regolith.

Section 3.1 explained the Gibbs energy minimization procedure. The goal of this procedure is to minimize the change in Gibbs free energy; in consequence, the products must have the smallest Gibbs free energy possible. During combustion, it is expected that additive metal oxide is generated. Figure 3.1 shows that calcium, magnesium and aluminum are in the most negative region of the Ellingham diagram, meaning a smaller amount of Gibbs free energy than the other metals shown. Calcium lies below the lines corresponding to the other metals for the temperature interval going from 0 to 2000°C. Magnesium lies slightly above the calcium line and only surpasses the aluminum line above ~1500°C. The aluminum line is significantly higher than the magnesium and calcium lines. This information gives an important clue on the

metals that might work well for combustion synthesis, specifically SHS, processes. Another important treat of these metals is the abundance of them on the Moon (Figure 1.3). Calcium can be found in the form of anorthite and wollastonite which are abundant in lunar soil. Magnesium and aluminum are also present in mineral form, and they can be recycled from the hardware used for space missions, such as spacecraft.

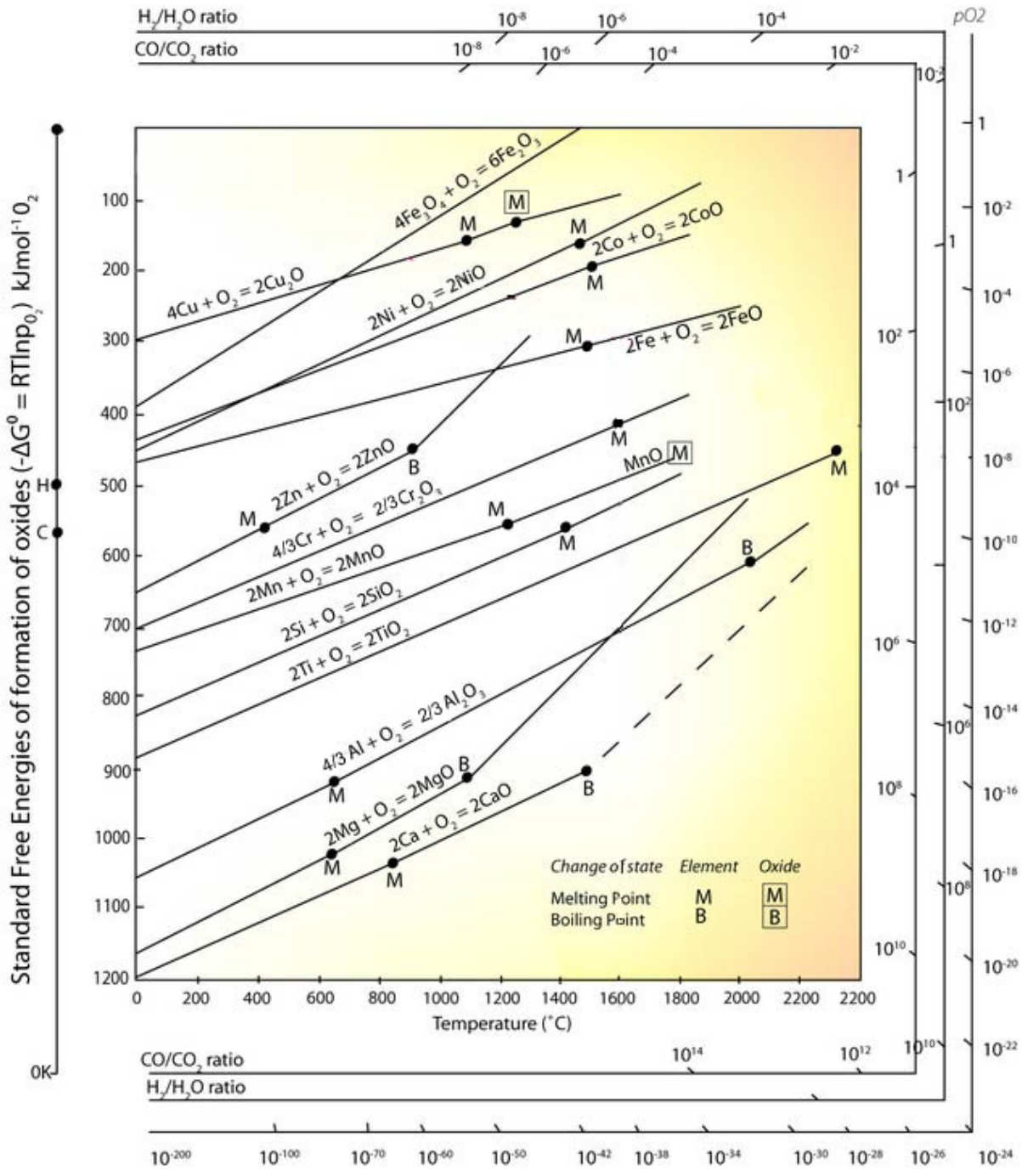


**Figure 3.1. Free energy-temperature diagram for some common metals [28]**

The calculations for the minimization of Gibbs free energy were performed with calcium, aluminum and magnesium metals.

## 3.3. Model Composition of JSC-1A for Thermodynamic Calculations

The JSC-1A mineral composition is shown in the third column of Table 3.1. Unfortunately, the THERMO software cannot handle such a large number of compounds in the initial mixture. To fix this problem, the minerals with the smallest concentrations were discarded (MgFeAl silicate, troilite, ilmenite, calcite magnetite and quartz), leaving just plagioclase, pyroxene and olivine minerals (the first eight minerals shown in the first column of Table 3.1), and glass.

The glass chemistry is known for JSC-1A; unfortunately, using this information would greatly increase the number of compounds present in the initial mixture. To solve this problem, the glass was assumed to have the same composition as the minerals in the simulant. This quantity was normalized to obtain the 100% composition shown in the fourth column of Table 3.1; this composition will be used for the calculations presented in the following sections.

## 3.4. THERMO Software

As stated in section 3.1, THERMO was used to perform the Gibbs minimization procedure. THERMO requires the input of the initial mixture composition and the regime (constant pressure or constant volume) that the combustion will occur under in order to calculate the adiabatic combustion temperature and the equilibrium product composition of the reaction under study.

**Table 3.1. Mineral Composition of JSC-1A and Model Composition used for Thermodynamic Calculations**

| Mineral | Formula | JSC-1A composition, wt% | Model regolith system composition, wt% |
|---|---|---|---|
| Anorthite | $CaAl_2Si_2O_8$ | 26.48 | 37.95 |
| Albite | $NaAlSi_3O_8$ | 11.35 | 16.27 |
| Orthoclase (K feldspar) | $KAlSi_3O_8$ | 0.07 | 0.10 |
| Wollastonite | $CaSiO_3$ | 7.77 | 11.14 |
| Enstatite | $MgSiO_3$ | 7.38 | 10.58 |
| Ferrosilite | $FeSiO_3$ | 4.28 | 6.13 |
| Forsterite | $Mg_2SiO_4$ | 9.08 | 13.02 |
| Fayalite | $Fe_2SiO_4$ | 3.36 | 4.81 |
| Glass | | 26.67 | 0 |
| MgFeAl Silicate | | 3.06 | 0 |
| Troilite | FeS | 0.17 | 0 |
| Ilmenite | $FeTiO_3$ | 0.11 | 0 |
| Calcite | $CaCO_3$ | 0.11 | 0 |
| Magnetite | $Fe_3O_4$ | 0.01 | 0 |
| Quartz | $SiO_2$ | 0.01 | 0 |
| Others | | 0.07 | 0 |
| Total | | 99.98 | 100.0 |

### 3.4.1. CALCULATION OF ADIABATIC FLAME TEMPERATURE

The first step to start using THERMO is to select the combustion regime; for this study, the constant pressure regime was assumed. After selecting the regime, THERMO needs the

input of the compounds in the initial mixture along with their phases (solid, liquid, or gaseous) and amounts (in mole). The JSC-1A/metal initial mixture is in the solid phase. Once the initial composition is input in THERMO, the initial temperature and the pressure of the system is required. The system pressure was set to 1 atm and the initial temperature of the mixture to 298 K (25°C). THERMO then searches in its database for the thermochemical data of the compounds present in the initial mixture; if any information is missing in the database, THERMO asks for the manual input of that information. Regarding the composition of JSC-1A, THERMO does not include the enthalpies of formation of albite ($NaAlSi_3O_8$) and ferrosilite ($FeSiO_3$), which are -3929.86 and -1193.45 kJ/mol, respectively [29]. After this information is introduced to the software, the Main Table appears and asks for the selection of the products that may appear in the products composition, i.e. the compounds that may be formed from the elements present in the initial mixture. This selection process allows for the discrimination of compounds that do not appear in the products of the reactions studied. Once the selection is finished, the iterative process of the Gibbs energy minimization begins. All the compounds were selected from the Main Table, because no information was available about the compounds that may be generated during these reactions.

In order to evaluate the effect of the concentration of the metal fuel on the adiabatic combustion temperature of JSC-1A/metal mixtures, the calculation was done at one percent increases in the weight concentration of metal fuel ranging from 0 to 100 wt% of metal. In order to make this set of calculations, a Microsoft Excel spreadsheet was created where the weight percent can be varied and the concentration of the compounds in the initial mixture is obtained.

When the iterations are over, the program displays the results. These results are stored in a separate file and are in the form shown in Figure 3.2, which shows one example of a run of THERMO with 75 weight % aluminum and with 25 weight % regolith. The results table shows the temperature of the reaction, the pressure of the gaseous products, the heat capacity, entropy and enthalpy of the products. Also, Figure 3.2 shows the products and the amounts (in mole) of each. THERMO can give the amounts in kilograms or mole, according to the user's preference. Also, when performing the Gibbs free energy minimization, THERMO calculates the adiabatic combustion temperature; this temperature is the temperature that will be reached if there is no heat transfer to the surroundings, i.e. all the energy liberated during the reaction goes to heat up the products.

```
    25% regolith
Volume of gas products    (litres)          0.0000
Pressure of gas products    (atm)           1.0000
Temperature                 (K)           740.0000
Gas products amount         (mol)        5.28E-0010
Products heat capacity      (J/K)           37.6400
Products entropy            (J/K)           61.6036
Products enthalpy           (KJ)          -122.1348
 Al 1                       (C) []            0.8659
 Al 2Ca 2O  7Si 1           (C)  [GEHLE       0.0103
 Al 2Mg 1O  4               (C)  []           0.0245
 Al 1Na 1O  2               (C)  []           0.0050
 Al 2O  3                   (C) []            0.0196
 Fe 1Si 1                   (C) []            0.0079
 K  1                       (L) []         1.65E-0004
 Si 1                       (C) []            0.0523
*
```

**Figure 3.2. Sample of the results display from THERMO**

The adiabatic temperature calculated at each point was then graphed as a function of metal fuel concentration to show the highest temperature possible for each of the metal-regolith mixtures. For each of these systems a maximum in temperature is expected due to the amount of additive present. If no additive is present no reaction will occur and the temperature

will remain constant; if the amount of additive increases the reaction will occur to a greater extent up to the point where the amount of metal fuel that can react. In this case, not all the metal fuel reacts; the extra additive has to be heated up to the equilibrium temperature and decreases the temperature reached. It will be seen that plateaus appear at some regions in the graphs of adiabatic combustion temperature; in general, these plateaus suggest a phase change of some of the compounds present in the reaction.

The metal fuel concentration for which the maximum adiabatic temperature is attained gives a hint of the amount of metal additive necessary for combustion to occur. For this temperature is the maximum temperature that the system will reach under adiabatic and isobaric conditions, this is the concentration ratio that will generate the greater amount of heat of reaction and thus will transfer more heat to the adjacent layers to ensure the self-propagative mode of the combustion. The maximum adiabatic flame temperature point does not mean, however, that combustion cannot occur below or above this metal fuel concentration.

### 3.4.2. ALUMINUM

Figure 3.3 shows the adiabatic flame temperature of JSC-1A/Aluminum mixtures. It is shown that the maximum flame temperature (1524.5 K or 1251.4°C) occurs for mixtures with 23% aluminum and 77% regolith simulant. Table 3.2 shows the equilibrium composition for the combustion of 1 mole of a 23% aluminum weight percent mixture. It is noteworthy that the amount of gas phase compounds produced during this reaction is very small approaching gasless combustion. Also, it is important to notice that nearly 15 wt% of the products is pure

silicon. Between 64 and 67 wt% we find a plateau due to the melting point of aluminum (933.52 K).

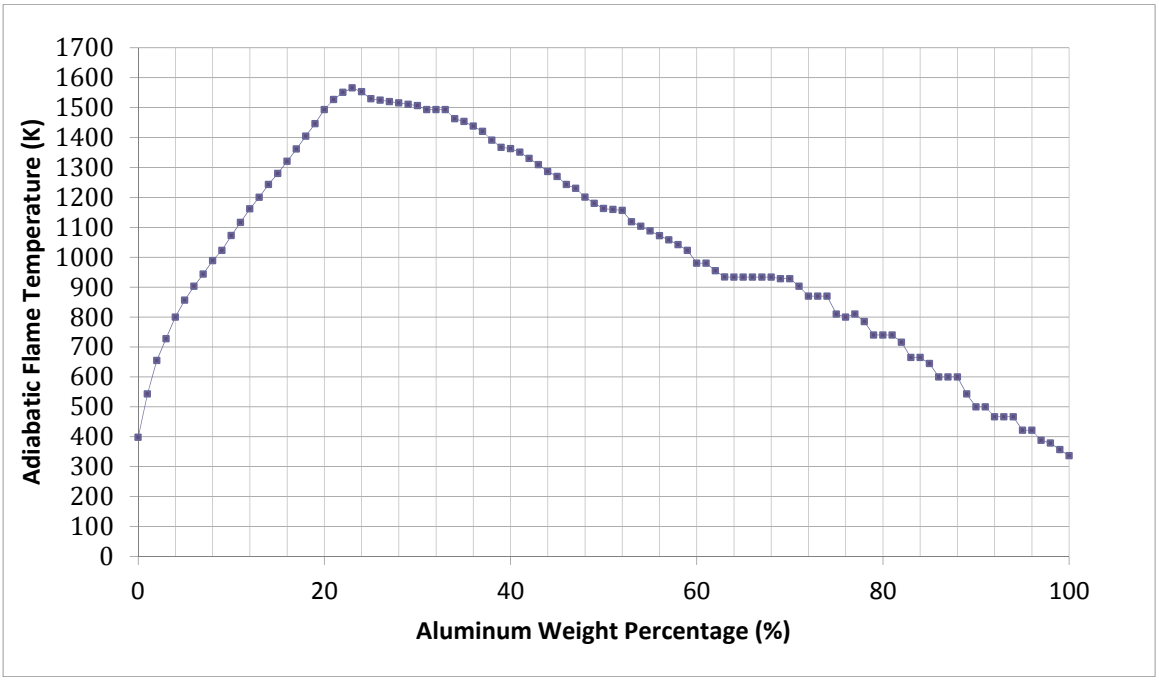


**Figure 3.3. Adiabatic Flame Temperature vs. Aluminum Weight Percentage for Regolith/Aluminum mixtures**

### 3.4.3. MAGNESIUM

Figure 3.4 shows the adiabatic flame temperature of JSC-1A/magnesium mixtures. It is shown that the maximum flame temperature (1689 K or 1416°C) occurs for mixtures ranging from 26 to 38 wt% magnesium. In order to decrease the necessary amount of metal fuel for sustained combustion, 26% magnesium mixtures were the most suitable for this study. Table 3.3 shows the equilibrium composition for the combustion of 1 mole of a 26% magnesium weight percent mixture. It is noteworthy that the amount of gas phase compounds produced during this reaction is very small. Also, it is important to notice that nearly 10 wt% of the products is pure silicon (in liquid and solid phases). Between 75 and 79wt% magnesium we find

a plateau due to the melting point of aluminum (922.9K). Please note the large amount of magnesium oxide (MgO) present in the equilibrium products.

**Table 3.2. Equilibrium composition of the JSC-1A/aluminum mixture (23 wt% aluminum)**

| Formula | Phase | Mole Percentage | Weight Percentage |
|---|---|---|---|
| $MgAl_2O_4$ | Solid | 21.012% | 31.97% |
| $CaAl_4O_7$ | Solid | 10.868% | 30.22% |
| Si | Solid | 49.994% | 15.02% |
| $Ca_2Al_2SiO_7$ | Solid | 2.891% | 8.48% |
| FeSi | Solid | 6.738% | 6.05% |
| $Al_2O_3$ | Solid | 3.978% | 4.34% |
| $NaAlO_2$ | Solid | 4.470% | 3.92% |
| K | Gas | 0.026% | 0.01% |
| Na | Gas | 0.023% | 0.01% |

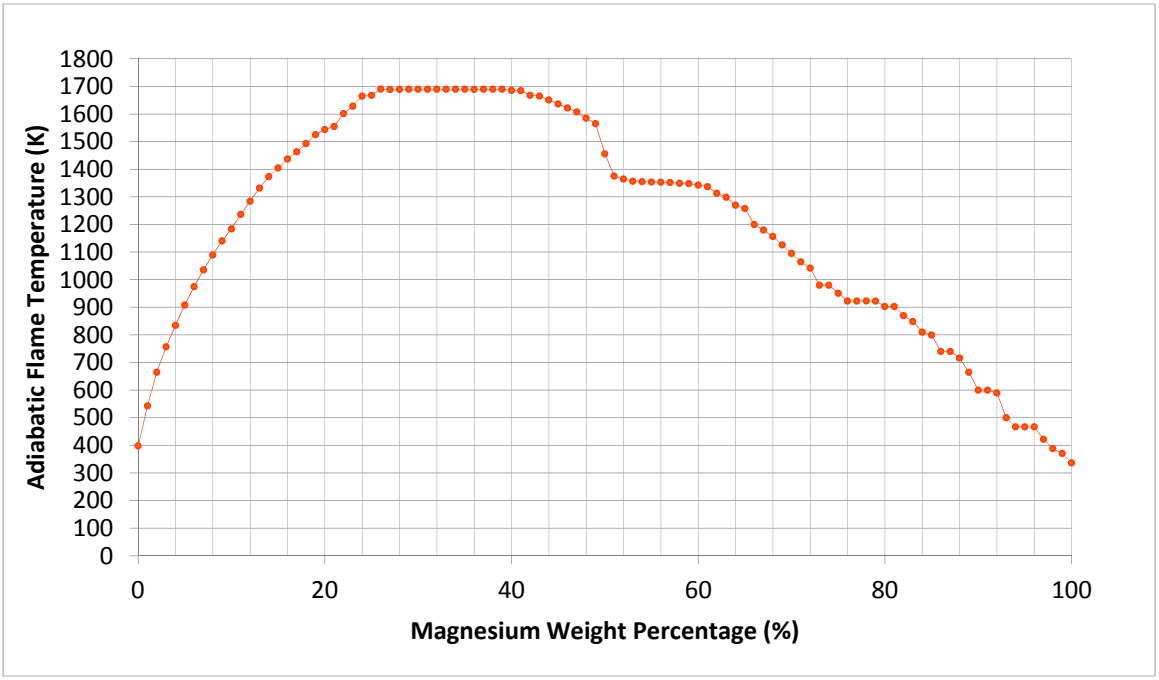


**Figure 3.4. Adiabatic Flame Temperature vs. Magnesium Weight Percentage for Regolith/Magnesium mixtures**

### 3.4.4. CALCIUM

Figure 3.5 shows the adiabatic flame temperature of JSC-1A/Calcium mixtures. It is shown that the maximum flame temperature (1786.82 K or 1513.67°C) occurs for mixtures having 51 wt% calcium. In order to decrease the necessary amount of metal fuel for sustained combustion, 51% calcium mixtures were the most suitable for this study. Table 3.4 shows the equilibrium composition for the combustion of a 51% calcium weight percent mixture. It is important to notice that a very large amount of the calcium present in the initial mixture appears in the products as calcium oxide (CaO). Also, the amount of pure silicon in the products (9.69%) is found in the liquid phase.

**Table 3.3. Equilibrium composition of the JSC-1A/magnesium mixture (26 wt% magnesium)**

| Formula | Phase | Mole Percentage | Weight Percentage |
|---|---|---|---|
| MgO | Solid | 48.63% | 39.77% |
| $MgAl_2O_4$ | Gas | 5.66% | 16.35% |
| $Ca_3MgSi_2O_8$ | Solid | 2.19% | 14.64% |
| Si | Solid | 16.99% | 9.68% |
| Na | Gas | 20.22% | 9.43% |
| FeSi | Solid | 3.12% | 5.32% |
| $CaMgSiO_4$ | Solid | 1.15% | 3.65% |
| Si | Liquid | 1.82% | 1.03% |
| Mg | Gas | 0.19% | 0.09% |
| Na2 | Gas | 0.02% | 0.02% |
| K | Gas | 0.01% | 0.01% |

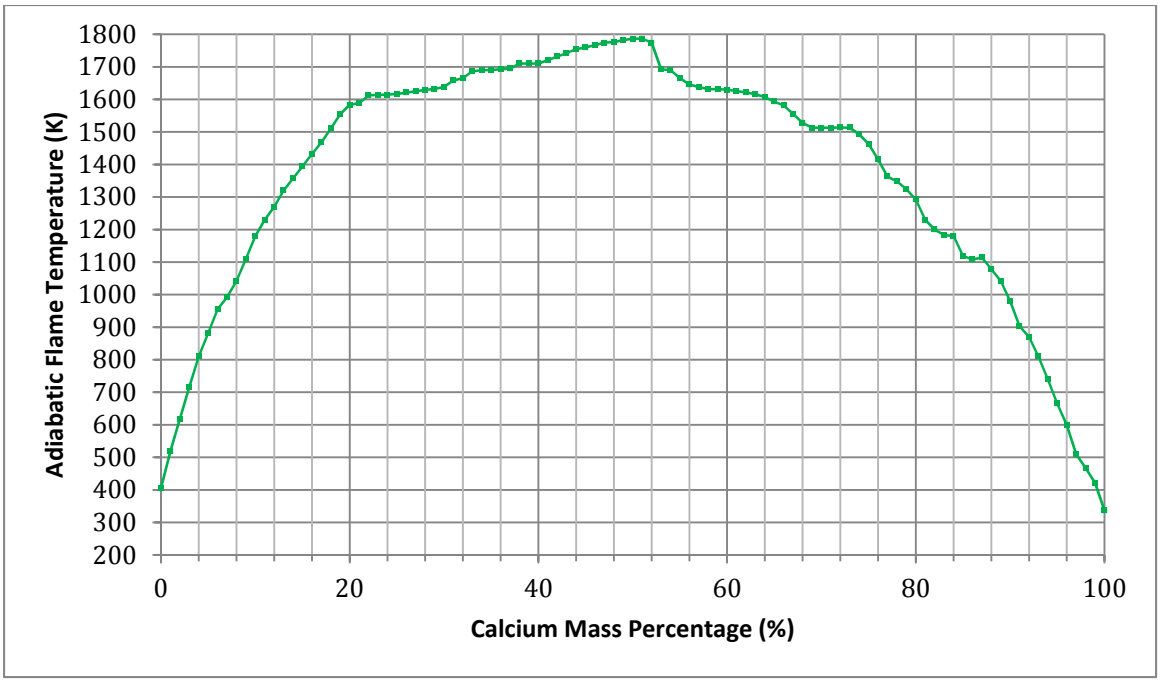


**Figure 3.5. Adiabatic Flame Temperature vs. Calcium Weight Percentage for Regolith/Calcium mixtures**

**Table 3.4. Equilibrium composition of the JSC-1A/calcium mixture (51 wt% calcium)**

| Formula | Phase | Mole Percentage | Weight Percentage |
|---|---|---|---|
| CaO | Solid | 65.54% | 69.96% |
| Si | Liquid | 18.12% | 9.69% |
| Ca $Al_2$ | Liquid | 4.26% | 7.62% |
| FeSi | Liquid | 2.38% | 3.80% |
| $CaMgO_2$ | Solid | 1.79% | 3.29% |
| Mg | Gas | 5.59% | 2.59% |
| $Ca_2SiO_4$ | Solid | 0.71% | 2.32% |
| Na | Gas | 1.51% | 0.66% |
| K | Gas | 0.05% | 0.04% |
| Ca | Gas | 0.05% | 0.04% |

### 3.4.5. Comparison of Results for Calcium, Magnesium, and Aluminum

Figure 3.6 shows a summary of the solution for the three metals analyzed in this study. It is shown that, as a general trend, the adiabatic temperature is higher for the metal which lies lower in the Ellingham diagram (Figure 3.1). For this reason, the calcium/JSC-1A mixture reaches a higher adiabatic temperature than the other mixtures, i.e. magnesium and the aluminum, respectively. However, at points close to the 20 percent metal concentration, magnesium shows a higher temperature. If the quantity of metal additive is to be reduced, this switch in the behavior of the adiabatic temperature may be an important parameter to take into account.

The plateaus that are observed in the adiabatic flame temperature versus metal concentration are, in general, because of a phase change of some of the compounds. For example, in the case of magnesium/JSC-1A mixtures a plateau is observed from the point at 26% to 43% at 1690; this temperature corresponds to the melting point of silicon. As explained earlier, if liquid elemental silicon is found in the products, it could be separated from the products relatively easy and be used for the production of photovoltaics.

Another important observation that needs to be made is the metal concentration at which the maximum adiabatic flame temperature occurs. In the case of calcium, the maximum occurs at a concentration of 51 wt% of calcium metal, while for magnesium occurs at 26 wt% and at 23 wt% for aluminum. The latter means that in order to reach the maximum adiabatic flame temperature a larger mass of calcium would be required. This big difference may be explained due to the difference in molecular mass of the metals. Magnesium has an atomic

weight of 24.31 g/mol, aluminum is next to magnesium in the periodic table and has a weight of 26.98 g/mol [30]. On the other hand, calcium lies below magnesium in the periodic table and has an atomic weight of 40.08 g/mol [30].

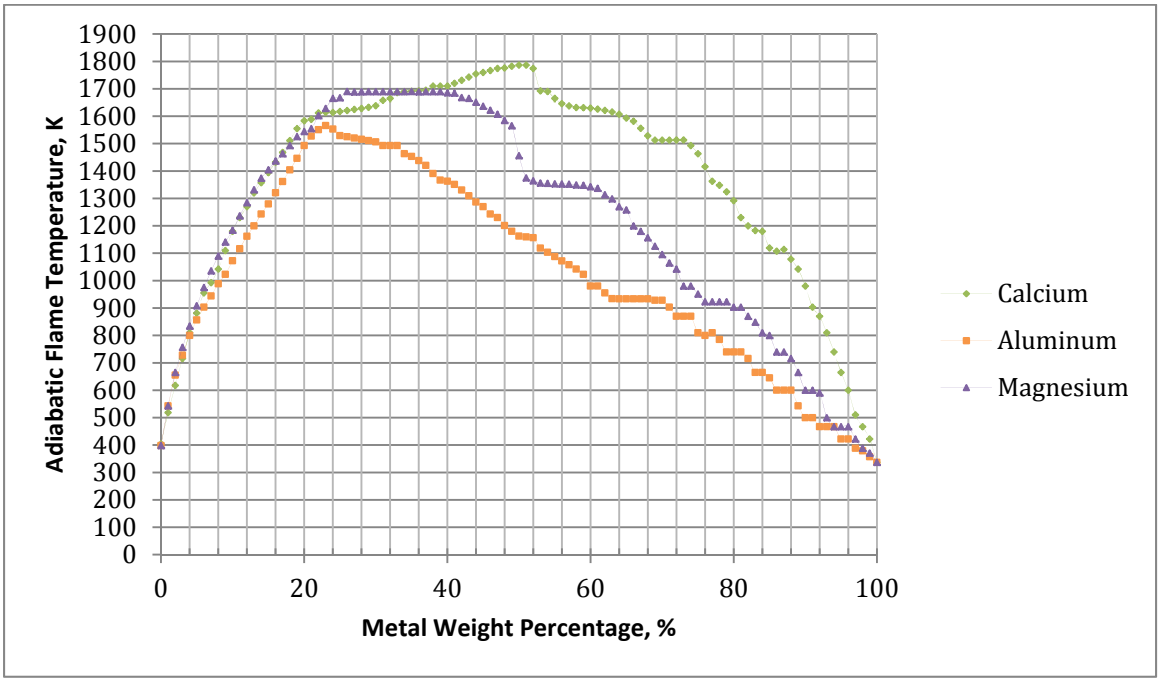


**Figure 3.6. Adiabatic flame temperatures for mixtures of JSC-1A/metal (metals: calcium, magnesium, aluminum)**

The difference in molecular weights explains the shift in the concentration to reach the maximum temperature, i.e. while the mass of calcium required attaining the maximum temperature is higher; the molar amount of calcium is comparable to those of magnesium and aluminum. For example, if 100 g of mixture are to be combusted to reach the maximum temperature, 51 g of calcium, 26 g of magnesium and 23 g of aluminum would be needed; these masses are the same as 1.27 mol of calcium, 1.06 mol of magnesium, and 0.852 mol of aluminum.

In practical terms, nonetheless, mass, and not mole amount, is the important parameter for transportation and storage. However, as explained in an earlier section, combustion can be achieved at lower concentrations than the optima shown in this section, and these points can be used as a good reference for starting experimental studies with the corresponding metal.

## 3.5. HSC Chemistry 7 Software

Martirosyan and Luss, from the University of Houston, study the combustion of lunar regolith with a pyrotechnic mixture of titanium and boron. They achieved combustion for a stoichiometric mixture of titanium and boron with JSC-1A [19]. To have a better understanding of the behavior of the JSC-1A/Ti+B mixtures, THERMO was to be used in order to determine the adiabatic flame temperature for different concentrations of this mixture using the same procedure used for calcium, magnesium and aluminum described in Section 3.4. Titanium and boron are selected due to the pyrotechnic nature of the reaction:

$$Ti + 2B = TiB_2 \quad (\Delta_f G^o(298.15\ K) = -275.334\ kJ/mol\ [31]). \qquad \text{(Eq. 3.6)}$$

Unfortunately, for this particular system, adding two elements to the composition of JSC-1A gives a large number of possible compounds in the products composition and THERMO cannot handle such a big number of compounds. To solve this problem, the commercially available software HSC Chemistry 7 was used. HSC Chemistry has 22 calculation modules, including the Equilibrium Composition module which uses the Gibbs minimization method to calculate the product composition of the reaction [32]. Moreover, HSC Chemistry incudes a thermochemical properties database (including $c_p$, H, and S) of 25,000 compounds, of which

60% are inorganic [33]. A detailed description of the use of HSC Chemistry 7 is presented in this section.

### 3.5.1. EQUILIBRIUM COMPOSITION

The equilibrium module in HSC Chemistry is capable of calculating the equilibrium composition of the products of a reaction given the initial mixture amounts. However, in order to calculate the adiabatic flame temperature of the reaction, the product composition is required by HSC Chemistry. Because of the complexity of the system, the product composition is not known and cannot be easily assumed. For this reason, HSC Chemistry and THERMO were used together to calculate the adiabatic flame temperature of the JSC-1A/Ti+B mixtures. HSC Chemistry was used to reduce the number of products to be selected in THERMO's Main Table by eliminating the compounds that will not be present once the reaction is complete.

The process to input the information to calculate the product composition is similar to what is done in THERMO. The initial composition is entered in HSC Chemistry and the iterative process for the Gibbs energy minimization is started for a given pressure and an interval of temperatures. Once HSC Chemistry has finished, the results are presented in graphical form as shown in Figure 3.7. The results are shown for a given interval of temperatures. For the example shown in Figure 3.7, a 40 wt% stoichiometric Ti+B mixture with 60% JSC-1A was analyzed. It is shown that $TiB_2$ is the main compound found in the equilibrium products, as expected, due to the pyrotechnic nature of the Ti+B reaction. The equilibrium composition calculations in HSC Chemistry were done for different concentration ratios (10%, 35%, 60%, 75% and 90% of regolith) to ensure that all the possible product compounds are selected in the

THERMO main table. All the results were tabulated and the compounds that were obtained for all the compositions used are shown in Table 3.5, where the compounds and the different phases that might be present are indicated.

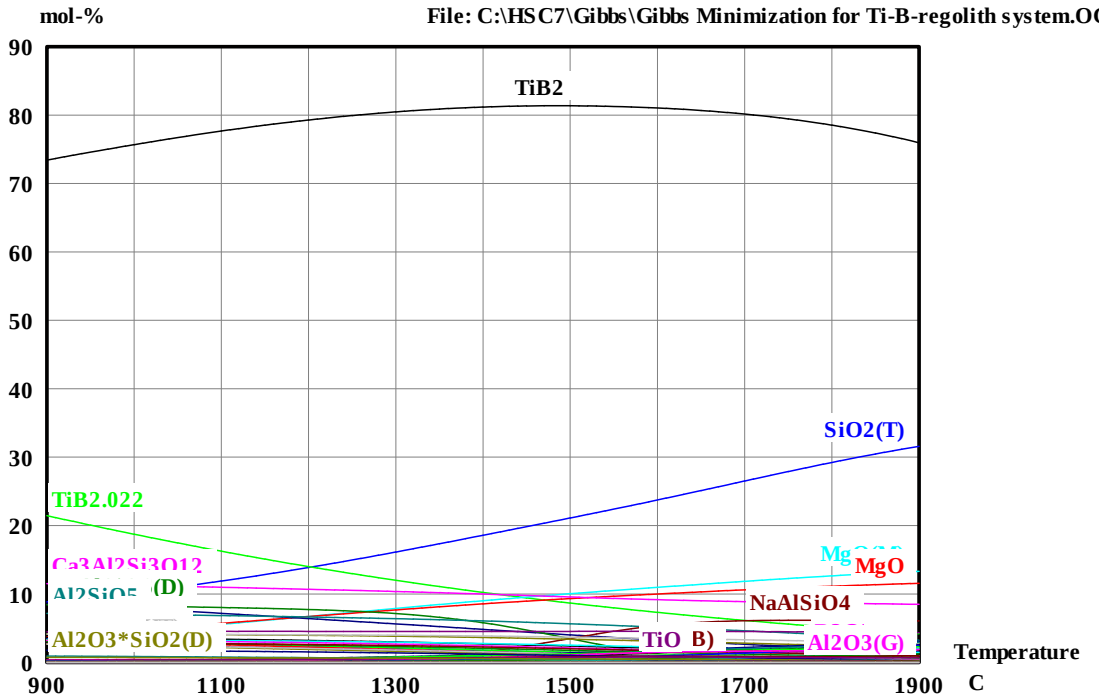


**Figure 3.7. Composition results for Gibbs energy minimization obtained from HSC Chemistry 7 for a 40wt % Ti+B/60 wt% regolith initial composition.**

**Table 3.5. Product equilibrium compounds for the combustión of regolith/Ti+B system**

| | | | | |
|---|---|---|---|---|
| $(BO)_2$(g) | Al | Al(FCC) | Al(g) | Al(HCP) |
| $Al_2$(g) | $Al_2O$(g) | $Al_2O_2$(g) | $Al_2O_3$ | $Al_2O_3$(C) |
| $Al_2O_3$(D) | $Al_2O_3$(G) | $Al_2O_3$(K) | $Al_2O_3$*$SiO_2$(D) | $Al_2SiO_5$ |
| $AlBO_2$(g) | AlO(g) | $AlO_2$(g) | AlTi | B |
| B(A) | B(B) | B(g) | B(GL) | $B_2$(g) |
| $B_2O$(g) | $B_2O_2$(g) | $B_2O_3$(A) | $B_2O_3$(g) | BO(g) |
| $BO_2$(g) | BTi | Ca(g) | $Ca_2$(g) | $Ca_2Al_2SiO_7$ |
| $Ca_3Al_2Si_3O_{12}$ | CaO(g) | Fe(g) | $Fe_2$(g) | $Fe_3Si$ |
| FeB | FeO(g) | $FeO_2$(g) | FeSi | K(g) |
| $K_2$(g) | $K_2O$(g) | $K_2O_2$(g) | $K_2TiO_3$ | $KBO_2$(g) |
| $KFeO_2$ | KNa(g) | KO(g) | Mg | Mg(g) |
| $Mg_2$(g) | $Mg_2SiO_4$ | $Mg_2SiO_4$(F) | MgO | MgO(g) |
| MgO(M) | MgO*$Al_2O_3$ | $MgSiO_3$ | $MgSiO_3$(G) | $MgSiO_3$(HP) |
| $MgSiO_3$(HT) | $MgSiO_3$(L) | $MgSiO_3$(L) | $MgSiO_3$(P) | Na |
| Na(g) | $Na_2$(g) | $Na_2O$(g) | $Na_2O$*$Al_2O_3$*$2SiO_2$ | $Na_2O_2$(g) |
| $NaAlO_2$ | $NaAlSiO_4$ | $NaAlSiO_6$(D) | $NaBO_2$(g) | NaO(g) |
| O(g) | $O_2$(g) | $O_3$(g) | Si | Si(g) |
| $Si_2$(g) | $Si_2O_2$(g) | $Si_3$(g) | $Si_3Ti_5$ | SiO(g) |
| $SiO_2$ | $SiO_2$(C) | $SiO_2$(CR) | $SiO_2$(CRS) | $SiO_2$(G) |
| $SiO_2$(H) | $SiO_2$(Q) | $SiO_2$(T) | $SiO_2$(V) | SiTi |
| Ti | Ti(A) | Ti(B) | Ti(g) | $Ti_2$(g) |
| $Ti_2O_3$ | $Ti_3O_2$ | $Ti_5Si_3$ | TiAl | TiB |
| $TiB_2$ | $TiB_{2.022}$ | TiO | TiO(B) | TiO(g) |
| $TiO_{1.01}$ | $TiO_2$ | $TiO_2$(g) | $TiO_2$(R) | TiSi |
| $TiSi_2$ | | | | |

### 3.5.2. THERMO

The compounds shown in Table 3.5 (obtained by HSC Chemistry) were then selected in THERMO's Main Table. HSC Chemistry allowed reducing the number of product compounds from about 200 to 121 (a number of products that THERMO is able to handle). As was performed with the metal additives (magnesium, calcium and aluminum), the weight percentage of regolith was increased one step at a time from 0 to 100 and the adiabatic flame temperature calculations were performed by THERMO. Figure 3.8 shows the adiabatic flame temperature variation with the percent of stoichiometric Ti+B mixture.

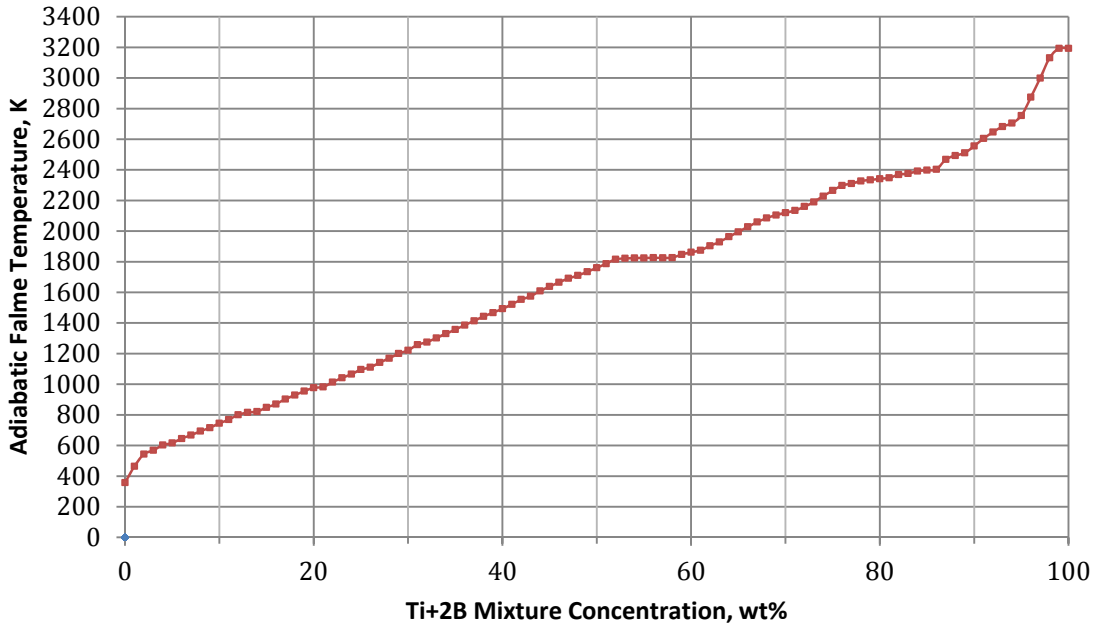


**Figure 3.8. Adiabatic flame temperature of regolith/Ti+B mixtures**

Figure 3.8 shows that there is no maximum adiabatic flame temperature for this system and that the temperature always increases for a higher percentage of Ti+B mixture. The reason for this behavior is the lack of reaction between the regolith and the Ti+B. Titanium and boron

react between each other releasing heat. The heat produced by this reaction is the responsible for the sintering of the regolith.

### 3.5.3. HSC Chemistry and THERMO for Metallic Additives

To make a fair comparison between the different systems studied in this document, HSC Chemistry and THERMO were used together to calculate the adiabatic flame temperature as function of metal concentration for calcium, magnesium and aluminum. As explained in section 3.5.2, HSC Chemistry was used to determine the possible compounds present in the products equilibrium composition. The new calculation of the adiabatic flame temperatures will allow for the comparison between the regolith/Ca,Mg,Al, Ti+B systems. Also, it will permit to assess the validity of the calculations for the regolith/Ti+B mixtures (at least theoretically), because, if the similarity of the graphs for the regolith/metal systems is significant, the conclusion that both methods give the same results can be made.

### 3.5.4. Calcium

Figure 3.9 shows the results for the adiabatic flame temperature for different concentrations of calcium metal. Figure 3.10 shows the comparison between the two methods. Both graphs are very similar and no important differences are notices. HSC Chemistry and THERMO give basically the same result.

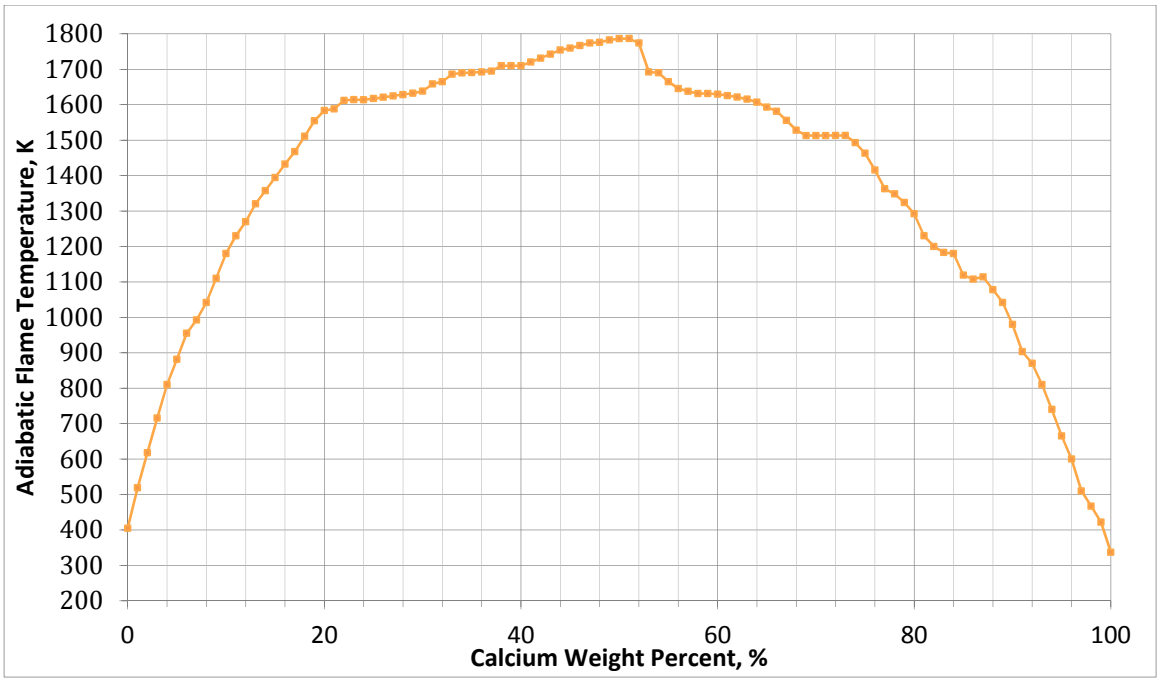


**Figure 3.9. Adiabatic flame temperature vs calcium weight percent using HSC Chemistry and THERMO software**

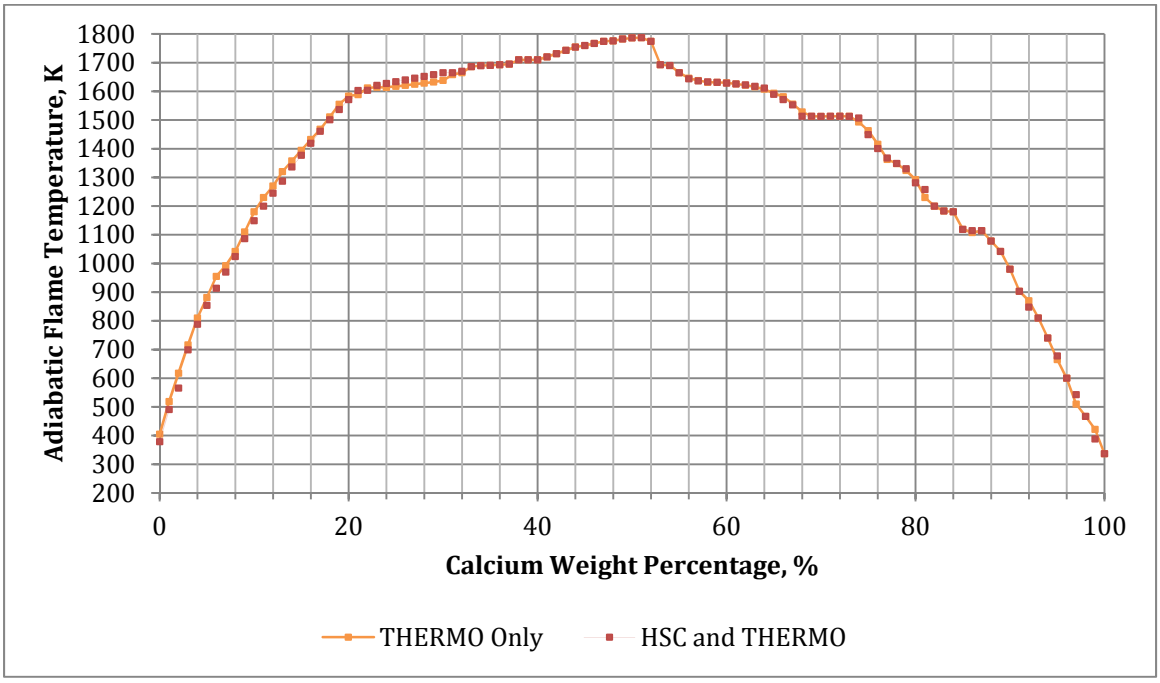


**Figure 3.10. Comparison of the adiabatic flame temperature calculated with HSC Chemistry/THERMO and THERMO only for JSC-1A/Ca mixtures**

### 3.5.5. MAGNESIUM

Figure 3.11 shows the results for the adiabatic flame temperature for different concentrations of magnesium metal. Figure 3.12 shows the comparison between the HSC method and the THERMO method. Both graphs follow the same trend; however, the maximum temperature is reached at 27 wt. % magnesium (compared to 26 for THERMO only). The maximum temperature was the same (1690 K, silicon melting point). A plateau at this temperature is not observed.

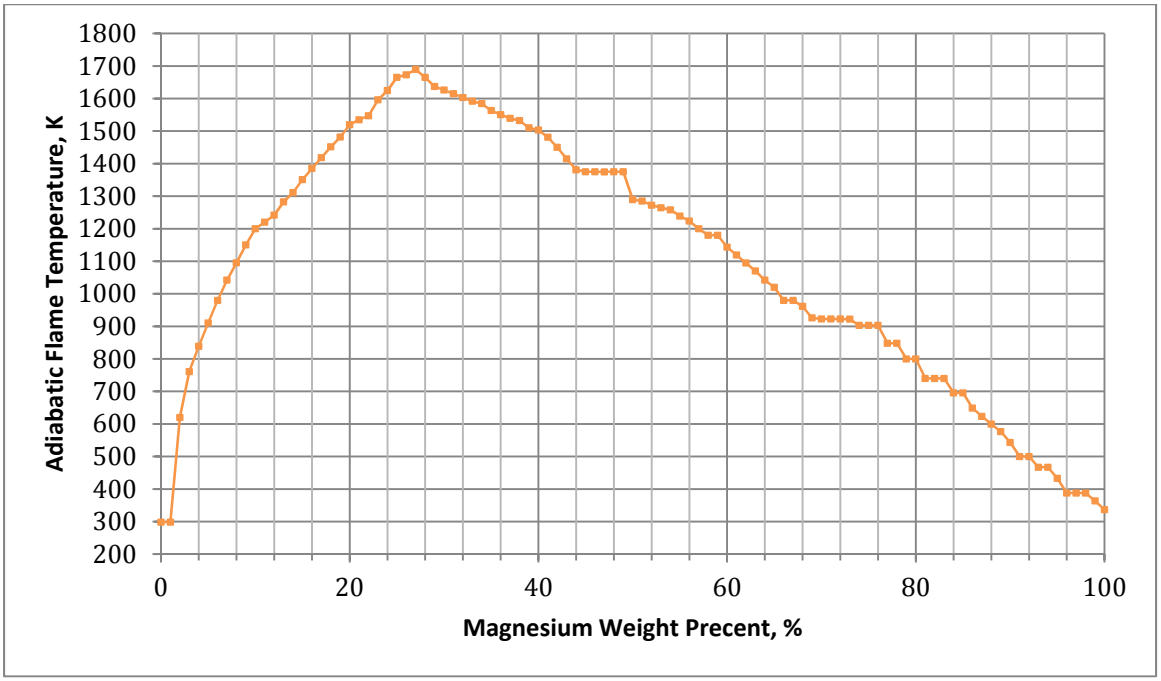


**Figure 3.11. Adiabatic flame temperature vs. magnesium weight percent using HSC Chemistry and THERMO software**

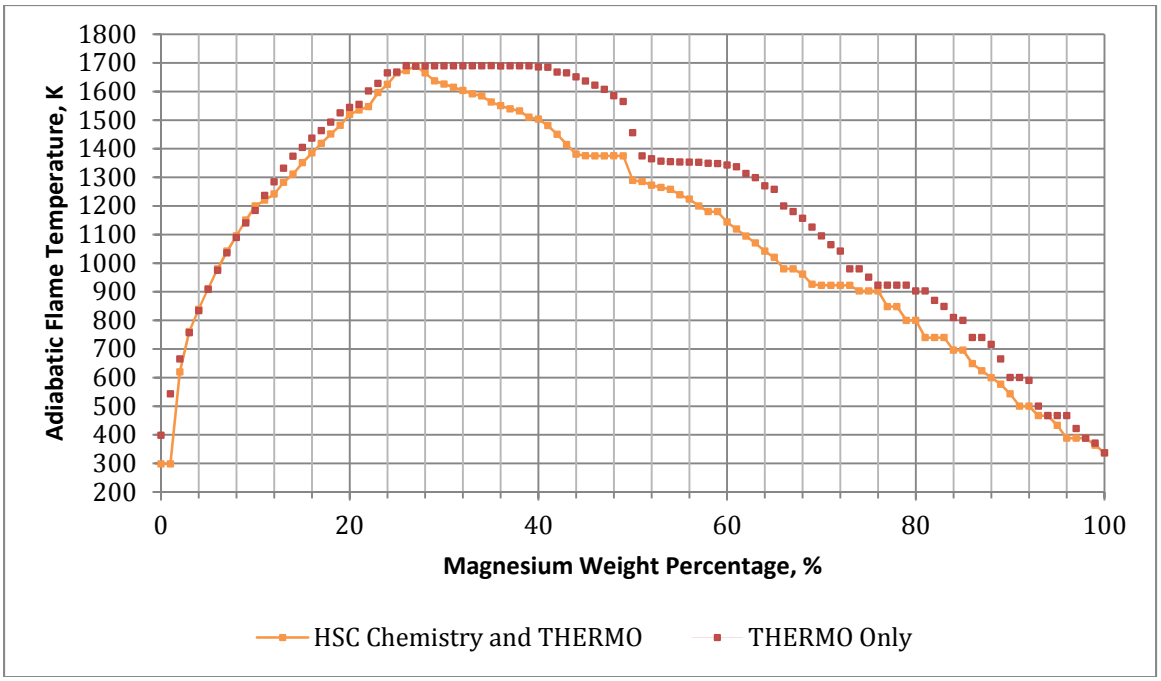


**Figure 3.12. Comparison of the adiabatic flame temperature calculated with HSC Chemistry/THERMO and THERMO only for JSC-1A/Mg mixtures**

### 3.5.6. ALUMINUM

Figure 3.13 shows the results for the adiabatic flame temperature for different concentrations of aluminum metal. The maximum temperature (656 K) is reached at 21 wt. % aluminum (lower than for THERMO alone and shifted from 23 wt. %). The trend of the chart shows the same behavior for both results.

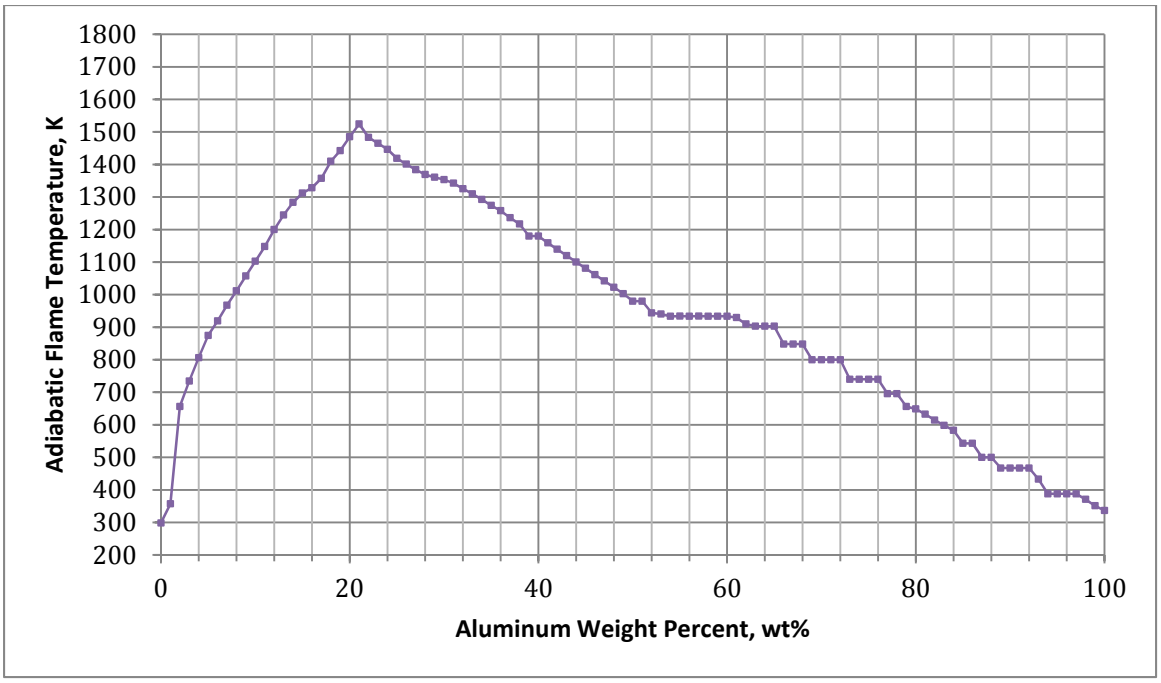


**Figure 3.13. Adiabatic flame temperature vs. aluminum weight percent using HSC Chemistry and THERMO software**

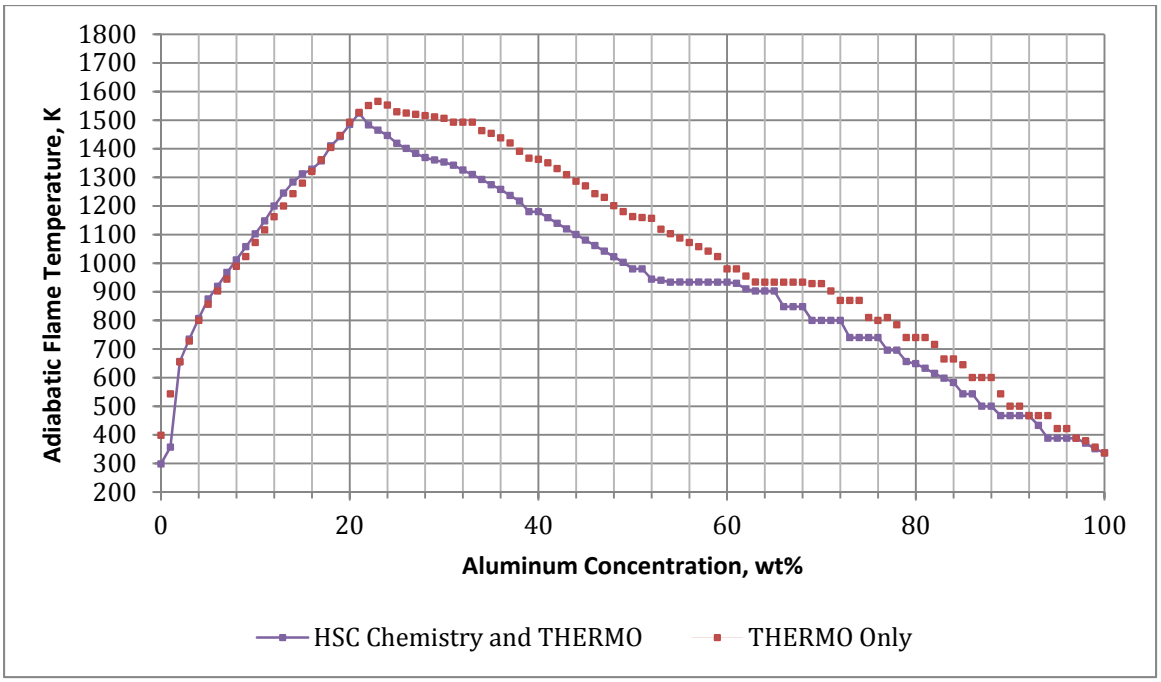


**Figure 3.14. Comparison of the adiabatic flame temperature calculated with HSC Chemistry/THERMO and THERMO only for JSC-1A/Mg mixtures**

### 3.5.7. Comparison of Metals with HSC

Figure 3.15 shows a comparison between the three temperatures calculated with HSC and THERMO. The trend for this method is the same as that calculated with THERMO only. Again, for concentrations in the low 20 wt. %, the magnesium and calcium change the maximum values.

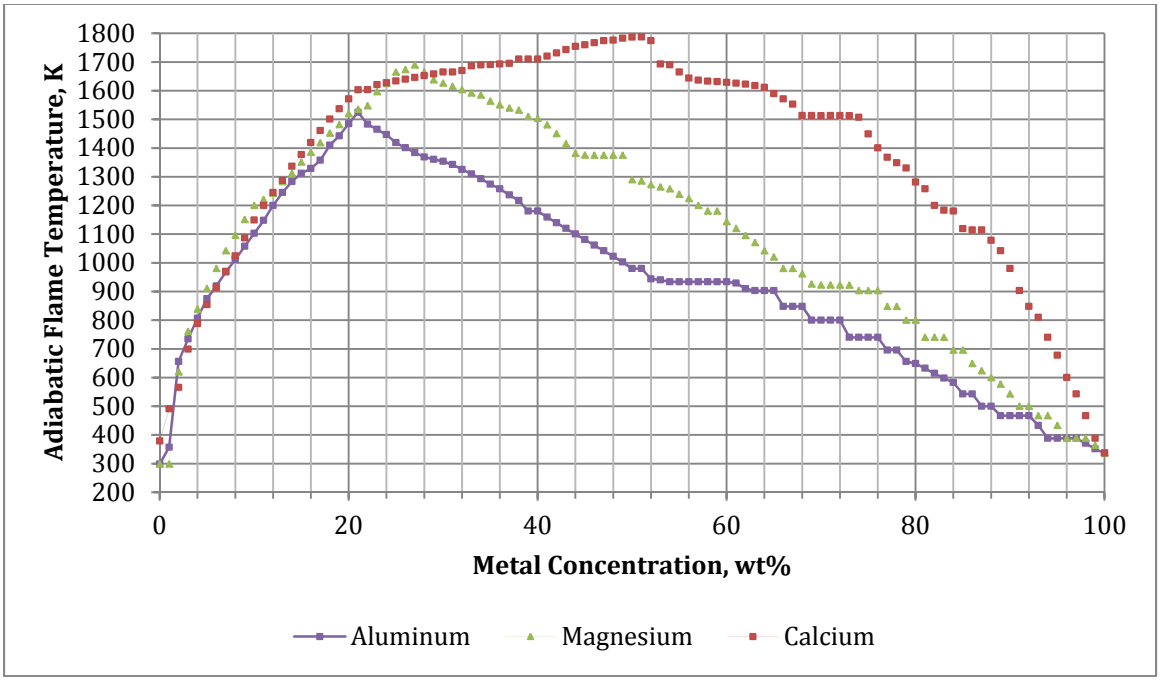


**Figure 3.15. Comparison of adiabatic flame temperature for metallic additives calculated with HSC Chemistry and THERMO**

## 3.6. Conclusions

The graphs presented in this chapter provide an insight to the behavior of the combustion of JSC-1A with energetic additives.

### 3.6.1. METALLIC ADDITIVES

Two methods were used to determine the adiabatic flame temperature of JSC-1A/metal mixtures. The THERMO method showed a higher adiabatic flame temperature for all cases than the HSC Chemistry/THERMO approach. However, the overall trend for the metal additives remained the same for both cases. Following the behavior expected from the Ellingham diagram, calcium showed the highest temperature followed by magnesium and aluminum, respectively. However for concentrations close to 20 wt% of metal fuel, magnesium lies higher than the calcium adiabatic flame temperature. Because one of the goals of this project is to minimize the amount of metal additive required, this shift is important if the minimum amount necessary lies close to this region.

The behavior of the graphs herein presented gives a hint about the ease to combust the mixtures, being the JSC-1A/calcium mixture the easiest to propagate at the appropriate weight percentage. To study the propagation of the reaction, these mixtures will be experimentally studied.

Aluminum and magnesium are commercially available in powder form and are available in different particle size. Although calcium reduction has been studied for ISRU applications [34] [35], no metallic calcium powder is commercially available; and the cSETR ISRU team does not have access to the equipment to produce calcium powder. For this reason, only aluminum and magnesium mixtures will be experimentally studied.

### 3.6.2. TITANIUM AND BORON

The reaction of JSC-1A with Ti+B was previously studied [19] and sustained combustion for a 40% Ti+B/60% JSC-1A mixture. Although, experimentally, this reaction has proven to be feasible, the scarcity of titanium and boron on the Moon do not justify a more detailed experimental study for lunar ISRU applications.

# 4. EXPERIMENTAL SETUP FOR SELF-PROPAGATING HIGH-TEMPERATURE SYNTHESIS UNDER MICROGRAVITY CONDITIONS

The effect of microgravity on the SHS products has been largely studied in the last decades. These studies have proven that gravity affects the microstructure, the volume increase, the composition and the flame velocity [36] [37] [38]. Understanding the effects of microgravity on SHS processes for lunar production of materials is particularly important due to the reduced gravity that exists on the Moon (one-sixth of the terrestrial gravity). For this reason, the experiments of JSC-1A with magnesium were performed on board NASA's Zero-G aircraft thanks to the Minority University Research and Education Program (MUREP). This chapter describes the flight profile and characteristics, the design of the microgravity rack to fly on board this aircraft. The findings regarding the effect of microgravity on the flame velocity and the mode of combustion will be presented in Chapter 5.

## 4.1. Microgravity and NASA Minority University Research and Education Program

The combustion of regolith/energetic additive mixtures for the production of structural materials on the Moon is one of the technologies that needs to be proven under microgravity to ensure its success if it shows economically viable. If any experiment is to be performed under this condition, the ideal situation would be to conduct it in outer space. However, this privilege is very limited due to the cost of space flight. Zero-G Corporation provides research services to groups that require microgravity to conduct certain experiments for which this condition is

important without leaving Earth. Although, not as expensive as actual space flight, this service is not low-cost and is reserved for a select number of research groups.

The cSETR ISRU team was selected from among several other university teams to perform research on board Zero G thanks to the sponsorship of NASA's Minority University Research Education Program (MUREP). The selection consists on sending a technical and outreach proposal to NASA. From the applying teams, few are selected due to the technical feasibility and significance of the research towards NASA's objectives.

After the selection of the team (five students, one faculty advisor and one NASA mentor); the design of the microgravity rack and the experiment was started.

## 4.2. Design of Experimental Rack to Fly On-Board Zero-G Aircraft

At the time of the selection for the microgravity program, the ISRU team had already started the experimentation stage and had proven the combustion of JSC-1A/magnesium SHS reaction. The existing setup to perform combustion experiments under normal gravity at UTEP had to be modified in order to comply with the safety requirements and design specifications of NASA. This process required a continuous communication back and forth with NASA's scientists and engineers to guarantee the well-being of the flyers and the equipment during the flights.

To better understand the NASA requirements, it is important to describe the flight profile and the plane conditions. The Zero G aircraft is a modified Boeing 727 capable of withstanding the unusual stresses imposed on the aircraft by the parabolic profile of the flight (Figure 4.1). The flight consists of a series of parabolas with intervals of weightlessness (zero

gravity) and increased gravity (1.8 g's). Figure 4.1 shows that the interval of microgravity is approximately 25 seconds, although this is not a fixed value due to the variability of the flight conditions. The number of parabolas varies depending on the conditions required by the research teams. For the educational programs (such as the MUREP), the airplane performs 30 zero gravity parabolas, one lunar-gravity parabola, and one Martian-gravity parabola (the lunar and Martian parabolas are mainly for enjoyment of the teams). Each team flies two consecutive days; the same flier cannot fly in both occasions.

For this experiment, it is important to note that the atmospheric pressure decreases with increasing altitude. At the top of the parabola, the altitude is approximately 32,000 feet and the pressure is 3.99 psia, while at the bottom of the maneuver the altitude is 24,000 feet and the pressure is 5.70 psia. The atmospheric pressure at sea level is 14.7 psia [39].

The microgravity duration greatly influences the design of the experiment to be flown, because each experiment must last less than this period of time. The information presented in this chapter will take this restriction into consideration.

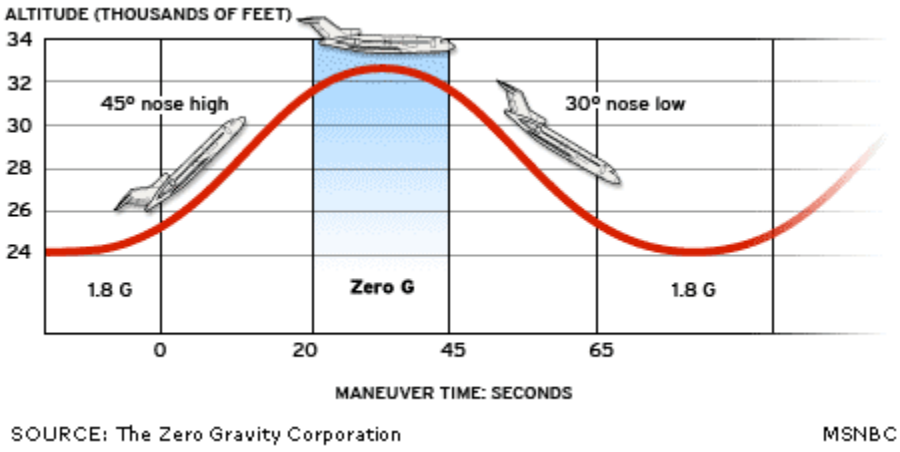


**Figure 4.1. Parabolic profile of the microgravity flight by the Zero G Corporation [40]**

### 4.2.1. Existing Experimental Setup and Modifications for Microgravity Flights

#### Existing Equipment and Experimental Procedures

The previous experiments done at UTEP were performed for mixtures of 74% JSC-1A/26% magnesium. This mixture ratio was selected because of the results of the thermodynamic calculations (Chapter 3). Unfortunately, the mixtures did not ignite for mixtures using the original JSC-1A. For this reason, the original JSC-1A was crushed using a roller ball mill (LabMill 8000) inside an alumina jar with burundum grinding media for different intervals of time. Increasing the milling time showed a decrease in the mean diameter of the particles, and for milling times greater than 2-hours, the reaction was completed [41]. Increasing the specific surface area (i.e. decreasing the particle diameter) might increase the reaction rate and, thus, the velocity of the reaction. The setup used by the team at UTEP consisted of a 30cmx40cm cylindrical steel combustion chamber (shown in Figure 4.2a) equipped with a pressure gauge (30 inHg vacuum to 15 psi), three glass windows and one steel port to access the interior of the chamber. The interior of the chamber is connected to an Argon tank and an external vacuum pump, and to an electrical system. The top and bottom lids of the chamber are connected through 12-1/4” steel bolts each.

a) b)



**Figure 4.2. a) Combustion chamber, b) Power supply**

The electrical system consisted of feedthroughs connected to a direct current power supply (shown in Figure 4.2b) which can deliver up to 20 A of current at a voltage of 30 V that could be transmitted to the ignition system which consisted of a highly resistive coiled wire (Nichrome) to initiate the ignition of the mixtures. A commercial camcorder was located outside one of the glass windows to record the reactions and obtain visual data.

The experimental procedure on Earth consists of the following series of steps:

1. The pellet is prepared to the desired concentration and pressure using the Craver hydraulic press.
2. The pellet is put inside the chamber and a good contact between the top part of the pellet and the ignition Nichrome wire is inspected. The chamber is closed.
3. The chamber is evacuated and refilled with Argon gas. Magnesium metal reacts with air oxygen, so the chamber must not contain oxygen gas.
4. The camera is turned on to record the reaction when started.

5. The power supply is turned on to heat up the ignition system and start the reaction at the top of the pellet. Once the reaction has started, the ignition system is turned off. When the reaction has finished it is let to cool down.
6. After the cool down process, the chamber is open and the reacted pellet is retrieved from the inside.

A visual example of the reactions is shown in Figure 4.3. The upper left picture (t=0) shows no reaction and a luminous Nichrome wire due to the energy being dissipated by the coil. Once the energy transferred to the mixture is sufficient to start the reaction the combustion front is visible (Figure 4.2 t=0-t=45).

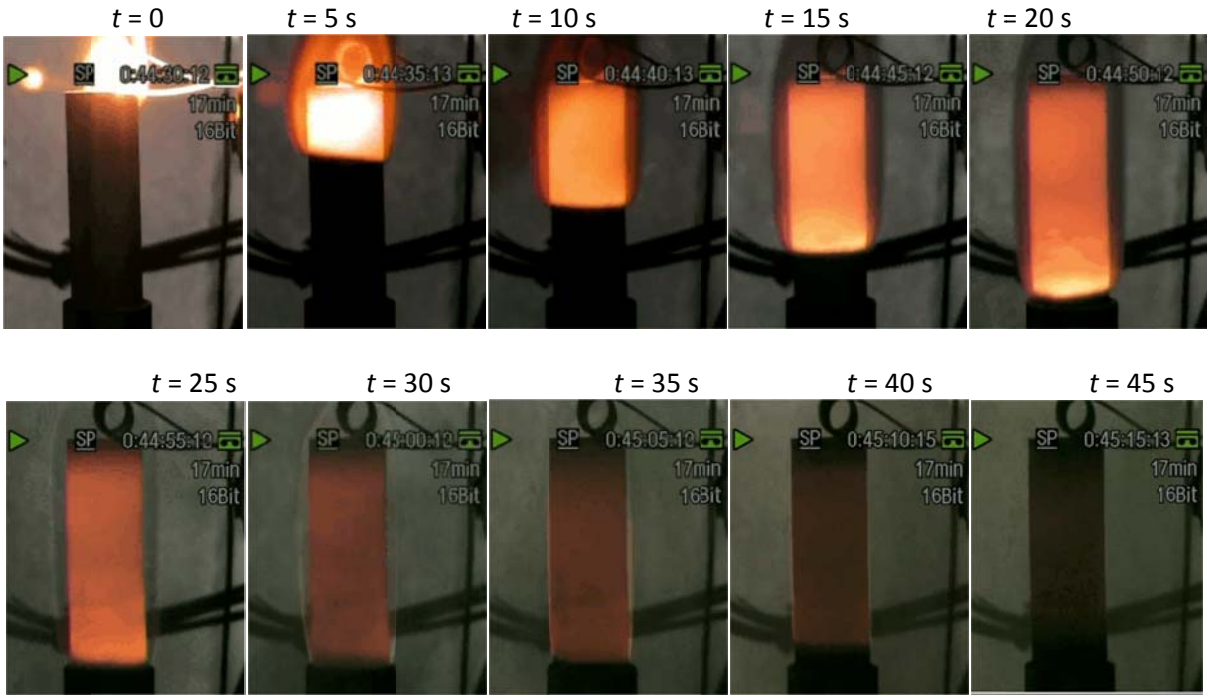


**Figure 4.3. Visual example of a 26%Mg/74% JSC-1A reaction**

The setup had to be modified to comply with NASA requirements and design specifications.

**Experimental Procedures and Equipment Modifications for Microgravity Conditions**

Due to the long time to complete the reactions for solid pellets (Figure 4.3), pressed mixtures could not be used. To ensure that the ignition and the completion of the reaction happen in the 25 seconds timeframe of reduced gravity, a planetary ball mill (Fritsch Premium Line Pulverisette 7) was used to generate JSC-1A particles as small as 1 µm. These mixtures had shown fast ignition on Earth. Quartz tubes were used to contain the loose powder mixtures. Quartz was selected due to its high melting point (approximately 1600°C) to guarantee the integrity of the tube while the reaction occurred.

Another important change that needed to be made to the experimental procedure is the need to increase the number of samples that can be burnt without opening the chamber, but still be able to record the combustion process. To accomplish this, a rotary device that could hold several samples and could rotate to the front of the camera so that the reaction could be recorded had to be envisioned. The ignition was completed by the resistive wire. The ignition wires for the fifteen samples were to be connected to a switchbox intended to select appropriate conducting wire for the sample in front of the camera.

At UTEP, the chamber was evacuated with the help of a vacuum chamber. NASA does not allow oil-operated vacuum pumps on board; however, the experimental rigs can be connected to the exterior of the airplane if necessary. The vacuum pressure generated between the inside of the chamber and the exterior of the plane during flight can be used as a “vacuum pump”. There are some gaseous products generated during each of the reactions; for this reason the chamber had to be flushed with Argon gas after each experiment. To allow enough

time to completely flush and cool down the combustion chamber (in case it warms up with the exothermic reactions), every other parabola was used for flushing purposes, i.e. the odd-numbered parabolas were used for combustion and the even-numbered were used for flushing.

To comply with NASA all the changes mentioned above had to be made on the existing equipment and, at the same time, comply with NASA. The NASA requirements pertinent to this experiment can be divided into four major topics: safety considerations, pressure system, electrical system and structural analysis. Previous to the flight, a Test Equipment Data Package (TEDP; found in Appendix A) has to be turned in to NASA engineers and scientists for their revision and approval. Also, prior to the flight, a Test Readiness Review (TRR) needs to be performed while at NASA facilities (i.e. Ellington Field). The following sub-sections will be explaining into more detail the development of the TEDP and the design of the microgravity rig taking into consideration the four major sections previously stated.

### 4.2.2. STRUCTURAL ANALYSIS

The structural analysis of the experimental rig to use on board Zero G is required in order to ensure the well-being of the passengers and the integrity of the aircraft if any of the components may come apart of the rack. In order to accomplish this task, a detailed force analysis of all the attachments between the components of the system and of the system with the plane is required following the standard NASA and Zero Gravity Corporation procedures [42] [43] [44] [45].

The structural analysis consists of studying the stresses imposed on the rack components in case of an emergency landing or take-off. The required analysis' loads are shown in Table 4.1.

**Table 4.1. Loads under emergency takeoff and landing conditions**

| Direction | Load |
|---|---|
| Forward | 9-g's |
| Aft | 3-g's |
| Down | 6-g's |
| Lateral | 2-g's |
| Up | 2-g's |

The number of g's stands for the number of times that the weight must be taken into account for the direction of the force being treated. For example, if the rig has a mass of 100 lbs., the force imposed when analyzing the forward direction must be 900 lbs. Each force is to be analyzed separately, i.e. loads are not to be imposed all at the same time. Figure 4.4 shows the combustion chamber, the power supply, the base plate and the framing material to be used. These are the heaviest instruments and were the components used to calculate the center of gravity of the overall system using the Advanced Weight Management tool in NX6. To account for the missing components, a 20% weight was added to the weight of the system. It is important to note that the heaviest component (i.e. the combustion chamber) has to be pointing in the forward direction in order to minimize the stresses on the bolts.

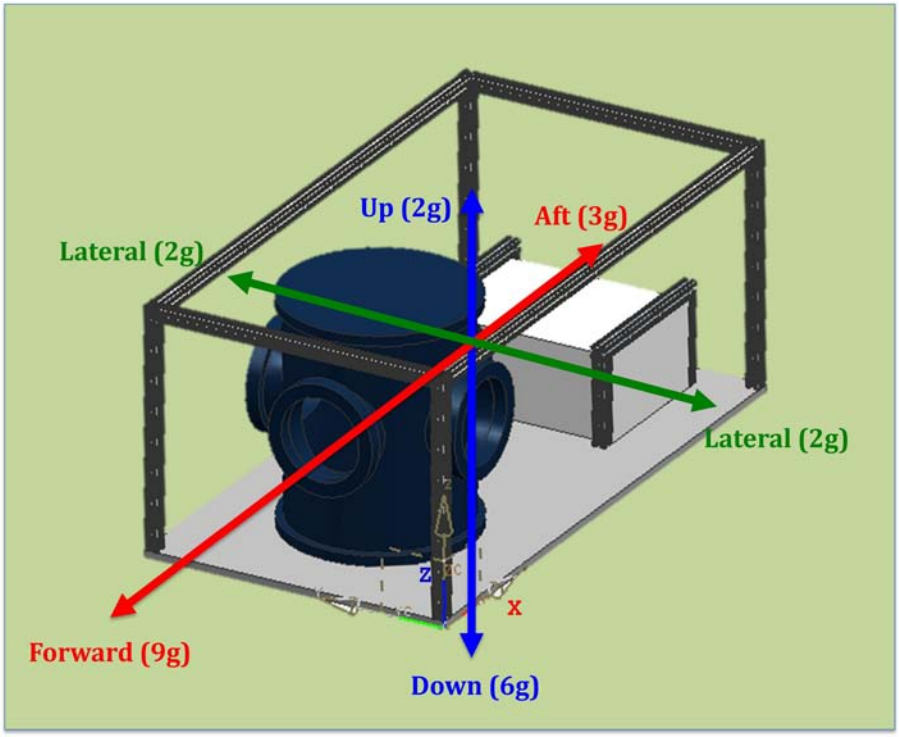


**Figure 4.4. Schematic of microgravity rig with imposed emergency takeoff and landing loads**

Three types of attachments were used for this system: ¼"-1215 steel bolts for the aluminum frame joints, ¼" Grade 5 steel for the chamber attachments and the frame attachments to the base plate, and 6-AN6 steel bolts (provided by NASA Reduced Gravity Office) were used for the floor attachments (to attach the base plate to the aircraft). For the floor attachments the allowable is given by the floor itself (tension allowable=2125 lbs. and shear allowable=2500 lbs) and not by the bolts. The bolted equipment to the aircraft (such as this system) must use the attach points arranged in a 20"x20" grid on the aircraft floor. All bolted equipment must use at least four attachment points; for the microgravity rig herein presented, six attachment points were used.

All the attachments must be analyzed. In order to comply with the structural requirements all margins of safety must be greater than zero. The margins of safety are calculated following the equation:

$$M.S._{yield} = \frac{\sigma_{yield\ strength}}{\sigma_{limit} \cdot F.S.} - 1. \quad \text{(Eq. 4.1)}$$

In Equation 4.1, $\sigma_{yield\ strength}$ is the allowable yield stress (tension or shear) for the joining component (bolt or strap), $\sigma_{limit}$ is the stress calculated based on the maximum loads expected during flight (in this case, these are the emergency takeoff and landing loads), and F.S. is any factor of safety applied to the analysis and depends on the aircraft, location, materials and other conditions. A summary of the margins of safety for the heaviest components is presented in Table 4.2, which shows that all the margins of safety are greater than zero and thus, is compliant with the specified requirements. A detailed calculation of the masses, the tension and shear forces, as well as of the margins of safety is included in the Structural Verification section of Appendix A.

**Table 4.2. Margins of safety summary**

| **Floor Attachments** | | | |
|---|---|---|---|
| **Configuration** | **Mode** | **Max. Load** | **MS** |
| 9g-Forward | Tension | 126.11 | 5.74 |
| | Shear | 318.95 | 2.14 |
| 3g-Afterward | Tension | 42.04 | 19.22 |
| | Shear | 106.32 | 8.41 |
| 2g-Lateral | Tension | 46.71 | 17.20 |
| | Shear | 70.88 | 13.11 |
| 2g-Upward | Tension | 109.61 | 6.75 |
| 6g-Downward | Tension | 212.63 | 3.00 |
| **Chamber** | | | |
| **Configuration** | **Mode** | **Max. Load** | **MS** |
| 9g-Forward | Tension | 257.97 | 3.19 |
| | Shear | 135.00 | 7.01 |
| 2g-Upward | Tension | 30.00 | 35.04 |
| **Power Supply/Inner Frame** | | | |
| **Configuration** | **Mode** | **Max. Load** | **MS** |
| 9g-Forward | Tension | 48.12 | 21.47 |
| | Shear | 63.45 | 16.04 |
| 2g-Upward | Tension | 14.10 | 75.68 |
| 2g-Lateral | Shear | 28.20 | 18.45 |
| **Outer Frame** | | | |
| **Configuration** | **Mode** | **Max. Load** | **MS** |
| 9g-Forward | Tension | 20.69 | 51.26 |
| | Shear | 31.73 | 16.29 |
| 2g-Upward | Tension | 7.05 | 152.36 |

### 4.2.3. HAZARDS ANALYSIS

The hazards analysis section includes all the risks that are inherent to the system and that are avoidable taking the appropriate mitigating measures. Examples of the hazards analyzed in this section are: temperature, toxicity, collisions, sharp points, and electrical potential. The detailed information can be found in the Hazards Analysis section in Appendix A. Table 4.3 shows the summary required by NASA. The Hazard column shows the category under which every risk falls under. All the categories can be found in References [43], [44], and [45]. To clarify Table 4.3, the example of Electrical Potential hazard will be explained. The Cause column shows the specific reason for which a safety issue may arise during flight; in the case of Electrical Potential overcharging the electrical outlet is a risk and represents a hazard. The Effect column shows the damage that may occur if the event shown in Cause happens; if the electrical outlet is overcharged, the electrical system may overcharge and a fire may be created. The Sev/Prob RAC column is the calculation of the Risk Assesment Code (RAC) for each of the hazards. The severity is the class consequence of the event and describes the damages that could occur. The class consequence is described by the terms catastrophic, critical, moderate, and negligible. The Probability is the likelihood estimate and depicts the chances of the event happening and is divided in five parts: likely to occur, probably occurs, may occur, unlikely to occur, and improbable. Once the severity and probabilities are determined, the RAC can be calculated according to Table 4.4. The RAC has 7 levels: 1 means that the hazard is unacceptable, 2 means that the hazard is undesirable, and a RAC of 3-7 suggests that the hazard is acceptable with controls.

At this point, the controls are to be introduced to the analysis. The column Controls shows the measures to be taken to avoid the cause to occur; to avoid overcharging the electrical outlet a 20 A fuse is to be used. The Verification column shows how the measure is going to be tested previous to the flight to ensure that it is working effectively at the time of the flight; the electrical system will be tested to ensure that the system is not electrically overcharged previous to the flight. After the controls are introduced the RAC's are calculated again with the measures implemented. All the RAC's must be greater than 3 in order to comply with NASA and Zero G Corporation.

**Table 4.3. Summary of the hazard analysis and Risk Assesment Codes (RAC)**

| HAZARD | CAUSE | EFFECT | Sev/Prob RAC | CONTROLS | VERIFICATION | DISPOSITION Sev Prob RAC |
|---|---|---|---|---|---|---|
| Electrical Potential | Overcharging the electrical outlet | Overheating and fire | II/C-3 | A 20 Amps fuse is installed to avoid overcharge | Electrical test previous to the flight | II/E-5 |
| Overpressurization | Gas generation inside the chamber | Cracking of windows in combustion chamber | II/E-5 | A relief valve is installed. A pressure gauge measures the internal pressure in the chamber. | Operators will monitor pressure using the gauge and will open the outlet valve when it is necessary. | II/E-5 |
| Fire | Uncontrolled combustion inside chamber | Overheating of internal components and steel chamber | II/C-3 | Flammable materials (wire insulation) cannot burn in argon atmosphere. | Operators will maintain argon atmosphere in the chamber. | II/D-4 |
| High Temperatures | The investigated combustion process generates high temperatures in the samples | Overheating of internal components and steel chamber | III/B-3 | Purging with argon after each experiment | Operators will purge the chamber after each experiment. | III/C-4 |
| Sharp Points or Edges | The experimental rig has sharp points or edges | Injury | III/C-3 | Foam will be attached to all sharp points and edges to avoid their exposure. | Visual inspection of the foam and the sharp edges | III/E-6 |
| Environmental Pollution | Fumes may form during the investigated process | Fumes may be accumulated in the chamber | IV/B-4 | Purging with argon after each experiment removes fumes from the chamber | Operators will purge the chamber after each experiment. The particles will be collected in filter. | IV/C-5 |

**Table 4.4. Risk Assessment Codes**

| Consequence Class | Likelihood Estimate | | | | |
|---|---|---|---|---|---|
| | A | B | C | D | E |
| I | 1 | 1 | 2 | 3 | 4 |
| II | 1 | 2 | 3 | 4 | 5 |
| III | 2 | 3 | 4 | 5 | 6 |
| IV | 3 | 4 | 5 | 6 | 7 |

### 4.2.4. Pressure System Analysis

The system is connected to an argon tank and to the overboard vent to flush the chamber every other parabola. This arrangement creates a pressure system and the integrity of the components had to be assessed to ensure the safety of the airplane. Figure 4.5 shows a schematic of the pressure system. The chamber is connected to the argon gas tank and the connecting valve is open when the chamber needs to be filled with argon. When the chamber needs to be evacuated, the valve connecting the chamber to the vent (right side of Figure 4.5) is open and the products pass through a 0.5 microns filter to avoid any toxic particles to go airborne.

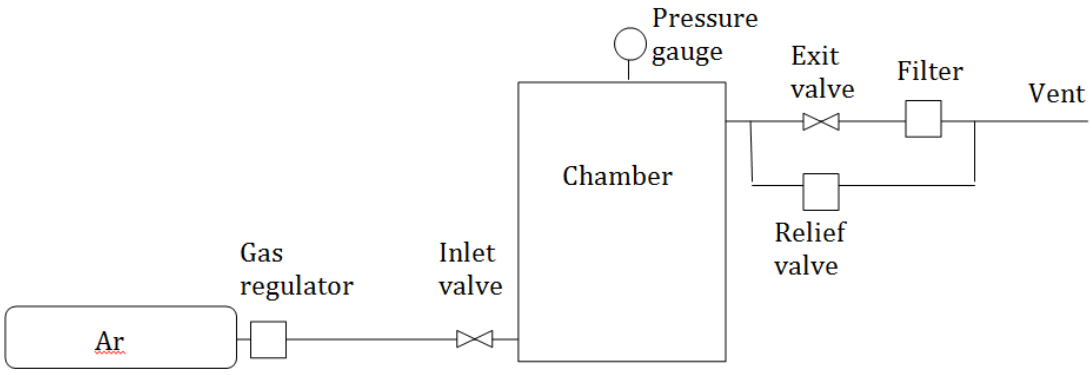


**Figure 4.5. Schematic of pressure system**

Although the experiments were to be performed at 0 psig, a sudden increase in pressure had to be considered and the system needed to be rated for a given pressure. The combustion chamber was tested to 20 psig (Pressure Vessel Verification in Appendix A). A relief valve of half the test pressure (as requested by NASA) was also installed to avoid the pressure from increasing higher than 10 psig. The pressure inside the chamber was monitored with the pressure gauge installed in the chamber.

The detailed information about the Pressure System Analysis can be found in Appendix A.

#### 4.2.5. ELECTRICAL ANALYSIS

The electrical components in the microgravity rig had to be analyzed to ensure that the electrical load on the airplane was below the allowed limit for the given outlet. In the case of this system a 115 VAC, 60 Hz, 20 Amps outlet was used. The electrical components used in this system are: a power supply, a camcorder, and a controller for a rotary stage. Table 5.5 shows that the current drawn from the airplane will not surpass the limit of 20 Amps and, if the appropriate hazard mitigating measures are in place, does not represent a risk.

**Table 5.5. Electrical load analysis**

| **Electrical Analysis** | | | |
|---|---|---|---|
| Power Source Detail | | Load Analysis | |
| Name | Power Cord A | Power Supply | 10 Amp |
| Voltage: | 115 VAC, 60 Hz | Stand-Alone Controller | 2 Amp |
| Wire Gauge | 12 | Camcorder | 1 Amp |
| Max Outlet Current: | 20 Amps | Total Current Draw: | 13 Amp |

#### 4.2.6. MICROGRAVITY RACK

After all the structural, electrical, pressure, and hazard considerations were taken into account the microgravity rig was finished and ready for the experimental step. NASA engineers and scientists

reviewed the setup to ensure that everything was in order and to clarify any final details. Figure 4.6 shows the experimental setup once it was installed on the aircraft. The camera is not shown because it could not be installed during takeoff and landing.

**Figure 4.6. Experimental setup installed on board Zero G aircraft (top view)**

A camera pole (provided by NASA) was installed on the system once the airplane was ready to start microgravity. On the left side of Figure 4.6, the combustion chamber is shown with the rotary stage controller on top. On the right side, the power supply (bottom) and the switchbox are shown. The switchbox is connected to the interior of the chamber (and to the ignition wire for each sample by feedthroughs. The electrical devices were connected to the kill switch (a switch to turn off the system

in case of emergency). Inside the chamber, the rotary stage with the samples was installed. Figure 4.7 shows a picture and a schematic of the cartridge.

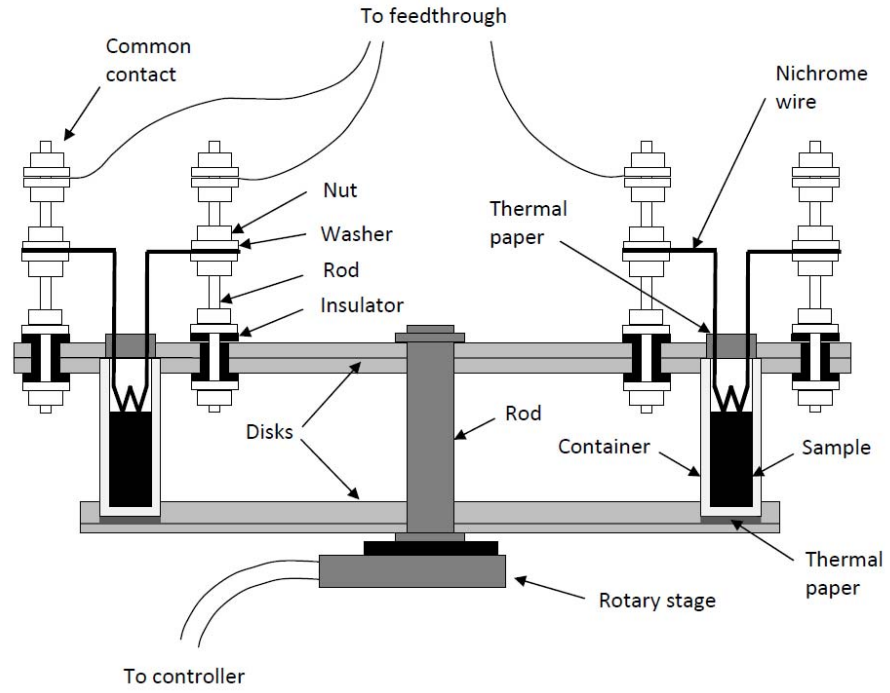


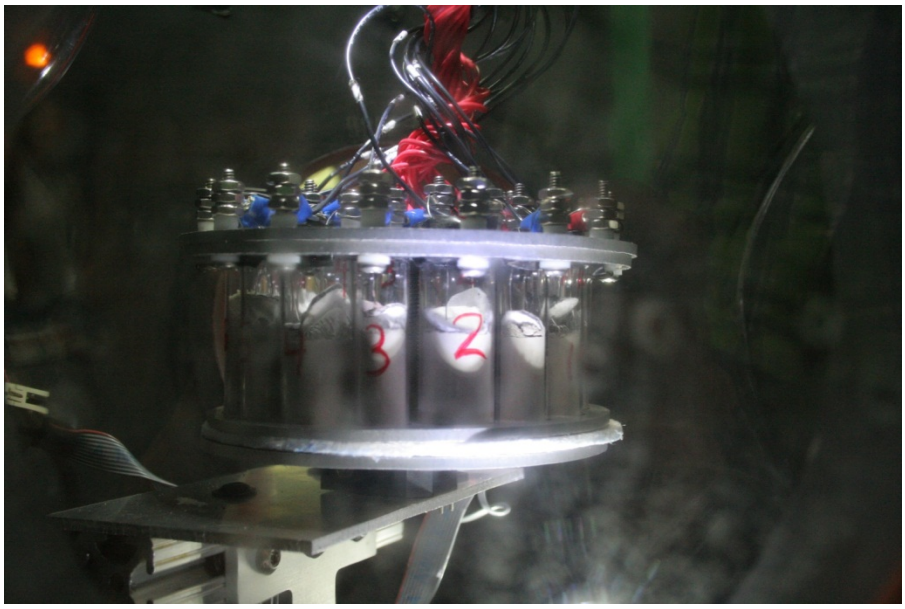


**Figure 4.7. Above: Schematic of cartridge and ignition system; below: cartridge with filled regolith/magnesium mixtures**

The tubes were numbered to ensure the position of the sample in front of the camera. The cartridge consists of four 1/16” aluminum plates. The two bottom plates are directly connected to the rotary stage. A layer of thermal paper (Fiberfrax) was installed between the two bottom plates to reduce the heat loss through the bottom plates. The top bottom plate and the two plates on top of the tubes have holes for the quartz tubes to fit in them. The top plate had a one millimeter reduced hole for the tube not to ‘fly’ once the microgravity period started. The top and bottom aluminum plates were connected through a ¼” steel rod to keep the alignment of the tubes and decrease the stress created on the tubes when rotating.

The microgravity rig showed to be successful. The experiment was performed twice (30 samples). Three different people worked inside the plane for each flight. Some of the results obtained will be presented in the next chapter.

# 5. EXPERIMENTAL RESULTS FOR THE COMBUSTION OF JSC-1A REGOLITH SIMULANT WITH MAGNESIUM ADDITIVE UNDER MICROGRAVITY CONDITIONS

After the experiments onboard the Zero G aircraft at Ellington Field were performed and the tubes collected from the microgravity rig, the analysis of the reacted samples started. This chapter will describe the results that involve velocity and visual considerations regarding the reaction of a mixture of 74% milled JSC-1A/26% magnesium metal, the reactants, the mixture preparation, and the analysis. Figure 5.1 shows some frames taken from the video recorded.

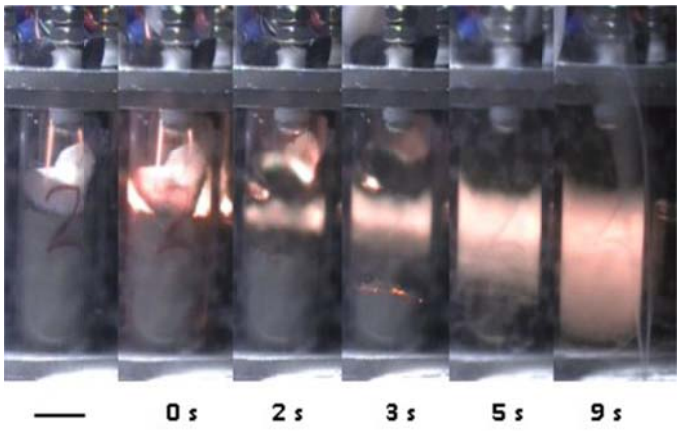


**Figure 5.1. Frames from reaction of JSC-1A/Mg mixtures under microgravity conditions**

## 5.1. Preparation of Mixtures

Due to the limited time of microgravity, the time of ignition was extremely important. Experience had shown that mixtures prepared with regolith milled using a planetary ball mill (Fritsch Pulverisette 7 Premium Line) was easier to ignite. For this reason, all the samples were made out of planetary ball milled powder (PBM) and magnesium powder (-325 mesh, 99.8%

pure, AlfaAesar). The regolith and the magnesium were mixed using the roller ball mill previously described for one hour inside a nalgene container with five burundum cylinders.

Once prepared, the quartz tubes were filled up with the mixture. Due to the fragility of the quartz tube, the mixture was compacted using just hand force to avoid breaking the tube. The ignition wire was introduced in the tube and located on top of the mixture. A piece of thermal paper was put on top of each sample to avoid any powder to come off the sample during the microgravity segments. The mass and the height of the compacted mixtures were recorded. Figure 5.2 shows a prepared sample previous to its installation in the rotary cartridge.

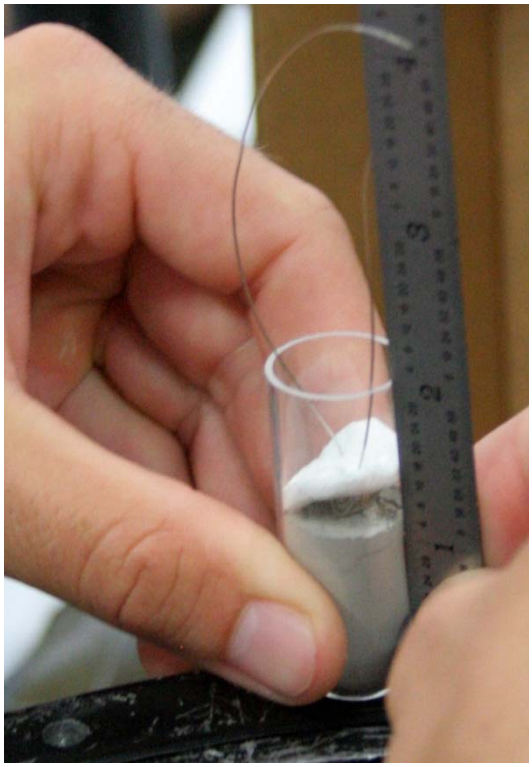

**Figure 5.2. Image of a mixture of 64% JSC-1A/26% magnesium inside a 20 mm OD with igniter and thermal paper**

The rotary stage with the samples was put inside the chamber the day before the flight in preparation for its installation inside the aircraft.

## 5.2. Velocity Measurements

The velocity was obtained with the help of the videos recorded and the sample heights measured. Figure 5.1 shows some frames recorded by the video camera (30 frames per second). The time since the initiation of the reaction until the finish of the propagation of the reaction is identifiable from the videos. The frame identified with the label 3s shows clearly an interface between the reacted area and the unreacted mixtures. After a conversion between the number of frame obtained and the camera velocity is made, the time in seconds can be obtained. The average velocity of the front is then the quotient between the height and the reaction time.

During the flights, when several zero gravity samples were obtained, the team decided to perform some experiments under increased gravity (1.5-1.8 g's). These experiments were reproduced on Earth under regular gravity conditions. Figure 5.3 shows the front velocity as a function of gravity condition.

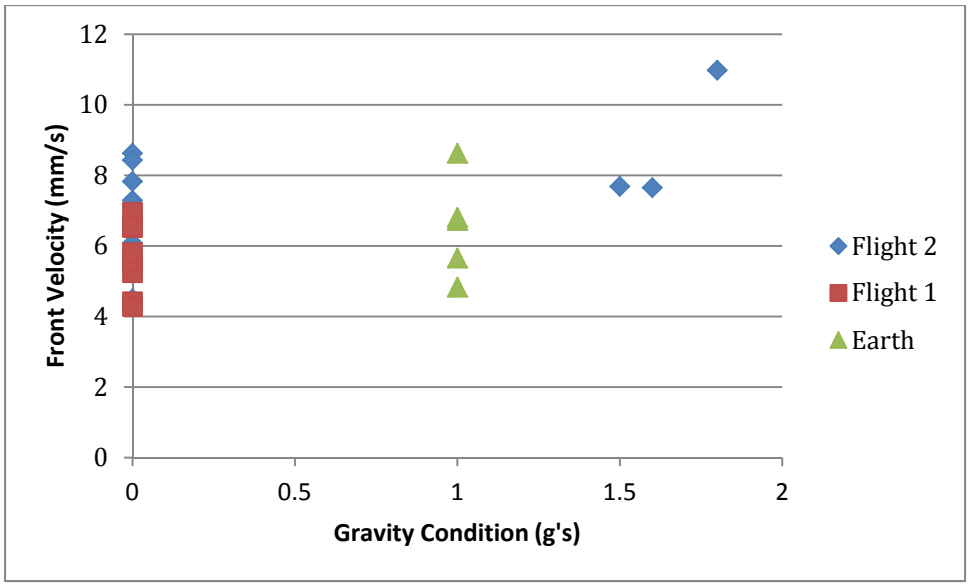


**Figure 5.3. Graph of front velocity against gravity condition**

To statistically asses the relationship between the gravity conditions and the velocity, an Analysis of Variance (ANOVA) analysis will be performed with a significance level of 0.05 ($\alpha$=0.05). Figure 5.4 shows the results for the ANOVA analysis, which illustrates that there is a difference in velocity as the gravity condition changes ($P < \alpha$). In order for the ANOVA analysis to be valid, the data must be normally distributed and each treatment must have equal variance. Figure 5.5 shows the normal probability plot, which allows to infer that the data follows a normal distribution and, thus complies with the normality condition necessary for the ANOVA analysis. Figure 5.6 shows the test for equal variances.

**One-way ANOVA: Velocity versus Gravity**

| Source | DF | SS | MS | F | P |
|---|---|---|---|---|---|
| Gravity | 4 | 22.83 | 5.71 | 3.00 | 0.045 |
| Error | 19 | 36.16 | 1.90 | | |
| Total | 23 | 59.00 | | | |

S = 1.380  R-Sq = 38.70%  R-Sq(adj) = 25.80%

**Figure 5.4. Analysis of variance for velocity versus gravity condition**

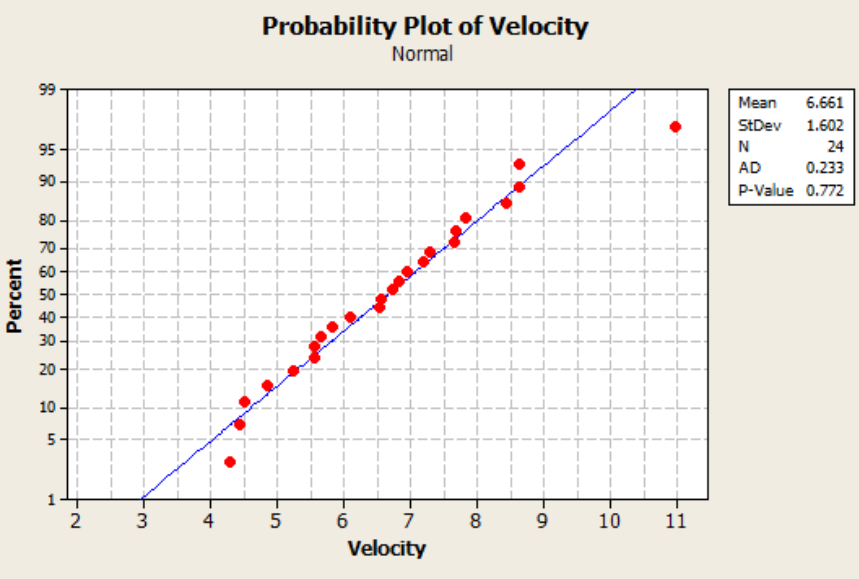


**Figure 5.5. Normal probability plot for velocity under microgravity**

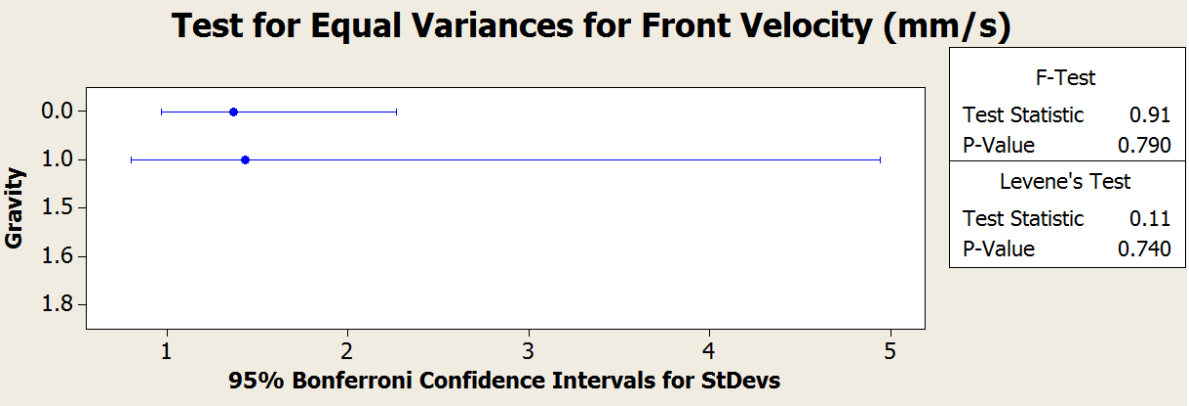


**Figure 5.6. Test for equal variances for front velocity versus gravity condition**

Figure 5.7 shows the velocities recorded for the two different tube inner diameters used (12 and 18 mm). The ANOVA analysis (Figure 5.8) illustrates the lack of significant difference for the front velocity for the two different tube diameters (P>α). Figure 5.9 shows the normal probability plot for the velocities recorded for the different tube diameters. Figure 5.10 shows the test for equal variances. The data set follows a normal behavior and equal variances so the ANOVA analysis is valid for this set of information.

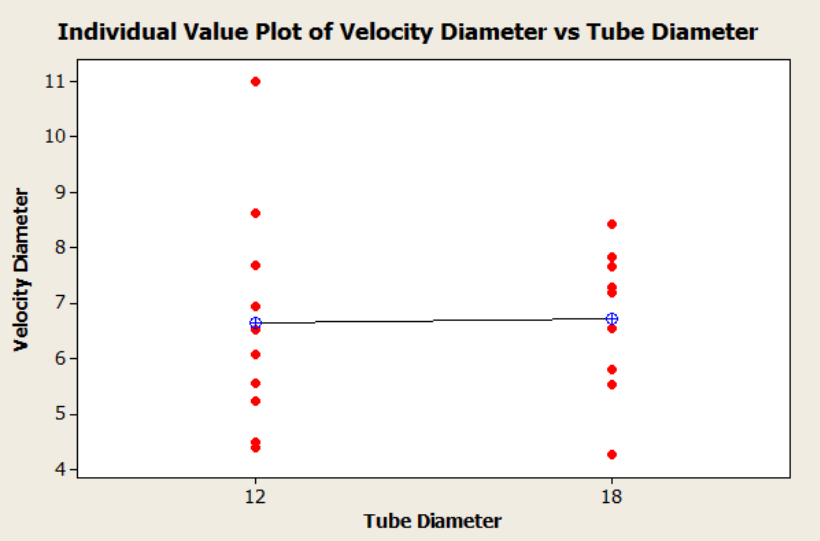


**Figure 5.7. Velocity versus inner diameter**

**One-way ANOVA: Velocity Diameter versus Tube Diameter**

| Source | DF | SS | MS | F | P |
|---|---|---|---|---|---|
| Tube Diameter | 1 | 0.03 | 0.03 | 0.01 | 0.927 |
| Error | 17 | 50.70 | 2.98 | | |
| Total | 18 | 50.73 | | | |

S = 1.727 R-Sq = 0.05% R-Sq(adj) = 0.00%

**Figure 5.8. Analysis of variance for the velocity with tube inner diameter as factor**

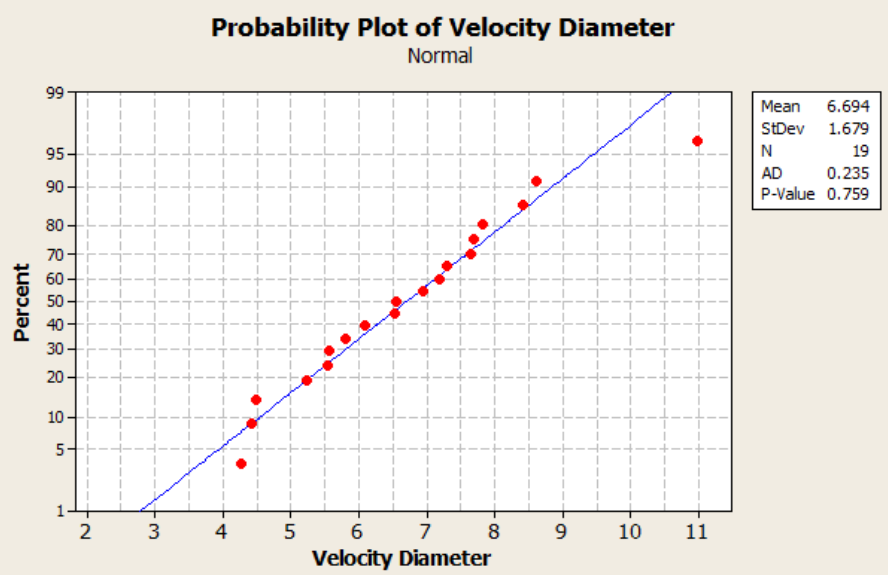


**Figure 5.9. Normal probability plot for the velocity for different tube diameters**

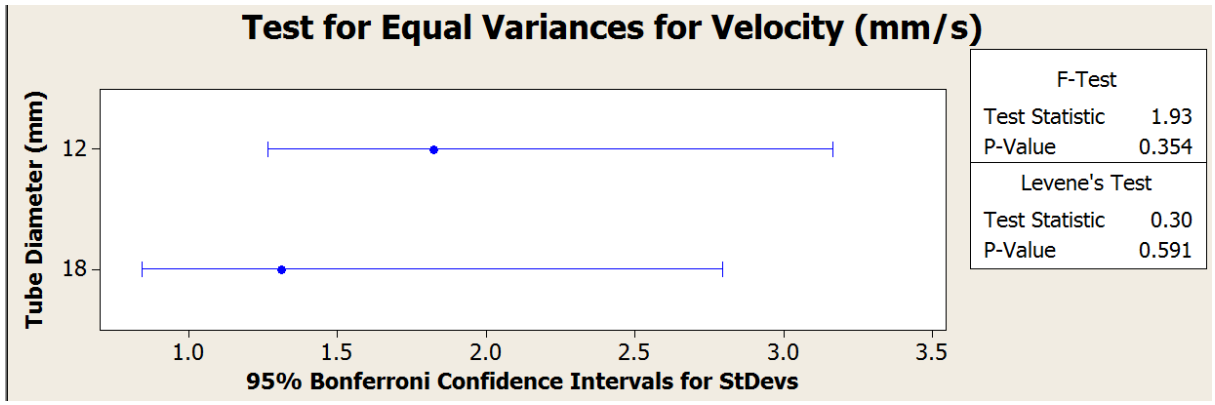


**Figure 5.10. Test for equal variances for velocity versus tube diameter**

## 5.3. Conclusions

The front velocity shows to be increasing as the gravity condition increases. Although this difference is statistically significant to a level of 0.05 (P=0.045, in the limit of the significance level), a greater number of experiments needs to be performed under increased gravity to improve the quality of the statistical analysis. The increase of velocity in the front is an expected response. When the system is subjected to a gravity field, the reactants are pulled down towards the center of the Earth and improve the contact between the particles before and during the reaction. During a microgravity period, this effect does not occur; during an increased gravity experiment, this effect is enhanced.

The front velocity does not show a significant difference for the two different tube diameters used. The P-value is much larger than the significance level ($P >> \alpha$) and allows inferring that the velocity is the same for both cases.

# 6. TEMPERATURE MEASUREMENTS FOR REGOLITH/MAGNESIUM MIXTURES FOR DIFFERENT PARTICLE SIZES

To better understand the effect of changing the particle size on the velocity, it is important to know one of the most important parameters of SHS (and of chemical kinetics): temperature. A series of experiments was designed to evaluate the effect of particle size on the velocity and temperature of the reactions. This chapter explains the preparation of the samples to be studied, the temperature measurements and the change in velocity and temperature as the particle size is changed.

## 6.1. Preparation of Samples

As previously done [41], mixtures containing 26% magnesium and 74 % JSC-1A were created. The magnesium powder was used as received from the manufacturer (-325 mesh, AlfaAesar). Four different types of milled JSC-1A were used: crushed powder using a roller ball mill (LabMill 8000) during 2, 3, and 4 hours, and crushed using a planetary ball mill PBM (Fritsch Pulverisette 7 Premium Line). The roller ball mill powder was crushed using an alumina jar and burundum cylinders as grinding media. Several pellets (1 inch diameter, 25 grams) of mixture were then produced using an axial hydraulic press (Carver); the force applied was 2 metric tons. Table 6.1 shows the difference in the median diameter as the milling time and method is changed. It is clear that the diameter decreases with milling time. Figure 6.1 shows one of the samples for this set of experiments.

**Table 6.1. Change in particle median diameter using different milling times and methods**

| **Powder** | Original JSC-1A | 2 hr | 3 hr | 4hr | PBM |
|---|---|---|---|---|---|
| **Median diameter (microns)** | 292.5058 | 73.68575 | 62.1655 | 50.27125 | 5.53 |

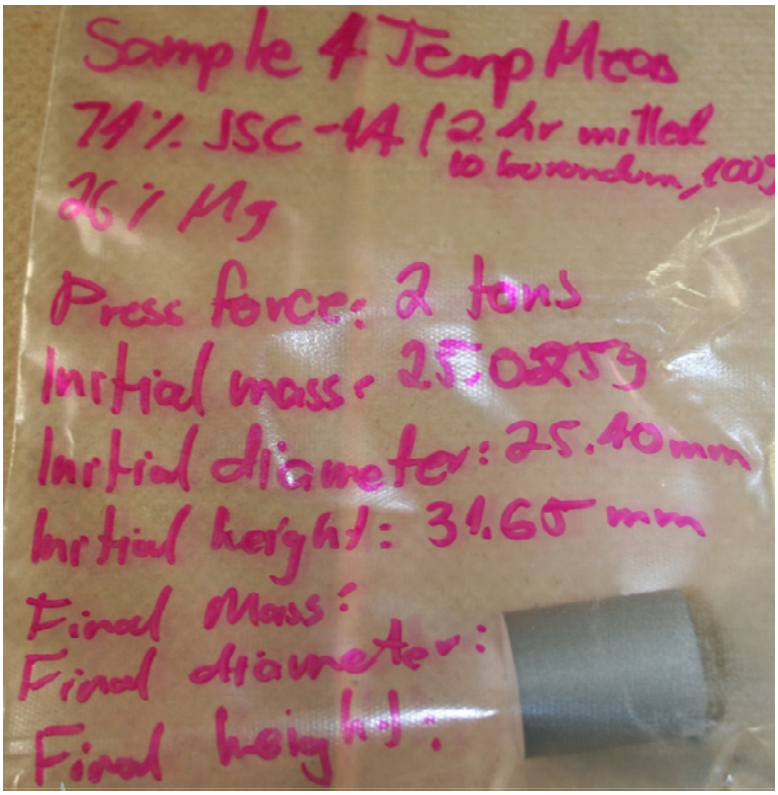


**Figure 6.1. Pressed pellet of JSC-1A/magnesium**

## 6.2. Experimental

Once the samples were made, a type K thermocouple (Chromel-Alumel) was introduced through a hole made in the sample (shown in Figure 6.2) to ensure that the thermocouple was as centered as possible inside the sample. The sample with the thermocouple was then put inside the combustion chamber and put in contact with the ignition wire (Nichrome) on top of

the sample. The thermocouple was connected via feedthrough to a portable data acquisition system (LabView) set to a sample rate of 6 Hz.

After the chamber was evacuated with argon gas, the ignition system was turned on and the sample burnt. The video was recorded using a commercial camcorder. Figure 6.2 shows a picture of a burnt sample after the thermocouple was removed. The pellets made with 2-hr and 3-hr milled powder did not ignite. The 4-hr powder and the planetary ball mill powder ignited, and the propagation of the reaction was stable. The results are explained in next section.

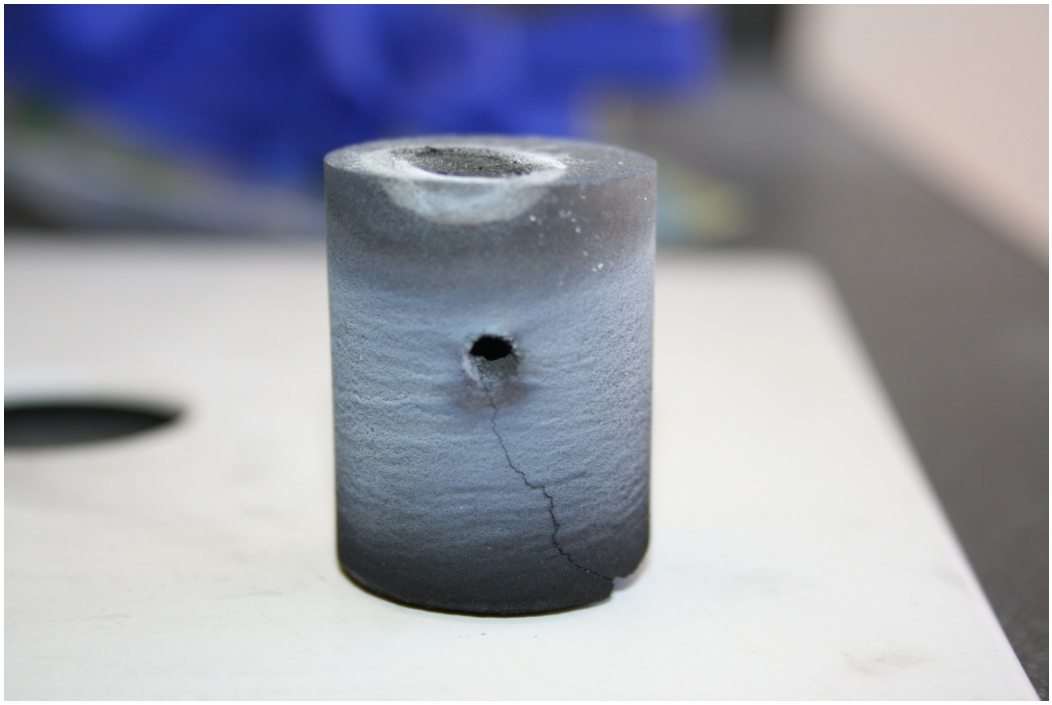

**Figure 6.2. Burnt pellet showing the thermocouple hole**

## 6.3. Results

The temperature measurements were exported to Microsoft Excel to analyze them. Figure 6.3 illustrates the temperature at the center of the sample (PBM JSC-1A) as a function of

time. The maximum temperature is shortly reached after the reaction starts to propagate close to ambient temperature. After the maximum temperature is reached, the sample is let to cool down.

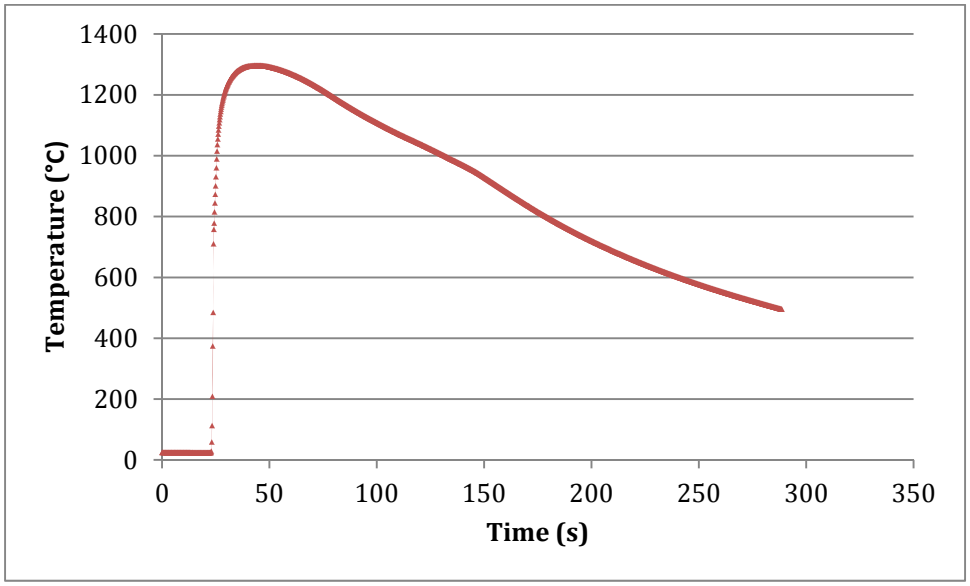


**Figure 6.3. Profile of temperature at the center of the sample during combustion**

The front velocity was calculated following the same procedure as with the microgravity samples. The frames were analyzed to obtain the moment at which combustion started and finished. This frame difference was then converted to time. Figure 6.4 shows the front velocity as a function of temperature. An increase in the velocity is observed as the temperature increases.

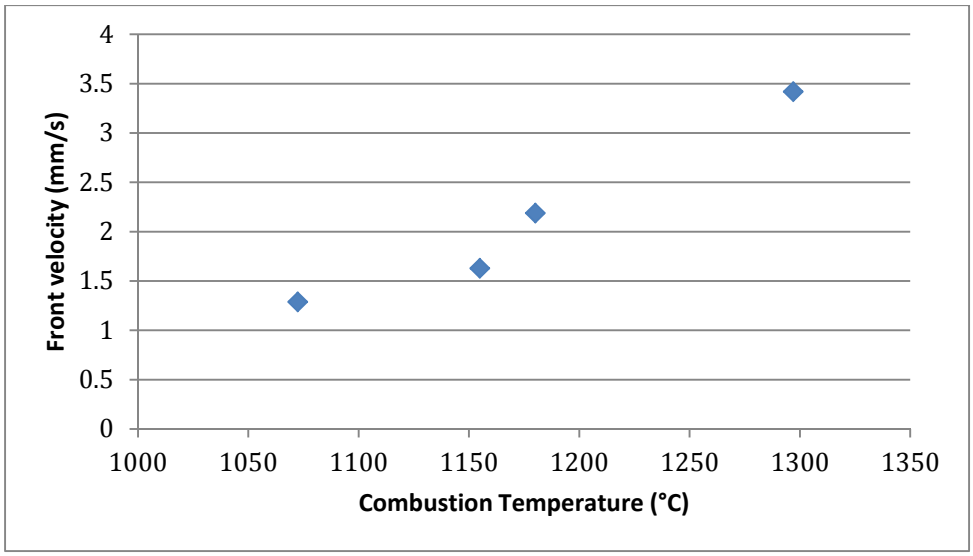


**Figure 6.4. Front velocity as a variation of temperature**

Figure 6.5 portrays the temperature change with the different particle sizes used, and Figure 6.6 shows the analysis of variance for these data. Due to the limited number of data points, the significance level was selected as α=0.1. Figure 6.7 shows the normality of the data points; Figure 6.8 shows the test for equal variances, and thus the validity of the ANOVA analysis.

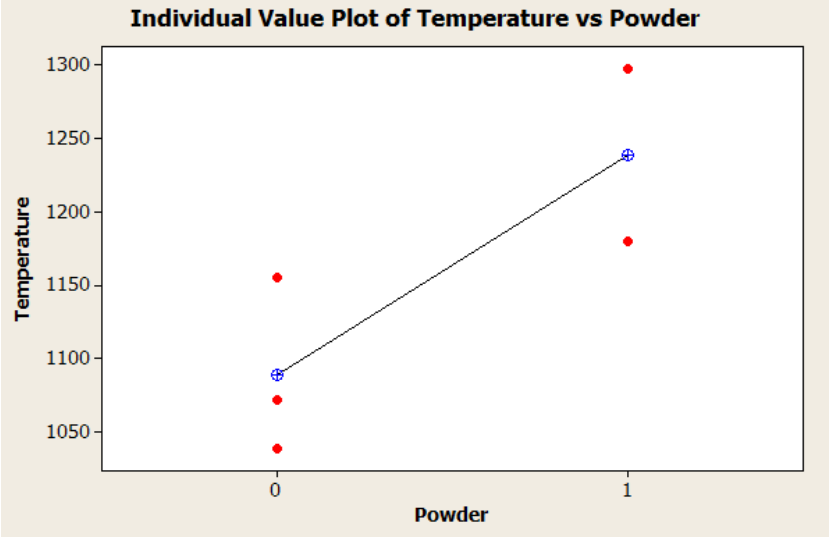


**Figure 6.5. Combustion temperature for 4-hr milled powder (0) and PBM (1)**

**One-way ANOVA: Maximum Temperature (Celsius)_1 versus Powder Temp**

| Source | DF | SS | MS | F | P |
|---|---|---|---|---|---|
| Powder Temp | 1 | 26882 | 26882 | 5.79 | 0.095 |
| Error | 3 | 13935 | 4645 | | |

**Figure 6.6. Analysis of variance for temperature versus powder**

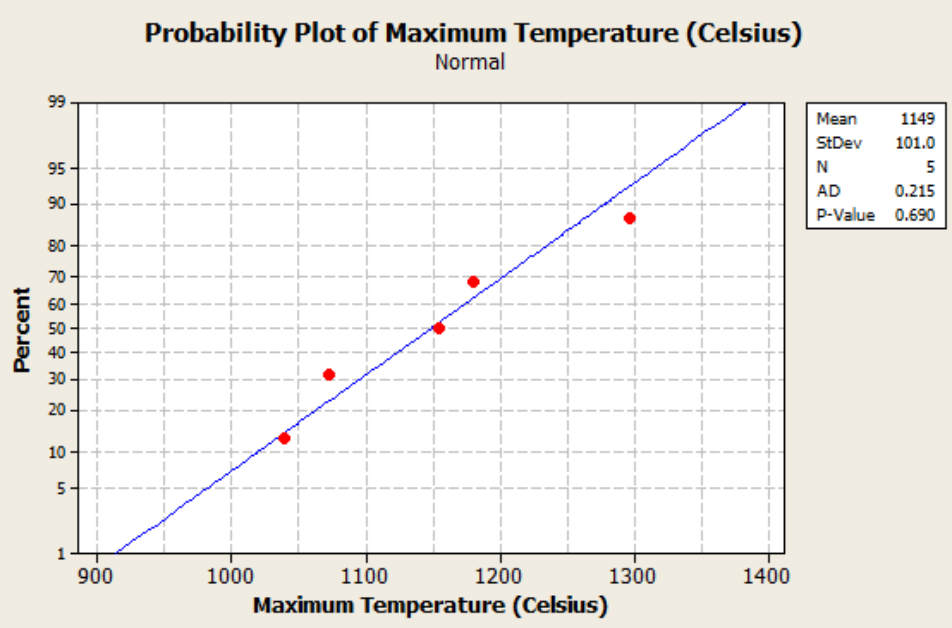


**Figure 6.7. Normal probability plot for temperature measurements**

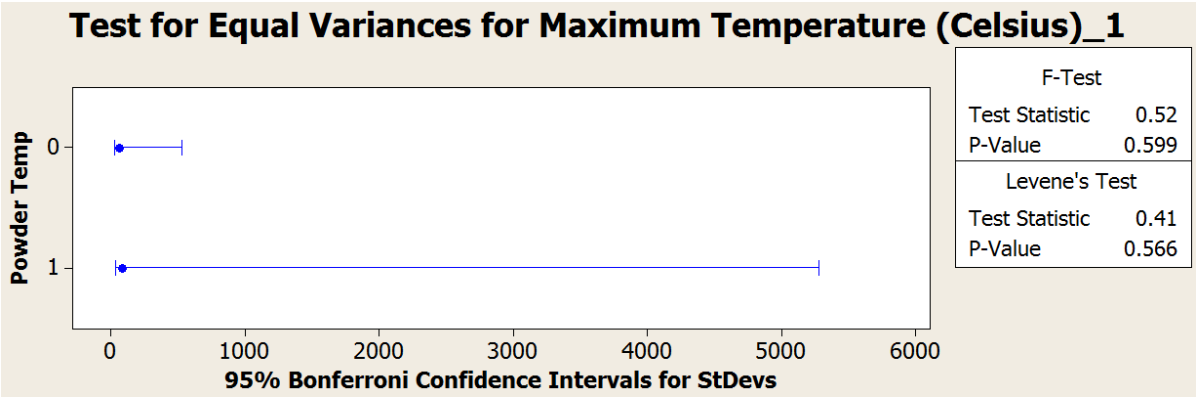


**Figure 6.8. Test for equal variances for maximum temperature versus particle size**

Figure 6.9, 6.10, 6.11, and 6.12 show the velocity measurements changes with the different powders, the ANOVA analysis, the normal probability plot, and the test for equal variances.

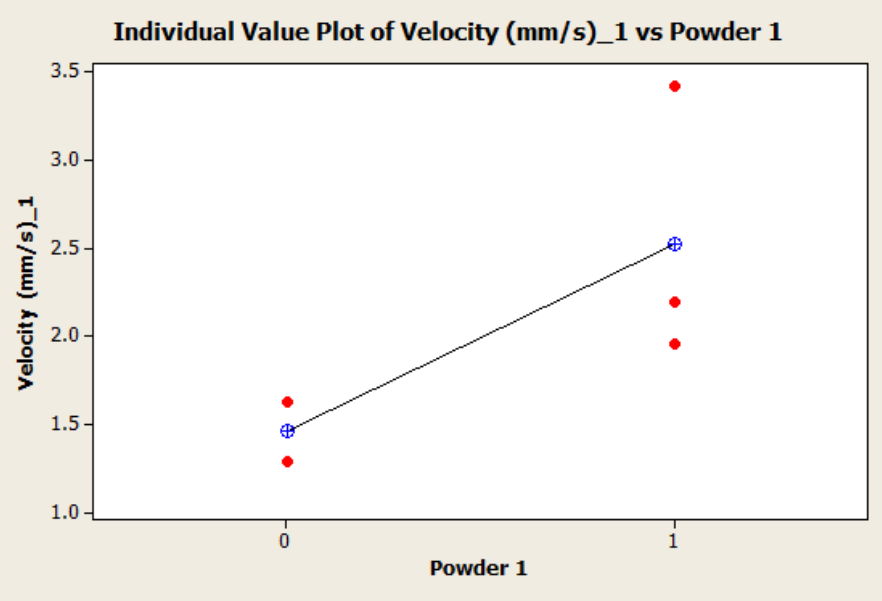


**Figure 6.9. Velocity measurement for 4 hr milled powder (shown as 0) and PBM (shown as 1)**

**One-way ANOVA: Velocity (mm/s)_1 versus C11**

| Source | DF | SS | MS | F | P |
|---|---|---|---|---|---|
| C11 | 1 | 1.357 | 1.357 | 3.16 | 0.174 |
| Error | 3 | 1.290 | 0.430 | | |
| Total | 4 | 2.648 | | | |

**Figure 6.10. Analysis of variance for velocity measurements versus powder type**

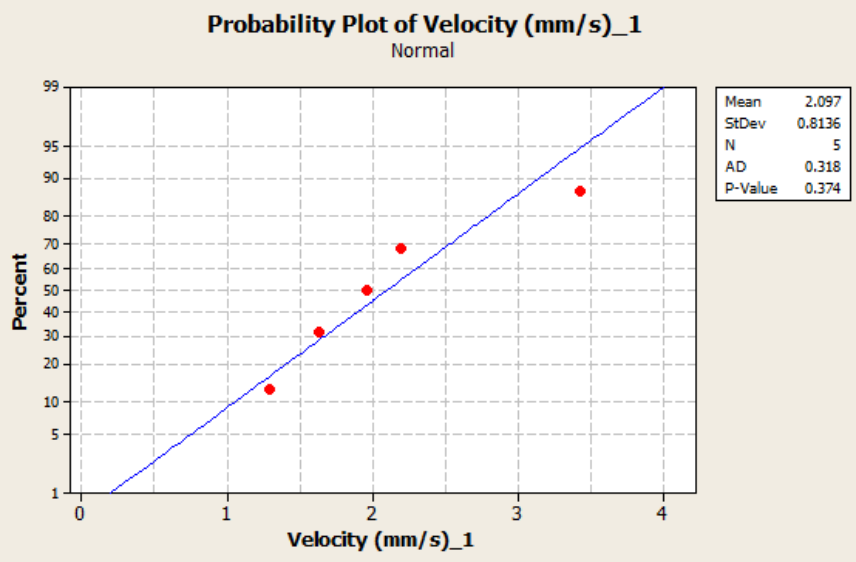


**Figure 6.11. Normal probability plot for velocity measurements**

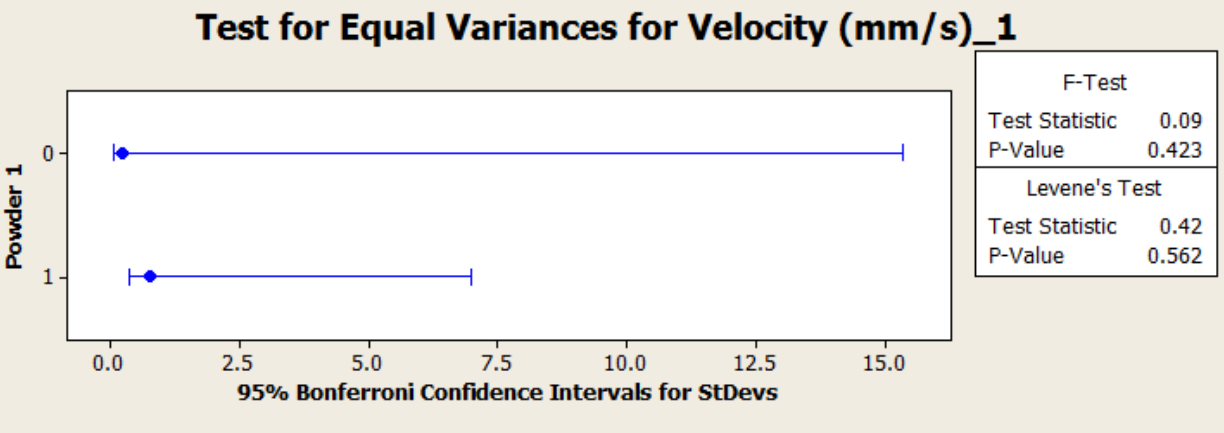


**Figure 6.12. Test for equal variances for velocity versus powder type**

## 6.4. Conclusions

Figure 6.4 shows an expected trend between velocity and temperature. According to chemical kinetics and to the Arrhenius equation, the reaction rate increases with increasing temperature. The increase in the reaction rate translates into a greater front velocity, a behavior clearly shown in Figure 6.4. From the analyses of variance presented in this chapter

(and using a significance level of 0.1), one can conclude that combustion temperature increases by decreasing the particle size, but not that velocity increases by the particle size.

These findings allow to conclude that for a higher temperature to be reached (which is generally desired to be higher to ensure the propagation of the reaction), a smaller particle size is necessary. The increase in temperature then creates a higher combustion front velocity.

# 7. COMBUSTION OF JSC-1A/ALUMINUM MIXTURES

The combustion of JSC-1AF (the finer fraction of JSC-1A) was performed at Virginia Tech [20] [21]. These experiments were performed under a regime between the simultaneous combustion mode and SHS. Simultaneous combustion is one of the modes of combustion synthesis (along with SHS) and consists in heating up the whole volume of the sample to study. What Faierson et al. did was to put a mixture of JSC-1AF and aluminum inside a silica crucible. Figure 6.1a shows a Nichrome wire going in and out of the sample. Inside, the wire makes loops so most of the sample is heated up. Figure 6.1b shows the reacted sample.

a.

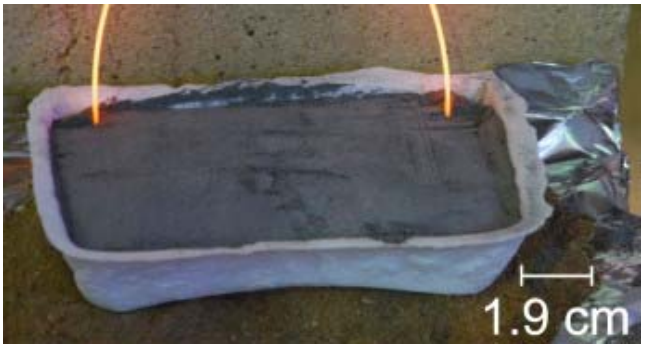


b.


**Figure 6.11. a. Mixture of JSC-1AF and magnesium inside a silica crucible; b. combusted sample [21]**

The cSETR ISRU team intends to repeat these experiments under a standard SHS mode; this is to start the combustion at the top of the sample with an ignition wire. The ISRU team is also developing a method to generate aluminum powder from aluminum foil using the Fritsch planetary ball mill obtaining promising results. Aluminum foil is a common material in space missions. If aluminum foil can be converted to powder, no extra aluminum should be brought from the Earth to the Moon, and this would greatly reduce the energy consumption and cost of this method.

## 7.1. Experimental

Two different samples were prepared for this set of experiments: pellet and loose powder. The pellets were made following the same procedure than the JSC-1A/magnesium pellets. Following the results obtained in Chapter 3, a mixture of 77% JSC-1A/23% aluminum was made. The aluminum used had a nanometric diameter (0.07 microns, AlfaAesar) to improve the combustion; also, the regolith simulant with the smaller diameter was selected (planetary ball mill, refer to Table 6.1) was used. The two powders were mixed using a roller ball mill (LabMill 8000) during one hour using five burundum pieces inside a Nalgene container.

The pellets were made of 25 grams of mixture under a force of 2 metric tons using an axial hydraulic press (Carver). The loose powder was put inside an 18mm ID tube (similar to the microgravity experiments). The pellet and the loose powder were put inside the combustion chamber and a tungsten wire was used as the ignition system. The tungsten wire was carrying a current of 17.2 A and a voltage of 24.0 volts (the maximum power allowed by the power source for this wire) and no ignition was observed for any of the samples.

To increase the temperature at the ignition point, a pyrotechnic mixture (stoichiometric mixture of 69% titanium and 31% boron) was put on top of the pellet to make a booster explosion. Figure 7.1 shows an unreacted pellet; the grey part is the JSC-1A/aluminum, the brown region is the booster mixture. The sample was then covered with a ceramic insulator (Fiberfrax) to minimize the heat transfer to the surroundings. Ignition of the sample was the same as described for the mixtures without booster mixture. The reaction of the titanium and boron (adiabatic temperature according to thermodynamic calculations is 3200 K) showed successful and started relatively easy, but did not propagate to the aluminum region. Figure 7.2 shows the reacted Ti+B mixture. The top shows the reacted boron and titanium; the white spots shown are pieces of the ceramic insulation. It is seen that the aluminum region did not react.

**Figure 7.1. Unreacted pellet of JSC-1A/aluminum with a titanium and boron booster mixture**

**Figure 7.2. Ignited pellet, the titanium and boron products are shown at the top of the picture; at the bottom, the unreacted aluminum and JSC-1A mixture is shown**

## 7.2. Conclusions

The SHS combustion of aluminum and JSC-1A mixtures showed to be unsuccessful. The failure to ignite the samples may be due to the low temperature reached during the ignition process. During the experiments performed at Virginia Tech, the whole sample was heated up, and had an increased temperature when the ignition started. The standard SHS process did not heat up the aluminum/JSC-1A mixtures to the appropriate temperature and, thus, did not ignite. The method follow at Virginia Tech is out of the scope of the cSETR ISRU team, and thus is not going to be continued at the moment.

# 8. FUTURE WORK

In order to better understand the reaction between JSC-1A and magnesium, more experimental studies are needed. The cSETR ISRU team will continue to look for ways to exploit the lunar resources for the production of lunar goods *in situ*. At the moment the production of structural materials and the extraction of volatiles from lunar regolith are ongoing projects at the Center for Space Exploration Technology Research.

## 8.1. SHS Compaction

The main goal of the cSETR ISRU team is to build structural materials on the Moon. The samples herein presented do not show high strength, and do not seem resistant enough for structural use. Currently, the cSETR ISRU team is studying the method called SHS Compaction. Typically, the SHS products are sintered but show a high porosity. SHS compaction consists on applying a mechanical load while the reaction materials are still hot. The application of this load allows for the densification and strengthening of the products. SHS compaction has been studied and it has been proven technologically feasible [46] [47] [48] [49] [50] [51] [52] [53] [54] [55] [56] [57] [58].

There are two main types of compaction schemes: dynamic and quasi-isostatic pressing. In dynamic pressing, the pressure is induced by a mechanical shockwave produced by an explosion or by the impact of an object. In the quasi-isostatic pressing scheme, the pressure is applied on a die press and is transferred to the combusted sample through a pressure-transmitting medium (PTM). The PTM redistributes the loads similarly to isostatic pressing. The PTM is made of a friable compound. Figure 8.1 shows an illustration of a SHS-quasi-isostatic pressing apparatus.

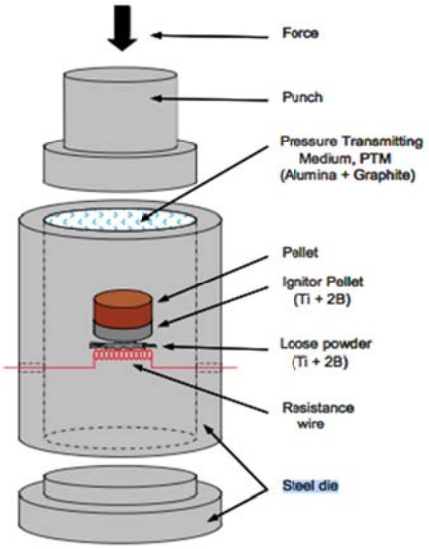


**Figure 8.1. Quasi-isostatic-SHS compaction apparatus [6]**

No studies involving SHS compaction of regolith/metal additives have been performed to date. In terms of ISRU, the best compaction option is quasi-isostatic pressing to avoid the necessity of bringing explosives to the mission site. Currently, the cSETR ISRU team is developing a SHS-quasi-isostatic pressing device to assess the feasibility of producing sufficiently dense and strong materials for construction applications on the Moon.

# BIBLIOGRAPHY


[1] A. G. Merzhanov and I. P. Borovinskaya, "Self-Propagated High-Temperature Synthesis of Refractory Inorganic Compounds," *Doklady Akademii Nauk,* pp. 366-369, 1972.

[2] E. I. Maksimov, A. G. Merzhanov and V. M. Shkiro, "Gasless Compositions as a Simple Model for the Combustion of Nonvolatile Condensed Systems," *Fizika Goreniya i Vzryva,* pp. 24-30, 1965.

[3] A. Merzhanov and I. Borovinskaya, "Historical Retrospective of SHS: An Autoreview," *International Journal of Self-Propagating High-Temperature Synthesis,* vol. 17, no. 4, pp. 242-265, 2008.

[4] J. J. Moore and H. Feng, "Combustion Synthesis of Advanced Materials: Part I. Reaction Parameters," *Progress in Materials Science,* vol. 39, pp. 243-273, 1995.

[5] J. J. Moore and H. Feng, "Combustion Synthesis of Advanced Materials: Part II. Classification, Applications and Modeling," *Progress in Materials Science,* vol. 39, pp. 275-316, 1995.

[6] M. Martínez Pacheco, "Self-sustained High-temperature Reactions: Initiation, propagation and synthesis," N/A, The Hague.

[7] A. Merzhanov, "Problems of Combustion in Chemical Technology and in Metallurgy,"

*Russian Chemical Reviews,* vol. 45, no. 5, pp. 409-420, 1976.

[8] J. F. Crider, "Self-Propagating High Temperature Synthesis - A Soviet Method for Producing Ceramic Materiala," US Army Foreign Science and Technology Center, [Online]. Available: http://www.ism.ac.ru/handbook/84crid.htm. [Accessed 28 November 2011].

[9] G. A. Landis, "Materials Refining on the Moon," *Acta Astronautica,* vol. 60, no. 10-11, pp. 906-915, 2007.

[10] G. Corrias, R. Licheri, R. Orru and G. Cao, "Self-propagating High-Temperature Reactions for the Fabrication of Lunar and Martian Physical Assets," *Acta Astronautica,* pp. In Press, Corrected Proof, 2011.

[11] C. C. Allen, J. C. Graf and D. S. McKay, "Sintering Bricks on the Moon," in *Engineering, Construction and Operations in Space IV*, Albuquerque, 1994.

[12] L. A. Taylor and T. T. Meek, "Microwave Sintering of Lunar Soil: Properties, Theory, and Practice," *Journal of Aerospace Engineering,* vol. 18, no. 3, pp. 188-196, 2005.

[13] R. Balasubramaniam, R. Wegeng, S. Gokoglu, N. Suzuki and K. Sacksteder, "Analysis of Solar-Heated Thermal Wadis to Support Extended-Duration Lunar Exploration," in *47th AIAA Aerospace Sciences Meeting Including The New Horizons Forum and Aerospace Exposition*, Orlando, 2009.

114] T. T. Pham and M. S. El-Genk, "Dose estimates in a lunar shelter with regolith shielding," *Acta Astronautica,* vol. 64, no. 7-8, pp. 697-713, 2009.

[15] R. Balasubramaniam, S. Gokoglu and U. Hegde, "The Reduction of Lunar Regolitlh by Carbothermal Processing Using Methane," *International Journal of Mineral Processing,* vol. 96, no. 1-4, pp. 54-61, 2010.

[16] R. J. Gustafson, B. C. White and M. J. Fidler, "2010 Field Demonstration of the Solar Carbothermal Regolith Reduction Process to Produce Oxygen," in *49th AIAA Aerospace Sciences Meeting Including the New Horizons Forum and Aerospace Exposition*, Orlando, 2011.

[17] Y. Zhao and F. Shadman, "Reduction of Ilmenite with Hydrogen," *Industrial and Engineering Chemistry Research,* vol. 30, pp. 2080-2087, 1991.

[18] Y. Zhao and F. Shadman, "Production of Oxygen from Lunar Ilmenite," The University of Arizona Press, Tucson, 1991.

[19] K. S. Martirosyan and D. Luss, "COMBUSTION SYNTHESIS OF CERAMIC COMPOSITES FROM LUNAR SOIL SIMULANT," in *Lunar and Planetary Science XXXVII*, 2006.

[20] E. J. Faierson, "Influences of Reaction Parameters on the Product of a Geothermite Reaction: A Multi-Component Oxidation-Reduction Reaction Study," 2009. [Online]. Available: http://scholar.lib.vt.edu/theses/available/etd-05072009-094913/unrestricted/FaiersonMSthesis.pdf. [Accessed 25 November 2011].

[21] E. J. Faierson, K. V. Logan, B. K. Stewart and M. P. Hunt, "Demonstration of Concept for Fabrication of Lunar Physical Assets Utilizing Lunar Regolith Simulant and a Geothermite

Reaction," *Acta Astronautica,* vol. 67, no. 1-2, pp. 38-45, 2010.

[22] C. Ray, S. Reis, S. Sen and J. O'Dell, "JSC-1A Lunar Soil Simulant: Characterization, Glass Formation, and Selected Glass Properties," *Journal of Non-Crystalline Solids,* vol. 356, no. 44-49, pp. 2369-2374, 2010.

[23] C. Schrader, D. Rickmann, C. McLemore, J. Fikes, S. Wilson, D. Stoeser, A. Butcher and P. Botha, "Extant and Extinct Lunar Regolith Simulants: Modal Analyses of NU-LHT-1M and -2M, OB-1, JSC-1, JSC-1A and -1AF, FJS-1, and MLS-1," 2008. [Online]. Available: http://isru.msfc.nasa.gov/lib/Documents/PDF%20Files/conf_pres_PTMSS2008_Schrader.pdf. [Accessed 26 October 2011].

[24] E. Hill, M. Mellin, B. Deane, Y. Liu and L. and Taylor, "Apollo sample 70051 and high and low-Ti soil simulants MLS-1A and JSC-1A: Implications for future lunar exploration," *Journal of Geophysical Research,* vol. 112, p. E02006, 2007.

[25] ORBITEC, "Characterization Summary of JSC-1AF Lunar Mare Regolith Simulant," 12 December 2006. [Online]. Available: http://www.orbitec.com/store/JSC-1AF_Characterization.pdf. [Accessed 26 October 2011].

[26] C. K. Gupta, Chemical Metallurgy Principles and Practice, Weinheim: Wiley-VCH, 2003.

[27] A. Shiryaev, "Thermodynamics of SHS Processes: Advanced Approach," *International Journal of Self-Propagating High-Temperature Synthesis,* vol. 4, no. 4, pp. 351-362, 1995.

[28] University of Cambridge, "The Ellingham Diagram," 2010. [Online]. Available:

http://www.doitpoms.ac.uk/tlplib/ellingham_diagrams/ellingham.php. [Accessed 25 October 2011].

[29] S. Saxena, "Systemization and Estimation of Thermochemical Data on Silicates," in *Modelling in Aquatic Chemistry*, I. Grenthe and I. Puigdomenech, Eds., Paris, OECD Publ., 1997, pp. 289-323.

[30] CRC Handbook of Chemistry and Physics, *Periodic Table Advanced,* Boca Raton: BarCharts, Inc., 2000-2001.

[31] M. W. Chase, "NIST-JANAF Thermochemical Tables," Journal of Physical and Chemical Reference Data, Gaithersburg, 1998.

[32] OUTOTEC, "Calculation modules," OUTOTEC, [Online]. Available: http://www.outotec.com/pages/Page____35373.aspx?epslanguage=EN. [Accessed 6 November 2011].

[33] OUTOTEC, "HSC Thermochemical Database," OUTOTEC, 2011. [Online]. Available: http://www.outotec.com/pages/Page.aspx?id=35541&epslanguage=EN. [Accessed 6 November 2011].

[34] G. A. Landis, "Calcium Reduction as a Process for Oxygen Production from Lunar Regolith," in *49th AIAA Aerospace Sciences Meeting including the New Horizons Forum and Aerospace Exposition*, Orlando, 2011.

[35] R. O. Suzuki, "Calciothermic Reduction of TiO2 and in situ electrolysis of CaO in the Molten

CaCl2," *Journal of Physics and Chemistry of Solids,* vol. 66, pp. 461-465, 2005.

[36] A. Merzhanov, A. Rogachev, E. Rumanov, V. Sanin, A. Sytchev, V. Shcherbakov and V. Yukhvid, "Influence of Microgravity on Slef-Propagating High-Temperature Synthesis of Refractory Inorganic Compounds," *Cosmic Research,* vol. 39, no. 2, pp. 210-223, 2001.

[37] A. G. Merzhanov, "SHS Processes in Microgravity Activities: First Experiments in Space," *Advanced Space Research,* vol. 29, no. 4, pp. 487-495, 2002.

[38] E. Medda, R. Orru, G. Cao, J. Fry, J. Y. Guigne and M. Zell, "Effects of Microgravity on High-Temperature Self-Propagating Reactions," in *Proceedings of the First International Symposium of the Microgravity Research and Aplications in Physical Sciences and Biotechnology*, Sorrento, 2000.

[39] Y. A. Cengel and J. M. Cimbala, "Property Tables and Charts (English Units)," in *Fluid Mechanics: Fundamentals and Applications*, New York, McGraw-Hill, 2006, pp. 903-915.

[40] MSNBC, "Zero-gravity flights go mainstream," MSNBC, 16 September 2004. [Online]. Available: http://www.msnbc.msn.com/id/5992077/ns/technology_and_science-space/t/zero-gravity-flights-go-mainstream/#.Tr3peqhTdAM. [Accessed 11 November 2011].

[41] C. White, F. Alvarez and E. Shafirovich, "Combustible Mixtures of Lunar Regolith with Metals: Thermodynamic Analysis and Combustion Experiments," *Journal of Thermophysics and Heat Transfer,* vol. 25, no. 4, pp. 620-625, 2011.

[42] Aircraft Engineering Branch, *Preparation of Stress Analysis Reports,* Houston: National Aeronautics and Space Administration, 2009.

[43] Aircraft Operations Division, *AOD 33896 Rev D Test Equipment Data Package Requirement and Guidelines NASA JSC RGO,* Houston: National Aeronautics and Space Administration, 2010.

[44] Aircraft Operations Division, *AOD 33897 Rev D Experiment Design Requirements and Guidelines for Microgravity Research,* Houston: National Aeronautics and Space Administration, 2010.

[45] Zero Gravity Corporation, *Interface Control Document Boeing 727-200 ZGC-ICD Revision A2,* Vienna, VA: Zero G Corporation, 2008.

[46] G. A. Adadurov, I. P. Borovinskaya, Y. A. Gordopolov and A. G. Merzhanov, Technological Fundamentals of SHS Compacting, vol. 63, Chernogolovka: Inzhenerno-Fizicheskii Zhurnal, 1992, pp. 538-546.

[47] A. P. Amosov, V. P. Radchenko, A. F. Fedotov and M. Ermolenko, "Effect of Shell Dimensions on Compaction and Shape Change During SHS-Pressing," *Powder Metallurgy and Metal Ceramics,* pp. 229-235, 2004.

[48] A. F. Fedotov, "Mechanism of Compacting and Forming in the Course of SHS Compaction with a Granular Shell," *Russian Journal of Non-Ferrous Metals,* pp. 290-296, 2008.

[49] I. Song, L. Wang and M. Wixom, "Self-Propagating High Temperature Synthesis and

Dynamic Compaction of Titanium Diboride/Titanium Carbide Composites," *Journal of Materials Sciences,* pp. 2611-2617, 2000.

[50] V. I. Yukhvid, "Modifications of SHS Processes," *Pure and Applied Chemistry,* vol. 64, no. 7, pp. 977-988, 1992.

[51] Y. Miyamoto and M. Koizumi, "High-Pressure Self-Combustion Sintering for Ceramics," *Journal of the American Ceramic Society,* vol. 67, no. 11, pp. C-224-C-225, 1984.

[52] M. Kholghy, S. Kharatyan and H. Edris, "SHS/PHIP of Ceramic Composites Using Ilmenite Concentrate," *Journal of Alloys and Compounds,* vol. 502, no. 2, pp. 491-494, 2010.

[53] I. Borovinskaya, V. Ratnikov and G. Vishnyakova, "Some Chemical Aspects of Power SHS Compacting," *Journal of Engineering Physics and Thermophysics,* vol. 63, no. 5, pp. 1059-1064, 1992.

[54] K. Epishin, A. Pityulin and A. Merzhanov, "Compaction of Materials Forming in Self-Propagating High-Temperature Synthesis," *Powder Metallurgy and Metal Ceramics,* vol. 31, no. 6, pp. 472-476, 1992.

[55] R. Raman, S. Rele, S. Poland, L. J. M. M. and A. and Niiler, "The One-Step Synthesis of Titanium-Carbide Tiles JOM, Vol. 47, 1995, pp. 23-25.," *JOM,* vol. 47, pp. 23-25, 1995.

[56] E. Olevsky, E. Strutt and M. Meyers, "Combustion Synthesis and Quasi-Isostatic Densification of Powder Cermets," *Journal of Materials Processing Technology,* vol. 121, pp. 157-166, 2002.

[57] Q. Xu, X. Zhang, J. Han, X. He and V. Kvanin, "Combustion Synthesis and Densification of Titanium Diboride–Copper Matrix Composite," *Materials Letters,* vol. 57, pp. 4339-4444, 2003.

[58] M. Martinez Pacheco, R. Bouma and L. Katgerman, "Combustion Synthesis of TiB2-based Cermets: Modeling and Experimental Results," *Applied Physics A,* vol. 90, pp. 159-163, 2008.

**APPENDIX A**

# Test Equipment Data Package

# TEST EQUIPMENT DATA PACKAGE (TEDP)

## NASA Reduced Gravity Flight Program for Minority Serving Institutions and Community Colleges

The Effect of Gravity on the Production of

Structural Materials from Lunar Regolith

**June 5th, 2011**

**Proposal # 2011-25330**


**The University of Texas at El Paso**
**Center for Space Exploration Technology Research (cSETR)**
**Department of Mechanical Engineering**
**500 West University Ave.**
**El Paso, Texas 79968-0521**

| | | | |
|---|---|---|---|
| Team Contact: | White, Christopher | cwhite2@miners.utep.edu | (915) 261-9836 |
| NASA Mentor: | Jones, Michelle | michelle.jones@nasa.gov | (281) 244-0066 |
| Faculty Advisor: | Shafirovich, Evgeny | eshafirovich2@utep.edu | (915) 747-6465 |

**Team Members:**

| | | |
|---|---|---|
| White, Christopher | Flyer/Graduate/Mechanical Engineering | cwhite2@miners.utep.edu |
| Alvarez, Francisco | Flyer/Graduate/Mechanical Engineering | falvarez@miners.utep.edu |
| Davis, Colin J. | Flyer/Senior/Mechanical Engineering | cjdavis@miners.utep.edu |
| Alvillar, Alan | Flyer/Junior/Mechanical Engineering | aalvillar@miners.utep.edu |
| Delgado, Armando | Flyer/Graduate/Mechanical Engineering | adelgado12@miners.utep.edu |

# 2.0. CHANGE PAGE

| Document Version | Date | Process Owner | Description |
|---|---|---|---|
| Version 1 | May 4th, 2011 | Francisco Alvarez, (915) 525-6708 | Initial Release |
| Version 2 | May 20th, 2011 | Francisco Alvarez, (915) 525-6708 | Updated team roster and Flight Manifest<br>Updated Allowables Table (Table A.3.3)<br>Updated Margins of Safety Tables (Tables A.5, A.6, A.7 and A.8)<br>Corrected Equations and Updated Figures in Section A.4 |
| Version 3 | May 27th, 2011 | Francisco Alvarez, (915) 525-6708 | Experiments with aluminum powder were discarded<br>Changed pressure relief valve (5 psig to 10 psig) and testing pressure (20 psig)<br>Corrected equations in Section A.4.1<br>Corrected Tables A.1 and A.5<br>Attached Appendix C: Pressure Vessel Verification.<br>Now Material Safety Data Sheets appears in Appendix D |
| Version 4 | June 3rd, 2011 | Francisco Alvarez, (915) 525-6708 | Flight Manifest updated (Section 5.0)<br>Camcorder to be used changed (Section 8.59<br>Bogen arm for camera attachment requested (Section 18.0)<br>RAC's (Appendix B) before and after safety measures were updated |
| Version 5 | June 5th 2011 | Francisco Alvarez, (915) 525-6708 | Corrected RAC's (Appendix B) |

# 3.0 QUICK REFERENCE SHEET

**Team Name:** Space Miners

**School Name:** The University of Texas at El Paso

**Principal Investigator:** Christopher White

**Contact Information:** cwhite2@miners.utep.edu, (915) 261-9836

**Experiment Title:** The Effect of Gravity on the Production of Structural Materials from Lunar Regolith

**Flight Date(s):** June 16th-June 25th, 2011

**Overall Assembly Weight (lbs.):** 144 lbs

**Assembly Dimensions (L x W x H):** 43" x 23" x 18"

**Equipment Orientation Requests:** The 43" side of the experimental setup must be parallel to the centerline of the plane.

**Proposed Floor Mounting Strategy (Bolts/Studs or Straps):** The floor mounting strategy of the experimental system to ZGC B-727 will be by 6 AN-6 bolts (provided by RGO).

**Gas Cylinder Requests (Type and Quantity):** 1 bottle (K or equivalent) of high purity Argon (Ar) gas with regulator and connecting tube (provided by NASA).

**Overboard Vent Requests (Yes or No):** Yes

**Power Requirement (Voltage and Current Required):** The available 115V, 60Hz, Single Phase, 20A connection will be used. The provided GFCI receptacle will be used.

**Free Float Experiment (Yes or No):** No

**Flyer Names for Each Proposed Flight Day:**
Day 1: Christopher White, Colin Davis, Michelle Jones
Day 2: Francisco Alvarez, Armando Delgado, Alan Alvillar

**Camera Pole and/or Video Support:** Yes. One camera pole is required for outreach purposes. One Bogen arm will be needed for experimental documentation.

# 4.0 TABLE OF CONTENTS

## 5.0 FLIGHT MANIFEST

The team is composed of three flyers for the first flight and three flyers for the second flight. The flyers are:

Day 1: Christopher White, Colin Davis, and Michelle Jones
Day 2: Francisco Alvarez, Armando Delgado, and Alan Alvillar

## 6.0 EXPERIMENT BACKGROUND

In-situ resource utilization (ISRU) is an enabling technology for future missions to the Moon, Mars, and beyond. A primary goal of ISRU is production of oxygen from lunar/planetary regolith for propulsion and life support. Another high-priority capability is to produce structural materials for landing/launching pads and for protection of habitats from radiation, meteorite impacts, and propulsion exhaust plume debris. Previously tested techniques include microwave heating of lunar regolith and combustion methods: sintering via exothermic reactions, either between elements such as titanium and boron, or between a reducing metal, such as aluminum (Al) or magnesium, and the regolith itself The latter option is based on thermite-type reactions between the added metal and regolith minerals, which are primarily oxides of silicon and some metals. These reactions generate temperatures (1550 K for Al and 1700 K for Mg) that are sufficient to maintain self-sustained combustion, which may lead to the formation of dense composite materials. This type of combustion is called self-propagating high-temperature synthesis (SHS) or combustion synthesis (CS). In contrast to microwave heating, SHS requires only small energy for initiation while the reactions are exothermic and self-sustained. Aluminum and magnesium could be recovered either from lunar/Martian regolith, or from used structures and parts of the vehicles, landers, etc. Thus, combustion of Al/regolith and Mg/regolith mixtures is a promising, low-energy consuming method for the in-situ production of structural materials.

Prior experiments with mixtures of regolith simulant and Al and Mg have demonstrated the combustibility of these mixtures. Those experiments were conducted in normal (Earth) gravity. The lower gravity on the Moon, however, may influence the properties of the products. Studies on combustion of thermite mixtures in microgravity have shown that reduced gravity influences the combustion wave characteristics and the product structure. Among the mechanisms by which gravity influences combustion is the formation of liquid phase in the combustion wave. During combustion of Al/JSC-1A and Mg/JSC-1A mixtures, liquid metal is present in the combustion front (the melting points of Al and Mg are 660°C and 650°C, respectively). Also, during combustion of Mg/JSC-1A mixtures, some amount of liquid silicon forms. Gravity-driven flow of liquid phase in the combustion front may influence the product composition and structure. In

addition, natural convection in the gas phase around the sample may influence the heat transfer from the reacting mixture to the surroundings and thus change the temperature and velocity of the combustion wave. As a result, the effect of gravity may be significant, leading to different process characteristics and material properties.

The research done on combustible mixtures of regolith/metals has been supported by the Center for Science Exploration Technology Research (cSETR). The cSETR is a NASA University Research Center at The University of Texas at El Paso.

# 7.0 EXPERIMENT DESCRIPTION

## 7.1 Purpose

The purpose of this experiment is to study the effect of gravity on the combustion of lunar regolith/metal mixtures and the obtained products.

## 7.2 Description

The combustible mixtures will be produced using lunar regolith simulant JSC-1A and magnesium powder. Combustion of regolith with the two metal powders will be studied. The regolith will be ball-milled to reduce the particle size and increase the reaction rate. The milled regolith will be mixed with the metal powder using a ball mill.

The regolith/metal mixtures will then be put into quartz tubes (inner diameter 12 mm, outer diameter 14 mm, length 50 mm). The mixtures will be manually pressed. The tubes will be installed vertically at the outer edge of a cartridge with space for 15 samples (spaced every 24 degrees). Each tube will be equipped with an igniter made of Nichrome wire to ignite the mixture at the top. Upon ignition, the combustion front will travel downwards. Each combustion process will be recorded using a camcorder. The cartridge will be installed on top of a motorized rotary stage and the system will be located in a sealed steel combustion chamber.

A controller located outside the chamber will control the rotary stage and it will be programmed to rotate 24 degrees every two parabolas. This rotation is necessary to locate the combustible mixture in front of the chamber window and allow for the video recording. The camcorder will be mounted outside of the chamber window and will record the whole experimentation process during the flight. The videos will be analyzed after the flight.

Prior to the experiments, the combustion chamber will be purged by argon from the compressed gas bottle, so that the initial atmosphere in the chamber will be argon. The combustion of regolith/metal mixtures produces mostly solid products. Some amount of liquid silicon may also form in the combustion front. The combustion may release only insignificant amounts of gases, which are present as impurities in the mixture

components or constitute vapors of the involved metals. During combustion of the mixtures, these gases, as well as argon initially in the pores of the sample, may carry some particles through the sample top outwards, creating fumes. The rotary stage system permits running the whole set of experiments without opening the chamber so that no gases or fumes can be released to the airplane cabin. After each experiment, the chamber will be purged by argon, so that the gases and fumes will be removed through the overboard vent and the atmosphere in the chamber before the next experiment will be pure argon again. The low atmospheric pressure outside the aircraft will facilitate purging.

The ignition will be started using electrical heating. A coiled nickel-chromium wire will be installed in each quartz tube and heated up using a commercial DC power supply. All the electrical connections between the exterior and interior of the chamber will be created by means of sealed feedthroughs. The electrical current will be transmitted to the sample through a set of switches connected to the DC power supply.

The chamber (with the interior components), the power supply and the camera will be installed in the microgravity rig made of 1”x1” 80-20 beams and attached to the airplane by six bolts. The rig will have a bottom aluminum plate to bolt the chamber to it and to permit for the placing of the camera and the power supply onto the rig.

After the flights, the average combustion front velocities will be determined using obtained DVD records, while the products will be characterized using X-ray diffraction (XRD), scanning electron microscopy (SEM), and energy-dispersive X-ray spectroscopy (EDS).

## 7.2 Goals

The characteristics of product composition and structure (e.g., XRD patterns and the grain size) and of the combustion process (the velocity of front propagation), obtained in the microgravity experiments, will be compared with those obtained at normal gravity. The conclusion will be made on the existence or absence of the gravity effect. In the former case, it will also be clarified which of the effects (i.e., natural convection in gas phase or liquid metal flow inside the sample) prevails. The gas convection should primarily affect the combustion front velocity while the liquid metal flow may influence the product structure.

## *7.3* Results Obtained in Normal Gravity

This section presents some of the results obtained in our experiments on the combustion of Mg/JSC-1A mixtures in normal gravity.

Figure 1 shows typical images of combustion front propagation over the Mg/JSC-1A mixture pellet, followed by cooling of the combustion products. The top row of images

demonstrates uniform propagation of the combustion front while the bottom row of images illustrates cooling of the sample.

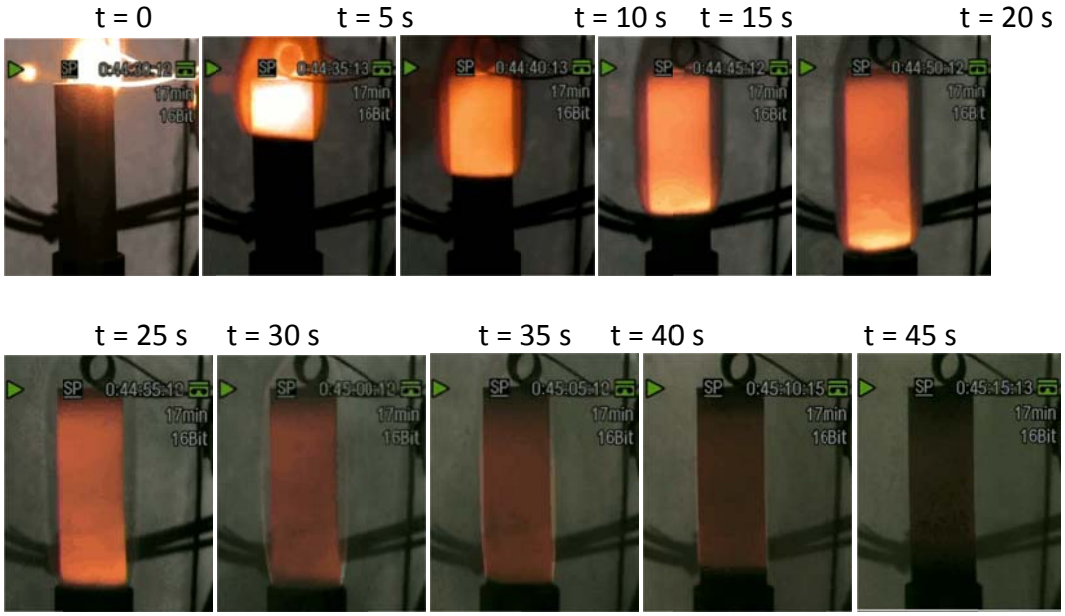


Figure 2. Images of combustion front propagation, followed by cooling, in Mg/JSC-1A mixture (26 wt% Mg) in Ar at 90 kPa under normal gravity conditions. The initial pellet length: 3.4 cm, the pellet diameter: 1.3 cm, the milling time: 4 h.

Figure 2 shows the effect of the milling time on the velocity of the combustion front, observed in our 1-g experiments. To avoid unsteady effects at the top and bottom of the sample, the velocity was determined as an average velocity in the middle part of the sample height.

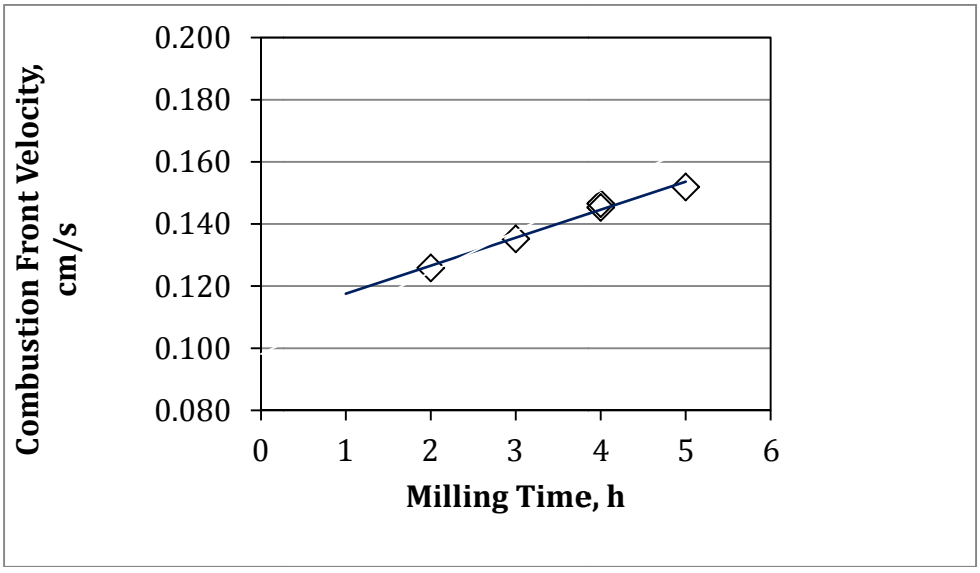

Figure 2. The combustion front velocity in Mg/JSC-1A mixture as a function of JSC-1A milling time at pressure 90 kPa and normal gravity.

# 8.0 EQUIPMENT DESCRIPTION

The setup herein presented is classified as Experimental. No special requirements are needed.

## 8.1 Powders and Preparation of Mixture Samples

**Note:** Powder preparation will be performed at The University of Texas at El Paso.

JSC-1A lunar regolith simulant was obtained from Orbitec. It was used in 1-g experiments and it will also be used in the proposed reduced-gravity experiments. To decrease the particle size to this value, the simulant will be ground in a ball mill (Labmill-8000) as described by White et al. or in a planetary ball mill (Fritsch Pulverisette 7 *premium line*). The particle size distribution of the milled JSC-1A powder will be determined using a laser diffraction particle size analyzer (Malvern Mastersizer 2000).

Magnesium (-325 mesh, 99.8% pure) was obtained from AlfaAesar and it will be used as received. The milled JSC-1A powder will be mixed with Mg using the ball mill. The mixture will contain 26 wt% Mg, which, according to our thermodynamic calculations, provides the maximum adiabatic combustion temperature, 1700 K. Figure 3 shows pictures of the powders used.

a) b)


Figure 3. Photos of the a) regolith simulant JSC-1A, b) magnesium powder

## 8.2 Bottom Aluminum Plate

The bottom plate is 43”x23” made of 6061 aluminum. The thickness of the plate is ½”. The plate will be directly bolted to the airplane attachment grid. Figure 4 shows a view of the microgravity rig (bottom plate shown).

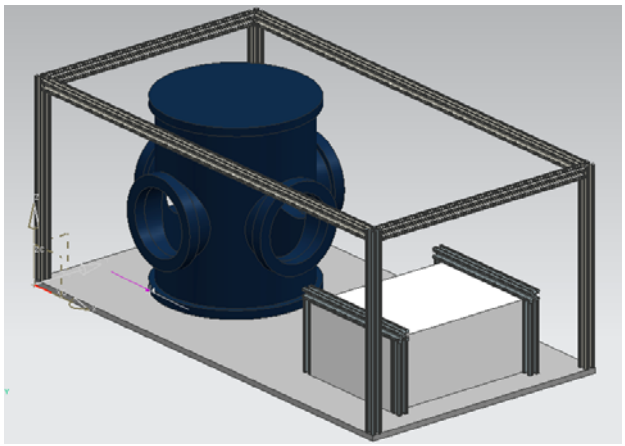

Figure 4. View of the frame (showing the 80/20 1010 beams in dark gray)

## 8.3 Frame

The frame is made of T-Slotted Aluminum 1010 beams (manufactured by 80/20®). This component is a 1.0" x 1.0" T-slotted shape made of 6105-T5 aluminum. Figure 5 shows the cross section of the 1010 beam and its properties. A model view of the frame with some components is shown in Figure 4.

a)

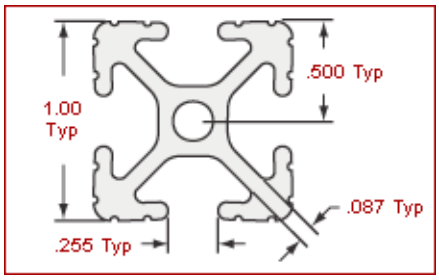


b)

| Part No. | Finish | lbs. / Ft. | Stock Length | Moment of Inertia | Area |
|---|---|---|---|---|---|
| 1010 | Clear Anodized | .5097 | 97, 145 or 242 In. | IX= .0442$^{*4}$<br>IY= .0442$^{*4}$ | .4379$^{*2}$ |

Figure 5. a) Cross section of 80/20 1010 beams and b) some properties of the beam (8020 Inc Website: http://www.8020.net/T-Slot-4.asp)

## 8.3 Combustion Chamber

The steel chamber (diameter 30 cm, height 40 cm) is equipped with a pressure gauge, two glass windows, one lateral plate for piping connections, and one port for the cartridge and sample installation (Fig. 6). The chamber has previously flown onboard KC-135 in a previous microgravity experiment program. The top and bottom lids are made of aluminum 6061. The chamber is equipped with a pressure gauge (Omega), which measures pressure in the range from 30 mm Hg vacuum to 15 psig.


Figure 6. Photographs of the reaction chamber

## 8.4 DC Power Supply 15950PS

The MASTECH Variable Benchtop Power Supply (P/N: HY3020E) will be used to power the ignition system. This device requires a 110 VAC, 60 Hz input. This power supply delivers 0-30 VDC or 0-20 A. The power supply output will not exceed 10 A of current and 20 V of voltage. The current and voltage outputs are monitored using the LEDs installed in the device. The dimensions are: width: 10-1/4" depth: 14-1/2" height: 6-1/4”. The weight is 15 lbs. A picture of the power supply is shown in Figure 7.

Figure 7. Photograph of the power supply

## 8.5 Digital Camcorder

A JVC 80GB Hard Drive Camcorder LCD (Figure 8) records at 832x624 and stores the information in HDD form. The camera will be connected to the electrical output to avoid the battery from discharging.

Figure 8. A photograph of the digital camcorder

## 8.6 Cartridge

The cartridge is made of four 3/16” 6061-aluminum disks (diameter 12 cm) (Fig. 9). The cartridge holds up to 15 samples and can be reused. The bottom plate consists of two disks, one with holes and the other one without holes. The top plate consists of two disks, both with holes but of different diameter. The holes in the top disks have a smaller diameter, so that the quartz tubes are fixed (see Fig. 9). A threaded aluminum rod holds the plates together. The rod is attached to the rotary stage. Figure 10 shows a CAD view of the cartridge.

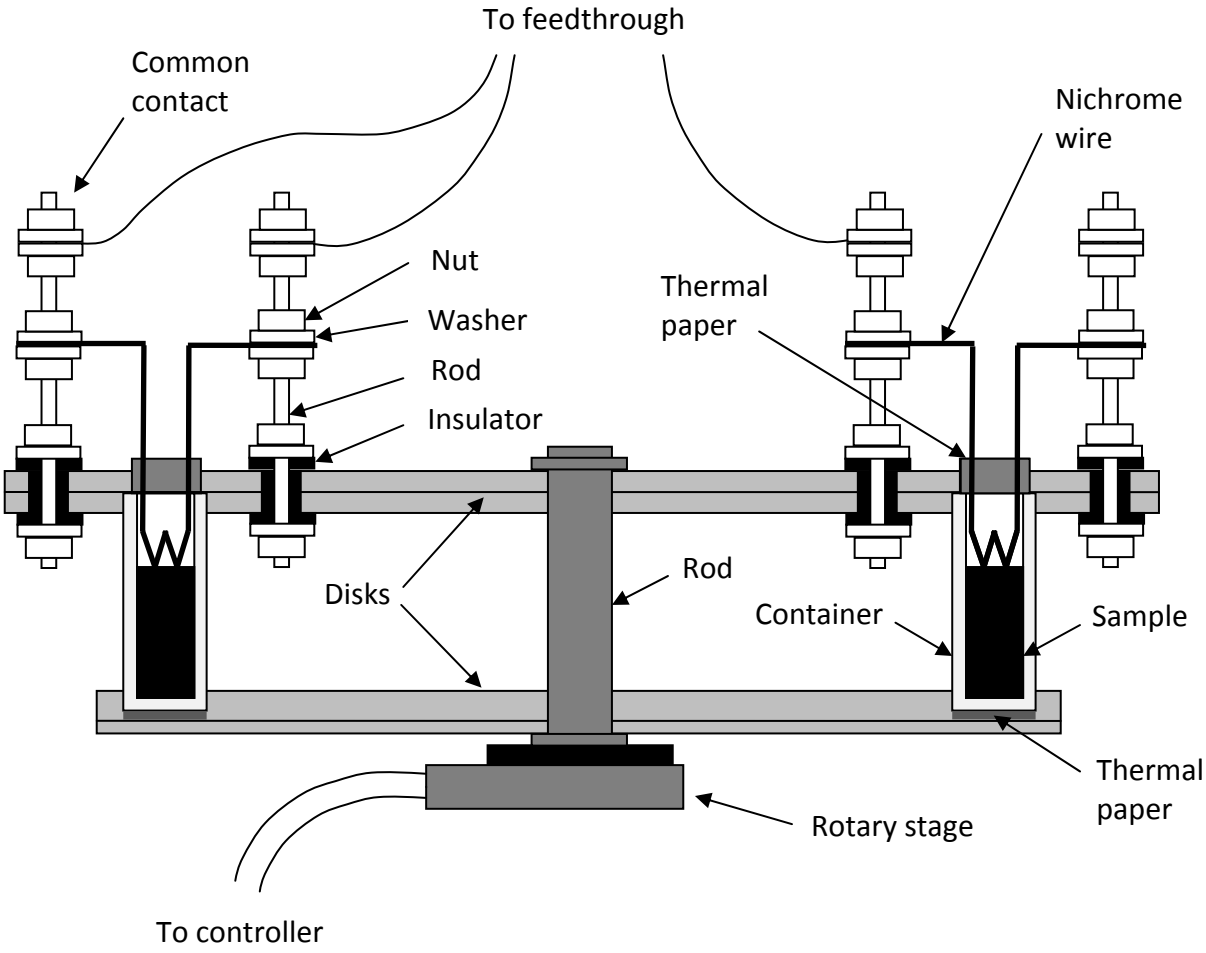


Figure 9. Schematic of the cartridge with samples

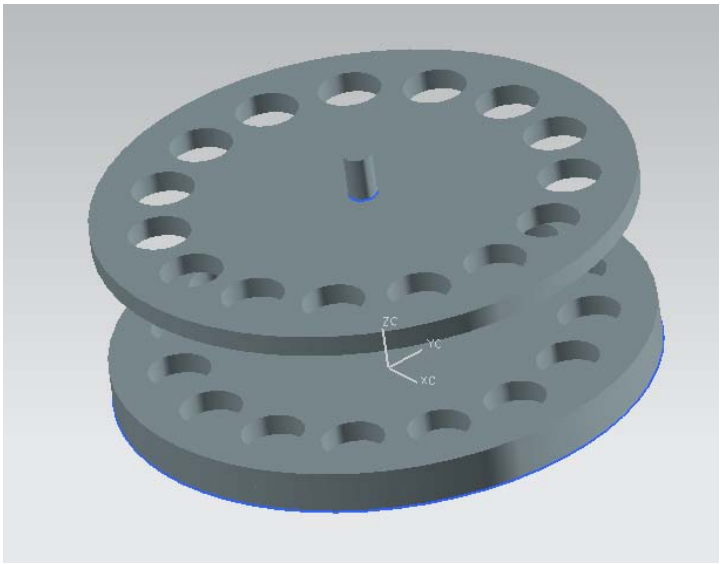

Figure 10. Model of the cartridge without holes for electrical connectors (The diameter of the disks is 120mm.)

## 8.7 Quartz Tubes

14 mm OD Quartz tubes are used to contain the regolith/metal mixtures. The quartz tubes (with the regolith/metal mixtures inside) will be installed in the cartridge as described in section 8.6. The experiments at normal gravity show that the combustion products are dense and they remain inside the tubes after the process. In addition, to prevent accidental ejection of particles from the top of the sample, ceramic fiber paper, also called Fiberfrax thermal paper, (a ¼"-thick disk with two holes for Nichrome wire) will be installed at the top of each tube (see Fig. 9).

## 8.8 Rotary Stage and Controller

The rotary stage and the controller are shown in Figure 11. The rotary stage is located inside the combustion chamber and is connected to the controller using a feedthrough in the lateral aluminum port in the chamber. The controller (weight: 2.75 lbs) will be outside and will be programmed to rotate the rotary stage 24 degrees every two parabolas (15 samples in the circular cartridge). The controller will require one button push to start the rotation.

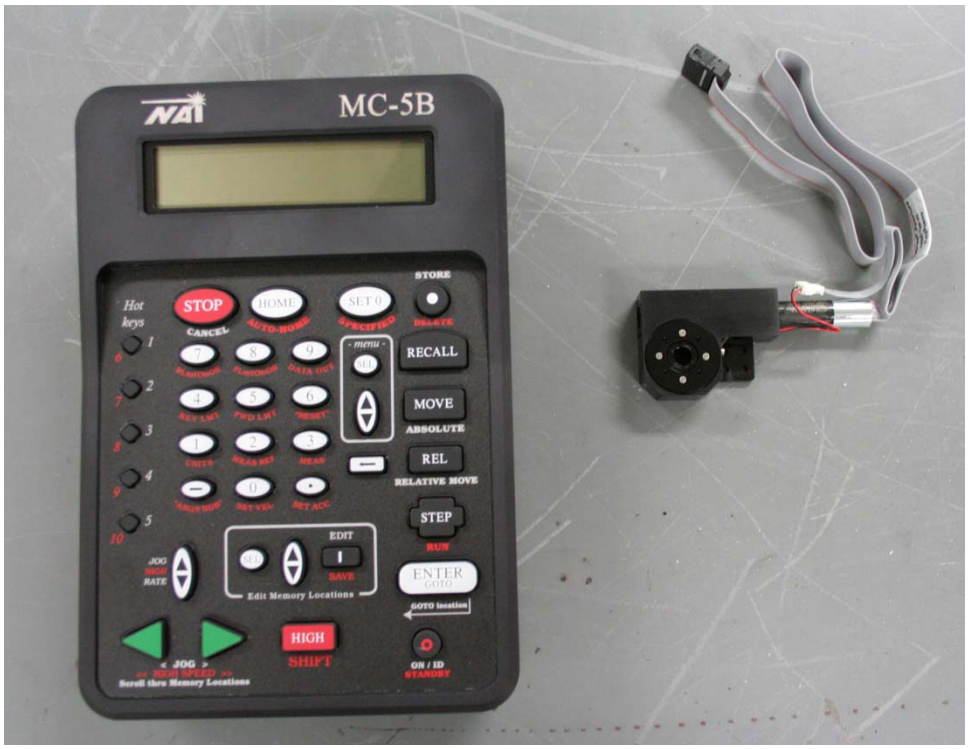


Figure 11. Left: controller, right: rotary stage.

### 8.9 Ignition Wires

The igniters consist of a coiled Nichrome wire to start the combustion of the samples through Joule heat. The coil will be embedded into the powder samples. The ends of the wire will be attached to the contacts on a connector (see Fig. X), which are connected to the DC power supply using the feedthrough in the chamber port. The connector contains 16 contacts, of which 15 are separately connected to the 15 igniters and one is a common contact for other ends of the igniters.

### 8.10 Feedthroughs

The feedthroughs (manufactured by Omega P/N: PFT2NPT-4CU) use 20 AWG wire stranded with PTFE insulation. It has a 600 V rating. Each feedthrough has 4 pairs of copper wires and a ½" NPT plug to install it on the lateral aluminum port in the combustion chamber.

### 8.11 Switches

The two poles-two positions (on-off-on) switches are used to select the igniter to be started at each experimental run. The switches are connected in parallel to a conventional power strip.

### 8.12 Pressure Regulators

The pressure regulators are connected to the argon tank and are manually controlled to manipulate the pressure and flow rate of gas into the chamber. The regulators are used as manufactured.

## 9.0 STRUCTURAL VERIFICATION

The structural analysis and verification can be found in Appendix A.

## 10.0 ELECTRICAL ANALYSIS

The airplane electrical power is requested for the following units:

- DC power supply (Mastech HY3020E) (Fig. 7)
- Stand-alone controller of the rotary stage (Edmund Optics NT57-575) (Fig. 1)
- Digital camcorder (Samsung MiniDV DigitalCam) (Fig. 8)

All these units are commercial off-the-shelf devices used in their intended manner, and powered from a single aircraft 115 VAC, 60 Hz, single phase, 20 Amp circuit distributed from a switched, surge and circuit breaker protected powerstrip. A single "kill switch" will be installed to shut down all equipment in case of emergency.

## 10.1 Schematic

Figure 8 shows a schematic diagram of the electric connections. For convenience, wires for only 4 igniters are shown.

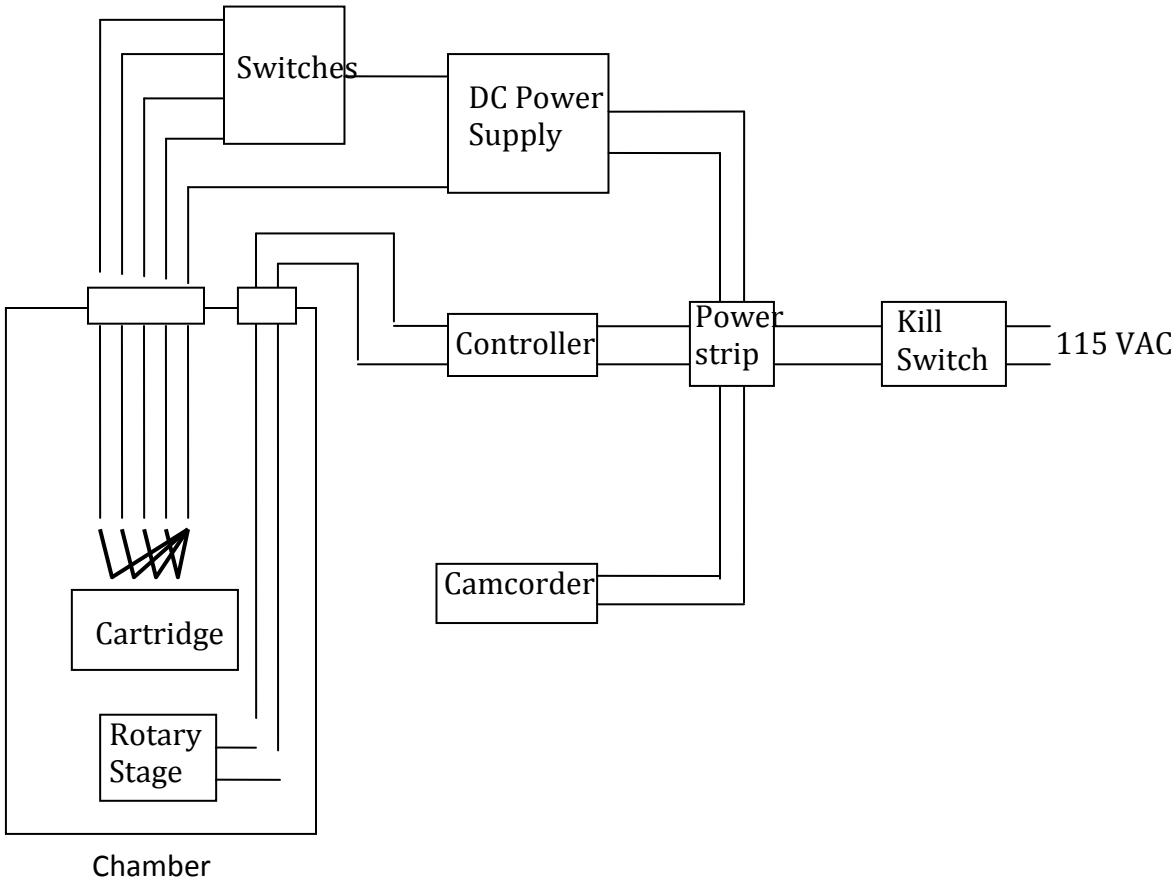

Figure 12. Schematic of the electrical connections

Table 1. Electrical load analysis

| **Electrical Analysis** | | | |
|---|---|---|---|
| Power Source Detail | | Load Analysis | |
| Name | Power Cord A | Power Supply | 10 Amp |
| Voltage: | 115 VAC, 60 Hz | Stand-Alone Controller | 2 Amp |
| Wire Gauge | 12 | Camcorder | 1 Amp |
| Max Outlet Current: | 20 Amps | Total Current Draw: | 13 Amp |

The DC power supply outputs are 0-30V and 0-20A, i.e. the maximum output power of this device is 600 W. In the experiments, the output voltage will be less than 20 V and the output current will be less than 10 A. A switch arrangement will be used for distributing electric power, obtained from the DC power supply, to the igniters.

The controller requires an electric current of 1.4 A to run the rotary stage. The controller has an internal fuse that prevents it from transmitting a current higher than 2 A.

The digital camcorder can be powered from an internal, rechargeable battery. During the flight experiments, however, it is preferable to use the 115 VAC power outlet, thus eliminating the possibility of low battery.

The switches to transfer the current to the igniter are Rocker Switch E-60272 LR-39145. These switches are rated for 21A/14V DC. The current passing through the switches will not exceed 10 A.

Experiments at the Center for Space Exploration Technology Research at UTEP have been performed connected to a single phase 115 VAC, 20 A, 60 Hz outlet (the same as onboard Zero- G Aircraft) and no electrical problems have been encountered.

The electrical devices used in the experiment will not be modified for the flights and will work according to the manufacturer specifications.

## 10.3 Kill Switch

The power delivered to the electrical system will be stopped in case of an emergency contingency while in flight. A kill switch will be installed between the power source and the power strip (as shown in Fig. 12). Closing the kill switch will power off the electrical devices.

### 10.4 Loss of Electrical Power

In case of a sudden loss of electrical power, the devices will turn off and the electricity shortage will not affect the performance of the electrical equipment. A test will be performed during the Test Readiness Review while in Ellington Field.

## 11.0 PRESSURE VESSEL OR SYSTEM

Figure 13 shows a schematic diagram of the pressure/vacuum system. The experiments will be conducted in an argon atmosphere at 0 psig pressure. One gas cylinder with compressed argon will be used. The chamber will be connected to this cylinder through a valve and a gas regulator. Another valve will connect the chamber to the overboard vent. A filter (Swagelok, 0.5 micron) will ensure that no particulates produced by combustion escape during purging of the chamber. Pressure in the chamber will be monitored using a pressure gauge (Omega) and the exit valve will be used if necessary. A pressure relief valve (Swagelok) rated at 10 psig will be installed to prevent uncontrolled pressure rise in the chamber.

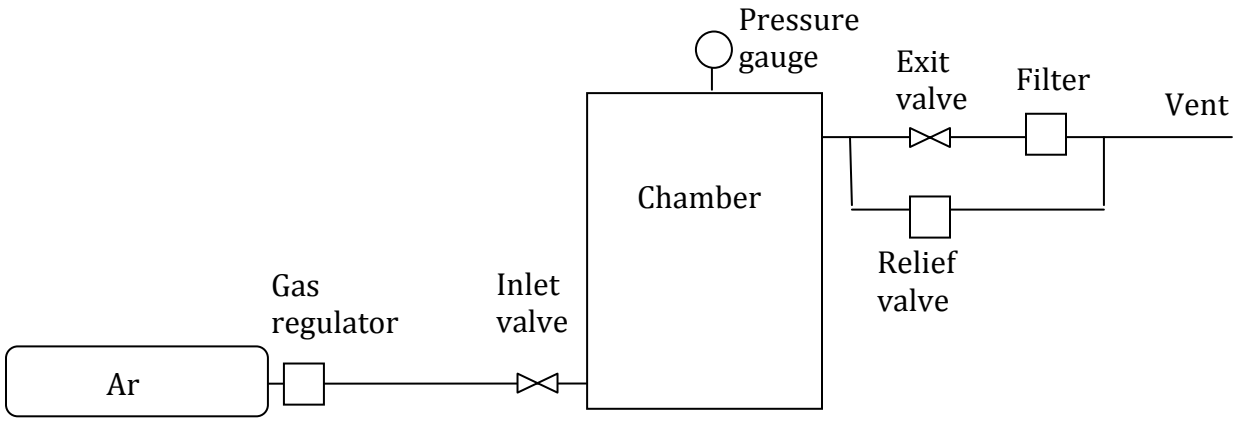


Figure 13. Schematic of the pressure/vacuum system

The chamber will be purged with argon after installation of the cartridge and after each experiment. To do this, first the exit valve, connecting the chamber with the vent, and then the inlet valve will be opened. The purging procedure before the first experiment will have to be relatively long in order to remove any tracks of air in the chamber. This procedure can be conducted before the flight. Purging between the experiments can be shorter because its goal is to remove fumes and any possible gas products, which are not expected to form in noticeable amounts. The experiments will be conducted during every odd parabola while purging will be carried out during every even parabola, so that a lower atmospheric pressure at the top of parabola will be effectively used. Purging

after the last experiment will be long again, to fully replace the gas atmosphere by pure argon.

Appendix C shows the pressure tests (at 20 psig) to assess the structural integrity of the chamber if an overpressure occurs.

## 12.0 LASER VERIFICATION

Laser verification is not required; this experiment does not involve the use of lasers.

## 13.0 PARABOLA DETAILS AND CREW ASSISTANCE REQUIRED

A special set of parabolas is not required for the described experiment.

## 14.0 FREE FLOAT REQUIREMENTS

The experimental setup does not require free float conditions.

## 15.0 INSTITUTIONAL REVIEW BOARD

An Institutional Review Board approval is not required; the experiment does not involve human test subjects, animal test subjects or biological tests.

## 16.0 Hazard Analysis Summary

### 16.1 Electrical Potential

To avoid electrical shock, the DC power supply and the experimental rack will be connected to the single-phase connection delivering 120 VAC, 20A, 60 Hz aircraft power. A kill switch will be installed to allow for the interruption of electric current if necessary. Also, a fuse rated at 20 Amps will be installed to avoid overcharging the system.

### 16.2 Shrapnel or Blast Wave Over-Pressurization

To avoid damage of the chamber due to unexpected increase in pressure, the chamber will be proof tested at 20 psig (test verification is shown in Appendix C) and a relief valve set to 10 psig will be installed.

## 16.3 Fire

The combustion process will be performed in argon atmosphere. Besides the tested mixtures, the only flammable materials in the chamber are insulation of electric wires and cables. Ignition of the insulating materials in argon atmosphere is impossible. Since the tested materials contain magnesium, a Class D fire extinguisher (for metal fires) should be onboard the plane.

## 16.4 High Temperatures

Immediately after ignition, the mixture may be heated up to 1400°C (this value is the adiabatic combustion temperature while the actual temperature will be lower). This temperature will be localized within the quartz container inside the chamber.

The mass of each sample will be less than 5 g. The mass of the chamber and its volume (0.03 $m^3$) are large enough to avoid any significant increase of the chamber temperature or pressure when such small samples are burned. Chamber walls will remain much colder than the permitted touch temperature (50°C) during or after combustion of all 15 samples. This will be verified in 1-g experiments in our laboratory prior to the flights. The aluminum cartridge will also function as a heat sink to prevent overheating of the rotary stage.

After combustion of each sample, the chamber will be purged with argon, which will remove hot gases and cool the solid products. It is expected that purging after the last experiment will cool the samples to the touch temperature. The chamber will be opened after landing. By this time, the samples will be at nearly room temperature.

## 16.5 Low Temperatures

No hazards are related to low temperature conditions.

## 16.6 Ionizing Radiation

No hazards are related to ionizing radiation.

## 16.7 High Energy Electromagnetic Fields

No hazards are related to high-energy electromagnetic fields.

## 16.8 Oxygen Deficient Atmospheres

No hazards are related to oxygen deficient atmospheres.

## 16.9 Toxic Atmosphere

Magnesium oxide fumes may be produced during the mixture combustion. Magnesium oxide is not toxic. Direct contact with them may result in minor irritation in skin, eyes,

and throat. The fumes will be contained inside the combustion chamber and will be flushed away by the argon gas.

### 16.10 High Sound Levels

No hazards are related to high sound levels.

### 16.11 Sharp Points or Edges

Foam will be attached to all sharp points and edges to avoid their exposure.

### 16.12 Collisions

No hazards are related to collisions.

### 16.13 Crushing Forces

No forces are related to crushing forces

### 16.14 Environmental Pollution

The magnesium oxide fumes will be flushed away of the chamber and will be collected in the installed filter. The fume particles will not be released to the atmosphere

### 16.15 Test Article

No hazards are related to the test article.

## 17.0 TOOL REQUIREMENTS

No special tools are required for the preparation of the experimental setup. During flight operation, no tools will be required.

## 18.0 PHOTO REQUIREMENTS

One camera pole is required to document the team performing the experiments. The videos obtained will be used for outreach purposes. Also, one Bogen arm will be required to attach the camera to the setup and record the experimental runs for further analyses.

## 19.0 AIRCRAFT LOADING

A forklift will be required to take the experimental setup to the interior of the airplane. Once inside the aircraft, the team will be able to move the setup and install it on the place designated by the RGO.

# 20.0 GROUND SUPPORT REQUIREMENTS

## 20.1 Electrical Connections

A 110 V/60 Hz connection will be required for ground testing.

## 20.2 Gas Tanks

One argon K-bottle will be required for purging of the combustion chamber during the flight. The gas regulators will be provided by the team.

## 20.3 Laboratory Desk

A conventional laboratory desk is required for ground testing and for preparation of the flight experiments.

## 20.4 Materials Cabinets

Two boxes with the mixture samples should be stored in a locked cabinet.

# 21.0 HAZARDOUS MATERIALS

Thirty-two samples of the investigated powder mixtures will be brought to Houston. The mixtures include JSC-1A lunar regolith simulant and magnesium. These mixtures are combustible but not pyrophoric. Please note that the mixtures will not be prepared at Ellington Field. The samples will be prepared at UTEP and brought ready to Houston. To be ignited, the mixtures need to be heated to high temperatures. During the experiment, such temperatures will be achieved locally using the Nichrome igniters heated by electric current.

The mass of each sample will be less that 5 g. Thus the total mass of these materials will not exceed 160 g. Each sample will be placed in a quartz container, closed by a plug. Plugs will be replaced by igniters before the flight. The igniters will include Nichrome wires with no chemical compounds. The containers will be stored and transported in boxes with special inserts (2 boxes with up to 16 containers in each).

A summary of the hazardous materials is presented in this section. Detailed information of the hazardous materials is given in Appendix B.

### 21.1 JSC-1A

Inhalation of dust may irritate nose, throat and lungs. Eye contact with solids may produce irritation. If irritation exists due to contact with the material, fresh air or water will mitigate the problems. During the experimentation, the JSC-1A powder will be contained inside the combustion chamber. Any powder that may escape from the experimental sample will be vented to the atmosphere through the overboard vent. JSC-1A is stable under normal conditions of storage and does not require any special handling.

### 21.1 Magnesium Powder

Magnesium powder may be reactive in contact with air and water. The container will be tightly sealed during its use and will minimize the contact with humidity and air. Magnesium powder must be kept away from hot surfaces and fire. If the container is kept in a dry and ventilated place, no special handling measures are required.

Contact with magnesium powder may cause irritation in eyes, nose, throat and lungs. During the preparation of the samples (performed at UTEP), protective mask and gloves will be used. In case of direct contact with eyes, skin, or nose, the affected person must be translated to a source of fresh air and the contact area thoroughly rinsed with water. During flight, the powder will be contained inside the combustion chamber and no direct contact will occur.

If the magnesium powder starts a fire, an extinguisher for metal fires (Class D) is necessary.

The quantity of magnesium powder utilized will not exceed 20 grams.

## 22.0 MATERIAL SAFETY DATA SHEETS

Appendix C contains the Material Safety Data Sheets of the materials used during the experiments.

## 23.0 PROCEDURES

### 23.1 Ground Operations

The setup will be installed on a laboratory desk in the service building. Several containers, filled with an inert material (lunar regolith simulant without any additives), will be equipped by Nichrome wire igniters and installed in the cartridge. The cartridge

will be installed in the chamber. The test of all electrical and measurement systems will be conducted during a simulation of the actual experiment, i.e. the cartridge will be rotated using the controller, the igniters will be consecutively heated by electric current, and the processes will be recorded by the digital camcorder.

## 23.2 Pre-Flight

Before each flight, the containers from one box will be installed in the cartridge and the plugs will be replaced by the Nichrome wire igniters. After that, the cartridge will be brought aboard in a special box and installed in the chamber using the port. The igniters will be connected to the contacts of the electrical scheme of the setup. The chamber will be closed and purged by argon. The “in” and “out” valves of the chamber will be closed.

## 23.3 In-Flight

At the beginning of each microgravity period, the igniter of a tested sample will be heated to initiate reactions in the sample. The combustion process will be recorded by the digital camcorder (the duration of the combustion process will be less than 18 s). After the process, using the programmed controller of the rotary stage, the cartridge will be rotated so that the next sample will be in position (in front of the camcorder) for the next experiment.

The next parabola will be used for purging the chamber by argon, which will create a pure, inert atmosphere for the next experiment. Thus, for example, odd parabolas could be used for the experiments while even parabolas could be used for purging. After the final experiment, the chamber will once again be purged with argon. The chamber will remain closed during the entire flight.

Two operators can conduct the experiments. One of them will turn on/off the power from DC power supply to ignite the samples and push the button on the controller of the rotary stage to rotate the cartridge while the other will be responsible for purging and maintaining the required pressure in the chamber (i.e., he will operate the two valves of the chamber, looking at the pressure gauge).

The sample located in front of the window (i.e. in the optimal position for video recording) will be ignited at the beginning of the reduced gravity period. According to our measurements at normal gravity [6], the 25-mm long samples will burn for less than 18 s, i.e. the combustion time of such samples is shorter than the reduced gravity period. The combustion process will be recorded by the digital camcorder in the miniDV format. Once combustion is complete, the cartridge will be rotated by 24° (360/15 = 24), so that the next sample is in the proper position for the experiment.

The next parabola will be used for purging the chamber by argon (the lower atmospheric pressure at the top of parabola will help purging), providing a pure, inert

atmosphere for the next experiment. Thus, for example, odd parabolas could be used for the experiments while even parabolas could be used for purging.

The proposed approach will allow us to conduct a large number of experiments during the flight without opening the chamber, i.e. without having to manipulate the mixture samples outside the chamber during the flight. Up to 15 parabolas can be used for the experiments during one flight.

### 23.4 Post-Flight

After landing, the chamber will be opened. The cartridge will be removed and transferred in its box to the service building. The containers will be removed from the cartridge and placed into their box. The used igniters will be replaced by the plugs and placed in a special box for disposal. New containers will be installed in the cartridge and new igniters in preparation for the next flight will replace their plugs.

## 24.0 BIBLIOGRAPHY


1. Munir, Z.A., and Anselmi-Tamburini, U., "Self-Propagating Exothermic Reactions: The Synthesis of High-Temperature Materials by Combustion," *Materials Science Reports* 3, 277–365 (1989).
2. Merzhanov, A. G., "Solid Flames - Discoveries, Concepts, and Horizons of Cognition," *Combustion Science and Technology*, Vol. 98, 1994, pp. 307-336.
3. Moore, J.J., and Feng, H.J., "Combustion Synthesis of Advanced Materials: Part I. Reaction Parameters, *Progress in Materials Science* 39, 243-273 (I995).
4. Moore, J.J., and Feng, H.J., "Combustion Synthesis of Advanced Materials: Part II. Classification, Applications and Modelling," *Progress in Materials Science* 39, 275-316 (1995).
5. Varma, A., Rogachev, A. S., Mukasyan, A. S., and Hwang, S., "Combustion Synthesis of Advanced Materials," *Advances in Chemical Engineering* 24, 79–224 (1998).
6. White, C., Alvarez, F., and Shafirovich, E., "Combustible Mixtures of Lunar Regolith with Aluminum and Magnesium: Thermodynamic Analysis and Combustion Experiments," 49th AIAA Aerospace Sciences Meeting, Orlando, Fl, January 4-7, 2011, AIAA Paper 2011-613.
7. Taylor, L.A., and Meek T.T., "Microwave Sintering of Lunar Soil: Properties, Theory, and Practice," *Journal of Aerospace Engineering* 18, 188-196 (2005).
8. Martirosyan, K.S., and Luss, D., "Combustion Synthesis of Ceramic Composites from Lunar Soil Stimulant," *Lunar and Planetary Science* XXXVII, 1896 (2006).
9. Faierson, E.J., Logan, K.V., Stewart, B.K., and Hunt, M.P., "Demonstration of Concept for Fabrication of Lunar Physical Assets Utilizing Lunar Regolith Simulant and a Geothermite Reaction," *Acta Astronautica*, Vol. 67, 2010, pp. 38-45.

10. Sen, S., Ray, C.S., and Reddy, R.G. “Processing of Lunar Soil Simulant for Space Exploration Applications,” *Material Science and Engineering A*, Vol. 413, 2005, pp. 592-597.
11. Characterization Summary of JSC-1AF Lunar Mare Regolith Simulant. Version 1.6.2. December 12, 2006. Orbital Technologies Corporation. http://orbitec.com/store/JSC-1AF_Characterization.pdf.
12. Mukasyan A.S., Lau, C, and Varma, A., “Influence of Gravity on Combustion Synthesis of Advanced Materials,” *AIAA Journal*, Vol. 43, 2005, pp.225-244.
13. Gökalp, I., Chauveau, C., Durox, D., Lacas, F., Legrand, B., and Shafirovich, E., “Preliminary Analysis of a Spray and Cloud Combustion Module for the ISS,” *Proceedings of the 5th International Microgravity Combustion Workshop, May 18-20, 1999, Cleveland, OH*, NASA/CP–1999-208917, pp. 127-130.
14. Chauveau, C., Legrand, B., Shafirovich, E., Vieille, B., and Gökalp, I., “Single Droplet and Cloud Combustion Experiments Using Parabolic Flights,” 4th International Symposium on Parabolic Flights, June 14-15, 1999, Paris – Le Bourget, France, p. 24.
15. Legrand, B., Chauveau, C., Shafirovich, E., Goldshleger, U., Carrea, E., Mounaim-Rousselle, C., Rouan, J.P., and Gökalp, I., “Combustion of Magnesium Particles in Carbon Dioxide Under Microgravity Conditions,” *Proceedings of the 6th International Microgravity Combustion Workshop, May 22-24, 2001, Cleveland, OH*, NASA/CP-2001-210826, pp. 225-228.
16. Shafirovich, E., and Varma, A., “Metal-$CO_2$ Propulsion for Mars Missions: Current Status and Opportunities,” *Journal of Propulsion and Power*, Vol. 24, No. 3, 2008, pp. 385-394.
17. Lau, C, Mukasyan, A.S., and Varma, A., “Materials Synthesis by Reduction-type Combustion Reactions: Influence of Gravity,” *Proceedings of the Combustion Institute*, Vol. 29, 2002, pp. 1101-1108.
18. Andrzejak, T.A., Shafirovich, E., Taylor, D.G., and Varma, A., “Apparatus for Studies of High-Temperature Chemical Reactions in Single Particle Systems,” *Review of Scientific Instruments*, Vol. 78, No. 8, 2007, art. 085102.
19. Andrzejak, T.A., Shafirovich, E., and Varma, A., “Ignition Mechanism of Nickel-Coated Aluminum Particles,” *Combustion and Flame*, Vol. 150, 2007, pp. 60-70.
20. Andrzejak, T.A., Shafirovich, E., and Varma, A., “Ignition of Iron-Coated and Nickel-Coated Aluminum Particles under Normal- and Reduced-Gravity Conditions,” *Journal of Propulsion and Power*, Vol. 24, No.4, 2008, pp. 805-813.

# APPENDIX A. STRUCTURAL VERIFICATION

A structural verification was performed on the rig and the components to comply with the Aircraft Operations Division (AOD) and safety requirements.

## A.1 Minimum Margin of Safety Summary Table

Table A.1 Margin of Safety Summery

| **Floor Attachments** | | | |
|---|---|---|---|
| **Configuration** | **Mode** | **Max. Load** | **MS** |
| 9g-Forward | Tension | 126.11 | 5.74 |
| | Shear | 318.95 | 2.14 |
| 3g-Afterward | Tension | 42.04 | 19.22 |
| | Shear | 106.32 | 8.41 |
| 2g-Lateral | Tension | 46.71 | 17.20 |
| | Shear | 70.88 | 13.11 |
| 2g-Upward | Tension | 109.61 | 6.75 |
| 6g-Downward | Tension | 212.63 | 3.00 |
| **Chamber** | | | |
| **Configuration** | **Mode** | **Max. Load** | **MS** |
| 9g-Forward | Tension | 257.97 | 3.19 |
| | Shear | 135.00 | 7.01 |
| 2g-Upward | Tension | 30.00 | 35.04 |
| **Power Supply/Inner Frame** | | | |
| **Configuration** | **Mode** | **Max. Load** | **MS** |
| 9g-Forward | Tension | 48.12 | 21.47 |
| | Shear | 63.45 | 16.04 |
| 2g-Upward | Tension | 14.10 | 75.68 |
| 2g-Lateral | Shear | 28.20 | 18.45 |
| **Outer Frame** | | | |
| **Configuration** | **Mode** | **Max. Load** | **MS** |
| 9g-Forward | Tension | 20.69 | 51.26 |
| | Shear | 31.73 | 16.29 |
| 2g-Upward | Tension | 7.05 | 152.36 |

## A.2 Loads and Allowables

### *A.2.1 Loads*

The equipment must withstand the loads designated by the AOD in takeoff or landing configurations shown in Table A.2:

Table A.2. Loads under Takeoff and Landing Conditions

| Direction | Load |
|---|---|
| Forward | 9-g's |
| Aft | 3-g's |
| Down | 6-g's |
| Lateral | 2-g's |
| Up | 2-g's |

### *A.2.2 Allowables*

Six bolts will be used to attach the setup to the aircraft plane. The bolts will be provided by the RGO. The combustion chamber is attached to the bottom plate by four 1/4" Grade 5 steel bolts. The 80/20 1010 beams are attached using L-brackets (shown in Figure A.1). Each L-bracket needs four bolts (1/4" 1215 Steel). For the aircraft attachments, the tension allowable load is 2125 lbs and the shear allowable load is 2500 lbs.

Table A.3. Load Allowables

| Part | Load | Allowable (lbs) |
|---|---|---|
| 1/4" Steel Bolts | | |
| Steel 1215 | Tension | 1908 |
| | Shear | 968 |
| Grade 5 | Tension | 2703 |
| | Shear | 1371 |
| Floor Attachments | | |
| | Tension | 2125 |
| | Shear | 2500 |

## A.3 Mass

The mass of the heavier components was used for the structural analysis calculation and 20% was added to their mass in order to account for components not expressly included (i.e. controller, rotary stage) in the force calculations and to add a safety factor for a not constructed apparatus. The center of mass was calculated using the Advanced Weight Management tool in NX 6.0. Table A.4 shows a table of the heavier components and the

addition of the 20 percent weight for analysis purposes. Figure A.1 shows a simplified model of the setup with the components with considerable mass.

Table A.4. Weight calculation of the experimental setup

| Part | Quantity | Material | Weight (lb) | Total Weight | Extra 20% | Weight for Analysis |
|---|---|---|---|---|---|---|
| 17.5" 80/20 1010 Beam | 4 | 6105 Aluminum | 2.12 | 8.48 | 1.696 | 10.176 |
| 21" 80/20 1010 Beam | 2 | 6105 Aluminum | 2.54 | 5.08 | 1.016 | 6.096 |
| 41" 80/20 1010 Beam | 2 | 6105 Aluminum | 4.96 | 9.92 | 1.984 | 11.904 |
| 6.25" 80/20 1010 Beam | 4 | 6105 Aluminum | 0.76 | 3.04 | 0.608 | 3.648 |
| 12.25" 80/20 1010 Beam | 2 | 6105 Aluminum | 1.48 | 2.96 | 0.592 | 3.552 |
| Bottom Aluminum Plate | 1 | 6061 Aluminum | 48.43 | 48.43 | 9.686 | 58.116 |
| Power Supply | 1 | Various | 15 | 15 | 3 | 18 |
| Steel Chamber | 1 | Steel | 50 | 50 | 10 | 60 |
| Controller | 1 | Various | 2.75 | 2.75 | 0.55 | 3.3 |
| Cartridge | 1 | 6061 Aluminum | 2 | 2 | 0.4 | 2.4 |
| | | | | | **Total Weight:** | **177.192** |

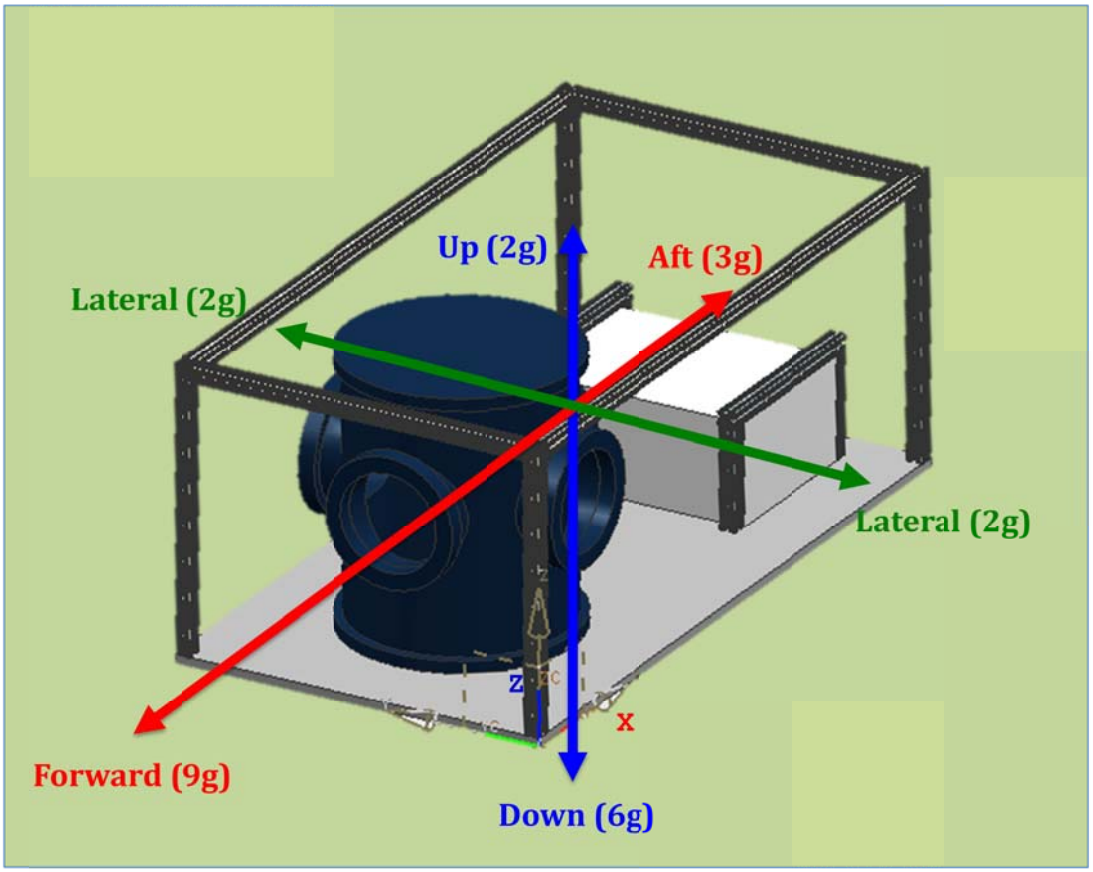


Figure A.1. CAD model of the setup with analysis loads

For the structural verification calculations a Minimum Safety Factor of 2 will be used. A Mass Factor (not measured center of mass) of 1.25 will be used as well.

## A.4 Floor Attachments

For the attachment of the apparatus to the aircraft, six AN-6 3/8" steel bolts (provided by RGO) will be used. A mounting grid on the floor of the aircraft with 20"x20" intervals between each bolt is utilized. A tensile and shear loading analysis was conducted to determine the stresses in the bolts. The loads were applied on the setup center of mass (x=19.38, y=12.26 in, z=6.59 in).

NOTE: The allowables for the floor attachments were used, not the allowables for the AN-6 bolts.

### *A.4.1 Forward Direction*

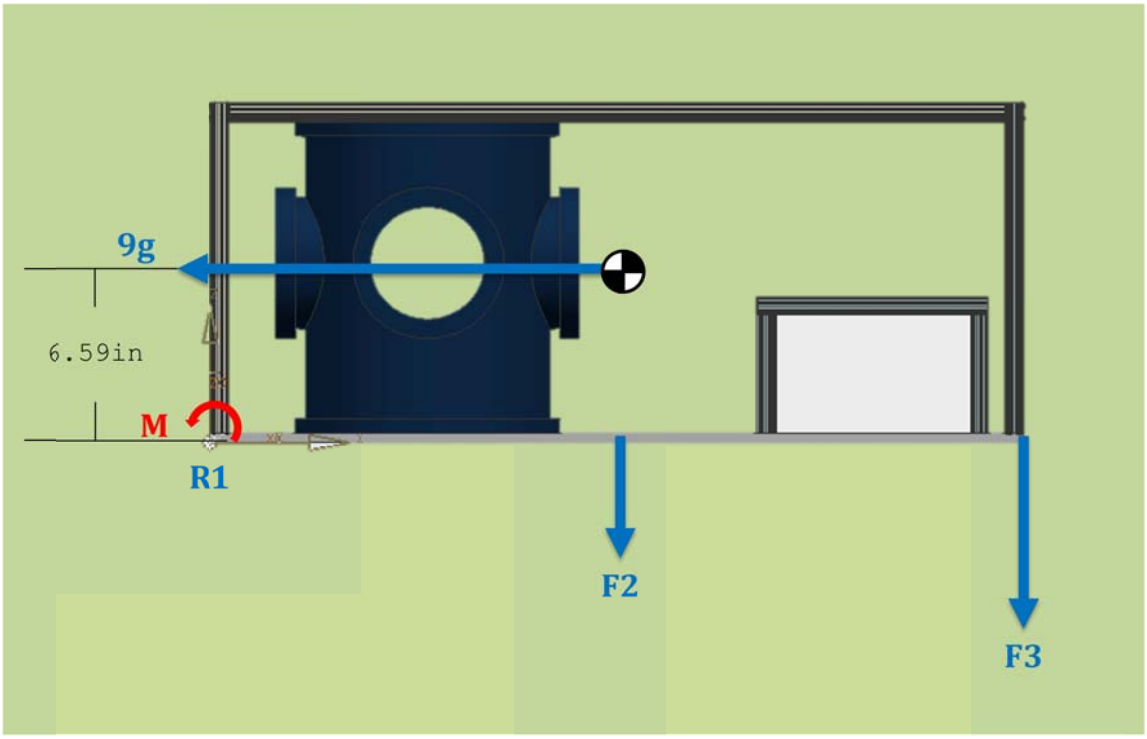

Figure A.2 Tensile forces exerted on mounting bolts by the forward G-load.

$$\Sigma M = 9g(6.59\ in) - 2F_2(20\ in) - 2F_3(40\ in) = 0$$
$$\frac{F_2}{20\ in} = \frac{F_3}{40\ in}$$
$$\therefore\ F_2 = 63.06\ \text{lbs.}$$
$$F_3 = 126.11\ \text{lbs.}$$

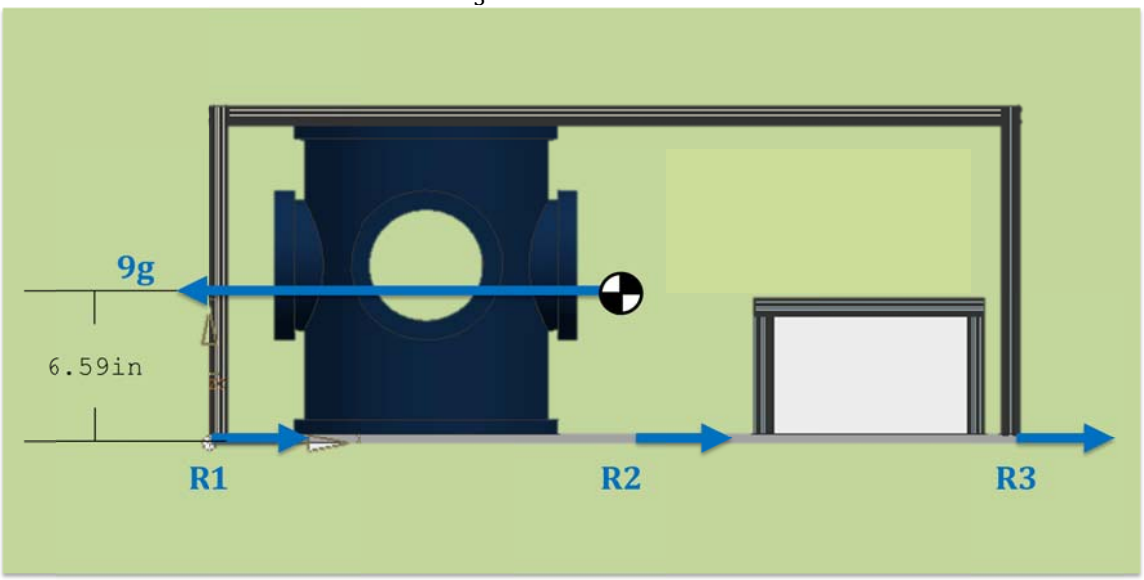

Figure A.3 Shear forces exerted on mounting bolts by the forward G-load.

$$\Sigma F = 9g - 6R = 0$$

$$\therefore R = R_1 = R_2 = R_3 = 318.95\ lbs.$$

### *A.4.2 Aft Direction*

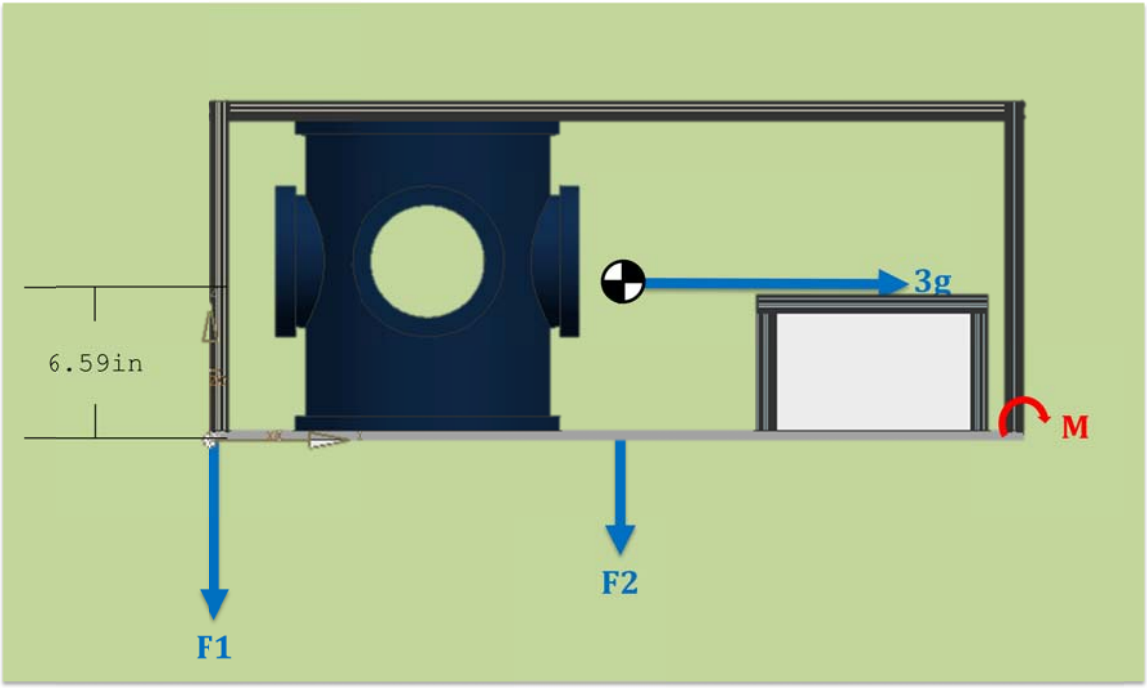


Figure A.4 Tensile forces exerted on mounting bolts by the afterward G-load.

$$\Sigma M = -3g(6.59\ in) + 2F_2(20\ in) + 2F_1(40\ in) = 0$$

$$\frac{F_2}{20\ in} = \frac{F_1}{40\ in}$$

$$\therefore\ F_1 = 42.04\ \text{lbs.}$$

$$F_2 = 21.02\ \text{lbs.}$$

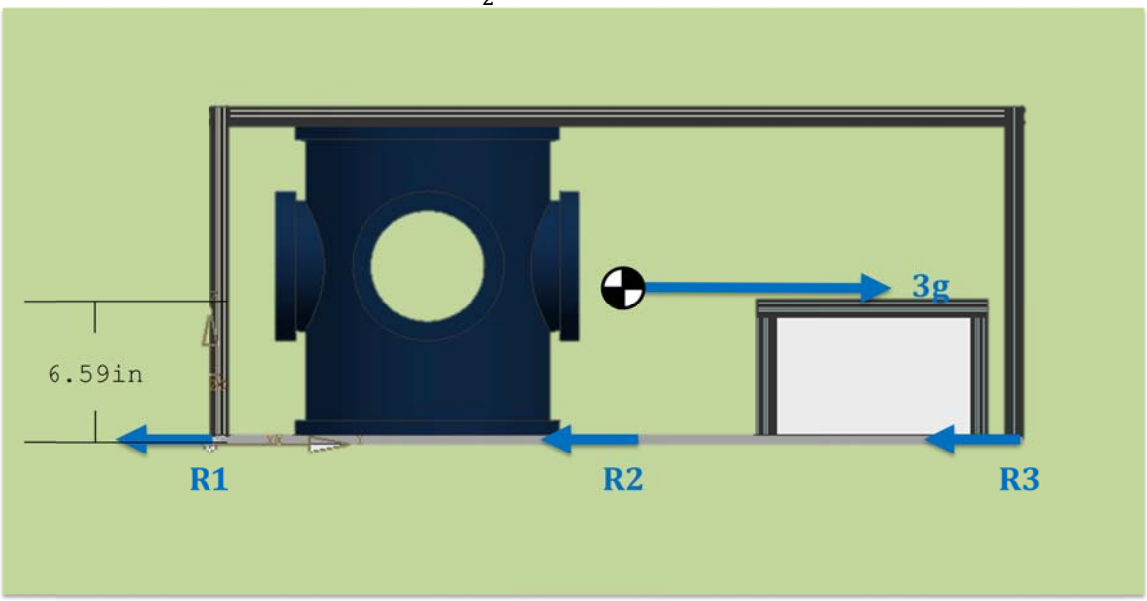


Figure A.5 Shear forces exerted on mounting bolts by the afterward G-load.

$$\Sigma F = 3g - 6R = 0$$
$$\therefore R = R_1 = R_2 = R_3 = 106.32 \text{ lbs.}$$

### *A.4.3 Upward Direction*

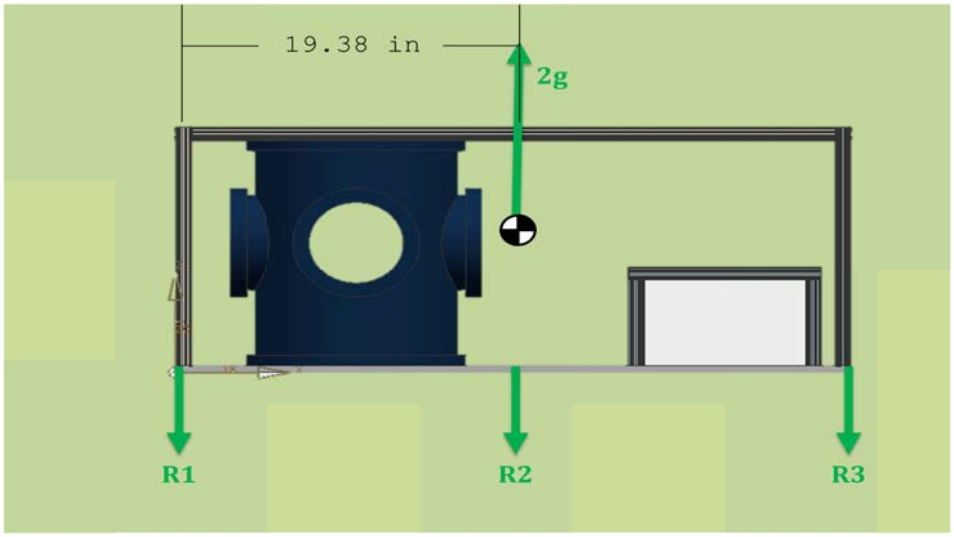


Figure A.6 Tensile forces exerted on mounting bolts by the upward G-load.

Assuming that it $R_2$ does not carry load, and a taking the moment about $R_1$:

$$\Sigma M = -2g(19.38\ in) + 2R_3(40\ in) = 0$$
$$\Sigma F = 2g - 2R_3 - 2R_1 = 0$$
$$\therefore R_1 = 103.02 \text{ lbs.}$$
$$R_2 = 0 \text{ lbs.}$$
$$R_3 = 109.61 \text{ lbs.}$$

### *A.4.4 Downward Direction*

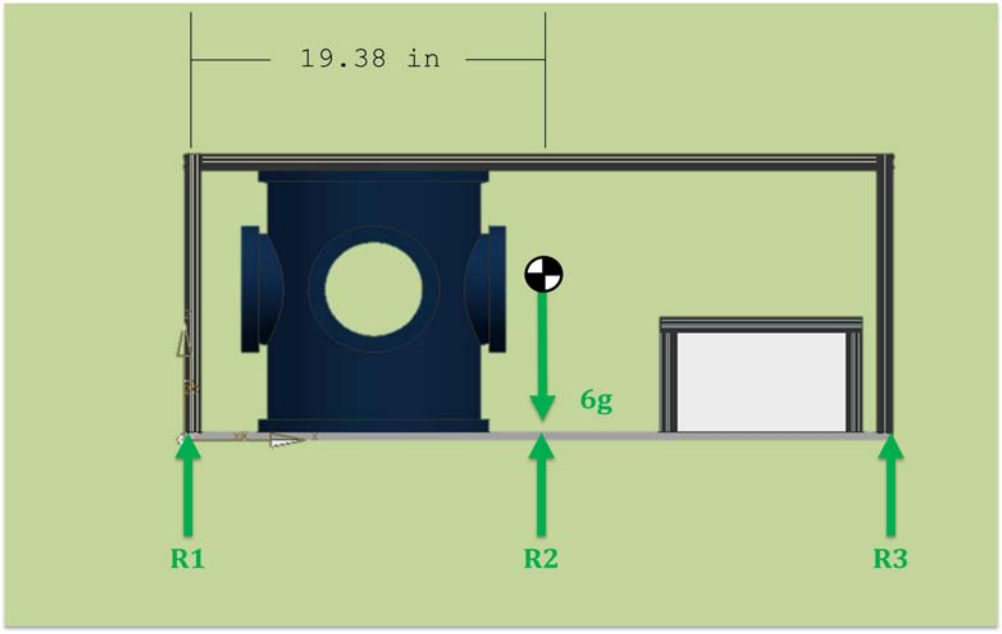


Figure A.7 Tensile forces exerted on mounting bolts by the downward G-load.

$$\Sigma F = 6g - 6R = 0$$

$$\therefore R = R_1 = R_2 = R_3 = 212.63 \text{ lbs.}$$

### *A.4.5 Lateral Direction*

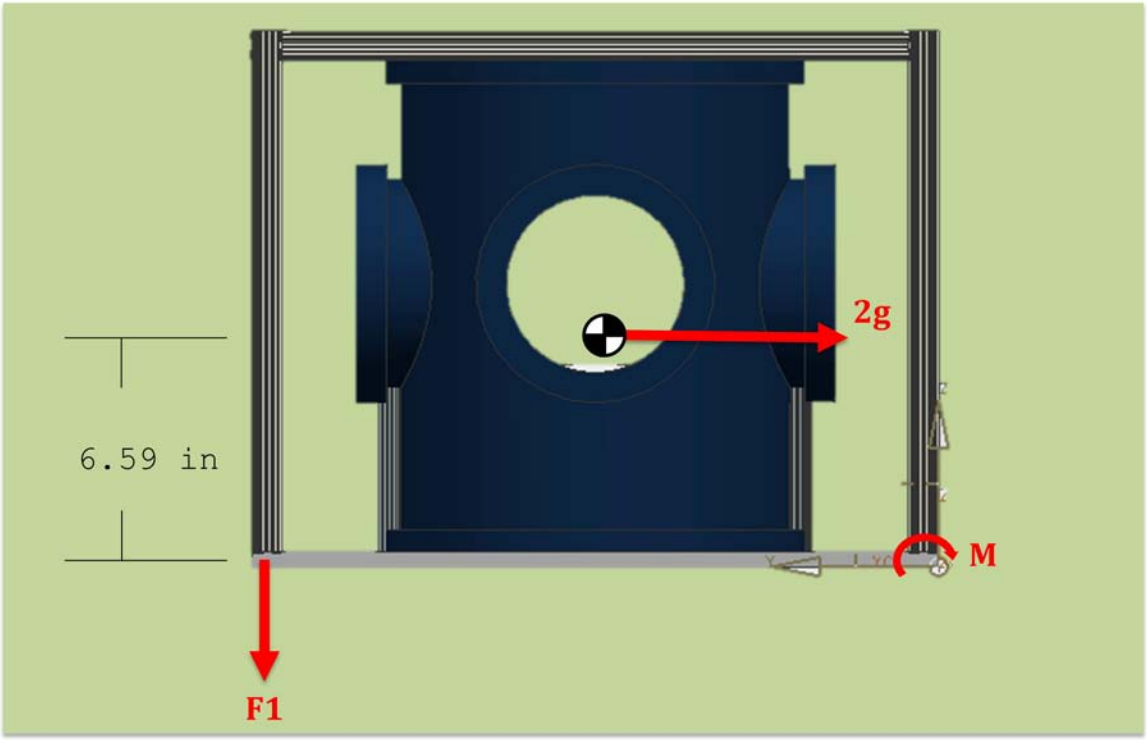


Figure A.8 Tensile force exerted on mounting bolts by the lateral G-load.

$$\Sigma M = -2g(6.2\ in) + 3F_1(20\ in) = 0$$
$$\therefore\ F_1 = 46.71\ \text{lbs.}$$

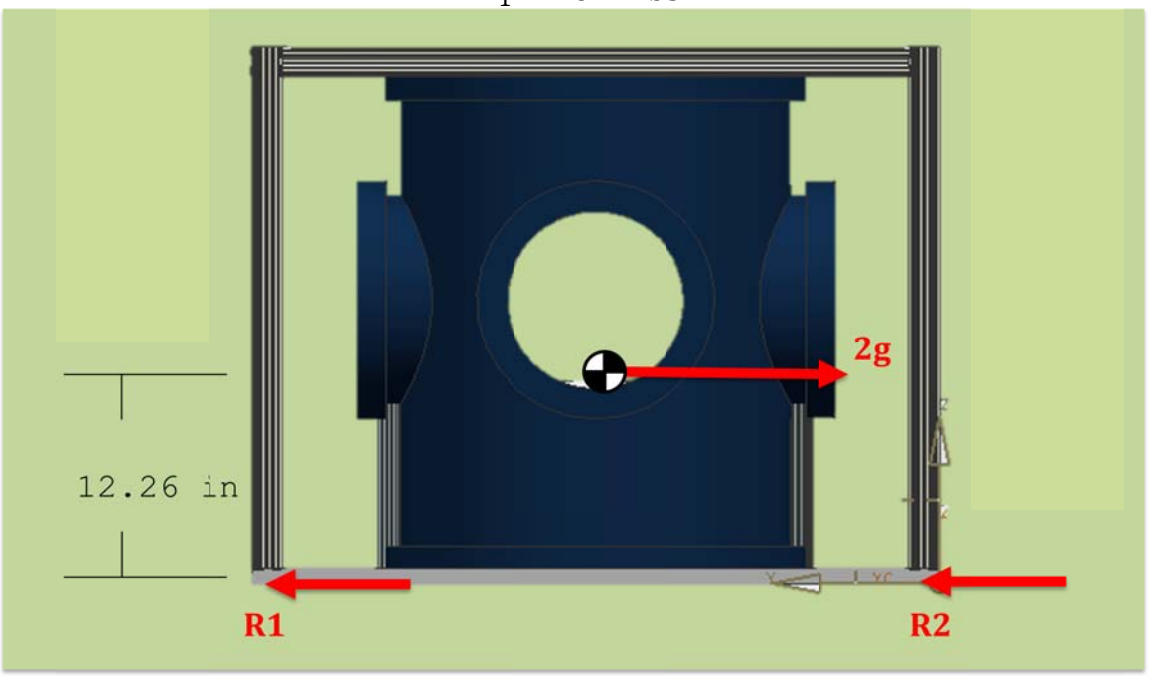


Figure A.9 Shear forces exerted on mounting bolts by the lateral G-load

$$\Sigma F = 2g - 6R = 0$$
$$\therefore R = R_1 = R_2 = 70.88\ \text{lbs.}$$

### *A.4.6 Margins of Safety*

The allowable for aircraft floor attachments was divided by the maximum load calculated for each configuration in order to obtain the margins of safety. Equation A.1 shows the method to calculate the margin of safety:

$$Margin\ of\ Safety = \frac{F_{allowable}}{F_{max} * FS_1 * FS_2} - 1 \quad . \qquad \text{(Eq. 1)}$$

$FS_1 = 1.5$ → Factor of safety for a non-measured/actual center of gravity
$FS_2 = 2$ → Minimum Factor of Safety

Table A.5 shows the margins of safety for the floor attachments. All the margins are greater than one, meaning that the attachments are safe for flight.

Table A.5 Margins of safety for floor attachments

| Configuration | Mode | Max. Load | MS |
|---|---|---|---|
| 9g-Forward | Tension | 126.11 | 5.74 |

| | | | |
|---|---|---|---|
| | Shear | 318.95 | 2.14 |
| 3g-Afterward | Tension | 42.04 | 19.22 |
| | Shear | 106.32 | 8.41 |
| 2g-Lateral | Tension | 46.71 | 17.20 |
| | Shear | 70.88 | 13.11 |
| 2g-Upward | Tension | 109.61 | 6.75 |
| 6g-Downward | Tension | 212.63 | 3.00 |

## A.5 Chamber

The most critical loads for the chamber attachments are the 9g forward load and the 2g upward load configurations. These loads are analyzed in this section. The weight for the chamber for this analysis (with an extra 20% is 60 lbs).

### *A.5.1 Mass and Allowables*

The chamber is attached to the bottom plate by four 1/4" Grade 5 steel bolts. A bolt below each of the window sites attaches the chamber to the aluminum bottom plate. Figure A.10 shows a schematic of the chamber and the forces. The center of mass was obtained geometrically (x=7 in., y=7 in. ,z=8.36 in.). The load allowables are shown in Table A.3.

### *A.5.2 Forward*

The 9g load configuration is the most critical of the lateral load configurations (9g>3g>2g).

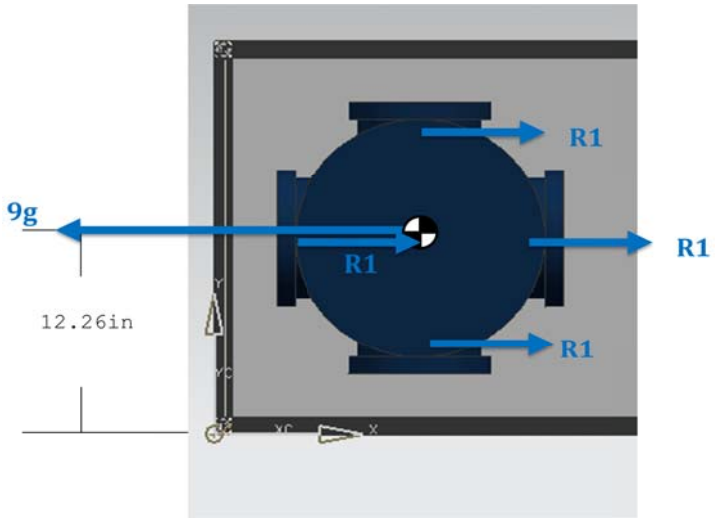


Figure A.10. Shear forces on chamber attachments and forward 9g force

$$\Sigma F = 9g - 4R1 = 0$$

$$\therefore R_1 = 135 \text{ lbs.}$$

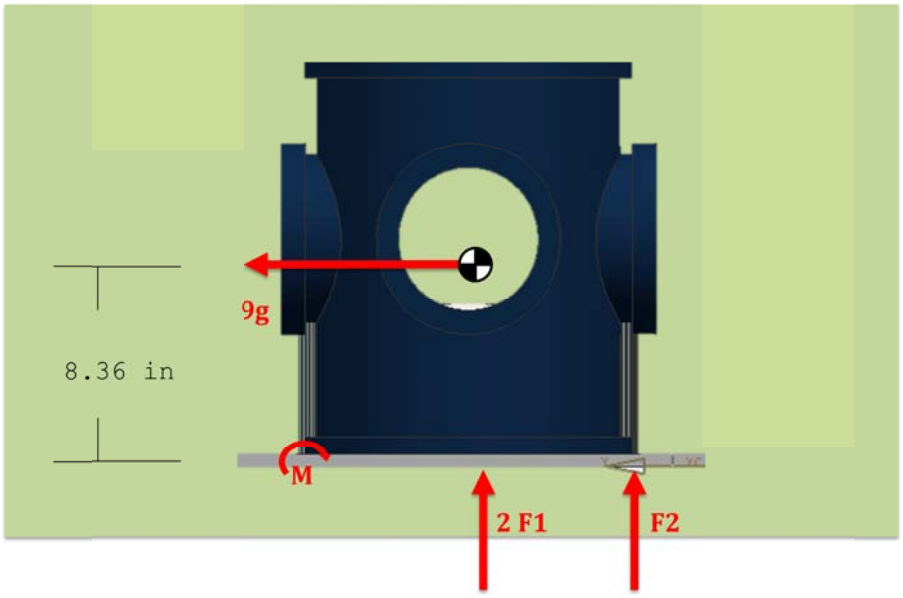


Figure A.11 Tension forces on chamber attachments and forward 9g force

$$\Sigma M = -9g(8.36\ in) + 2F_2(7\ in) + F_1(14\ in) = 0$$
$$\frac{F_2}{14\ in} = \frac{2F_1}{7\ in}$$
$$\therefore\ F_1 = 257.97 \text{ lbs.}$$
$$F_2 = 64.49 \text{ lbs.}$$

### *A.5.3 Upward*

The 2g load configuration is the most critical of the up-down loads.

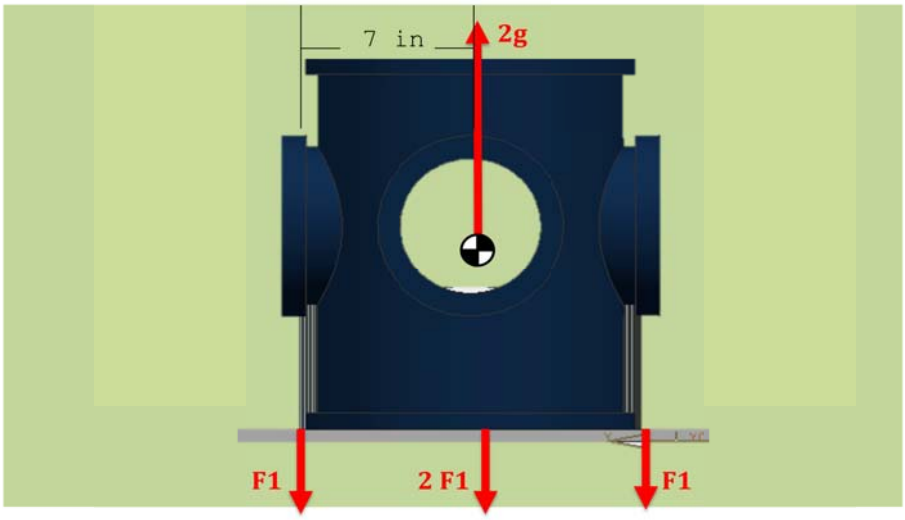


Figure A.12. Chamber attachments tension reaction to 2g upward force

$$\Sigma F = 2g - 4F1 = 0$$
$$\therefore F_1 = 30 \text{ lbs.}$$

### *A.5.4 Margins of Safety*

Table A.6. Margins of safety for chamber attachments

| Configuration | Mode | Max. Load | MS |
|---|---|---|---|
| 9g-Forward | Tension | 257.97 | 3.19 |
| | Shear | 135.00 | 7.01 |
| 2g-Upward | Tension | 30.00 | 35.04 |

## A.6 Power Supply and Inner Frame

The most critical loads on the power supply and inner frame are the 9g forward force, the 2g upward force and the 2g lateral force.

### *A.6.1 Mass and allowables*

The power supply is attached to the bottom plate by the inner frame shown in Fig 1. The frame is attached to the aluminum bottom plate by four L-brackets (two ¼" Grade 5 steel bolts each). The power supply is supported by two L-brackets (one ¼" bolt each), one on each side for the lateral 2g load. The weight for the power supply and inner frame for this analysis (with an extra 20%) is 28.2 lbs. The center of mass was obtained using NX 6 software (x=4.80 in., y=5.73 in., z=3.64 in.). The allowables are shown in Table A.3.

### *A.6.2 9g Forward Force*

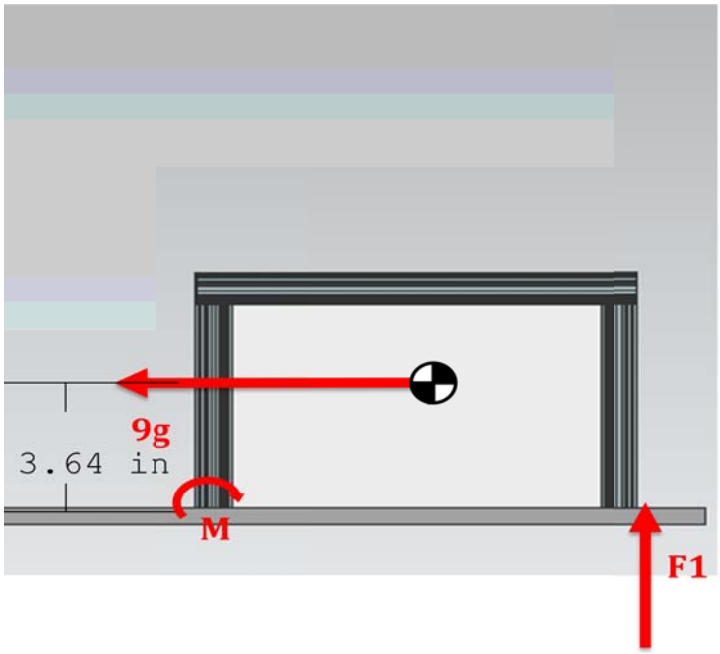


Figure A.13. Power supply tension reaction to 9g forward force

$$\Sigma M = -9g(3.64\ in) + 2F_1(9.60\ in) = 0$$
$$\therefore\ F_1 = 48.12\ \text{lbs.}$$

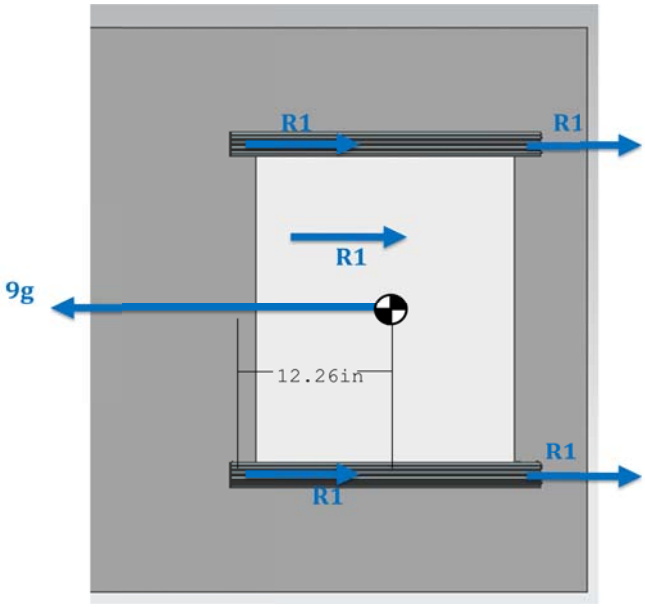


Figure A.14. Power supply shear reaction to 9g forward force

$$\Sigma F = -9g + 4R = 0$$
$$\therefore R = 63.45\ \text{lbs.}$$

### *A.6.3 2g upward*

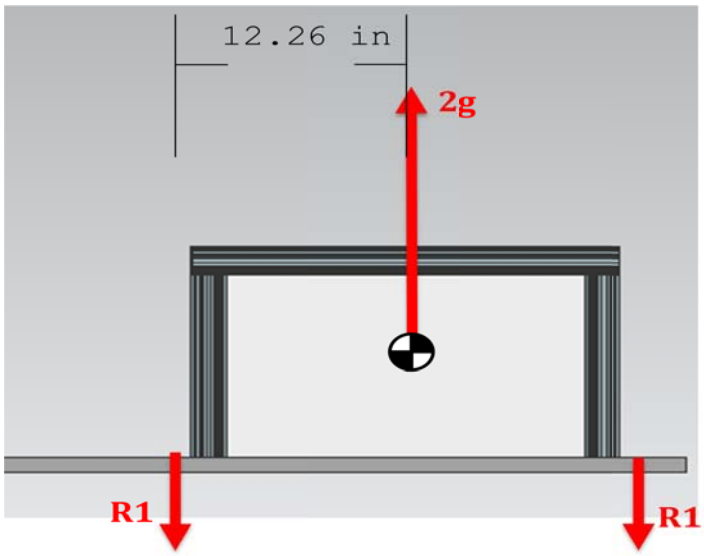


Figure A.15 Tension reactions of inner frame and power supply under 2g upward load

$$\Sigma F = 2g - 4F1 = 0$$
$$\therefore F_1 = 14.1 \text{ lbs.}$$

### *A.6.4 2g lateral*

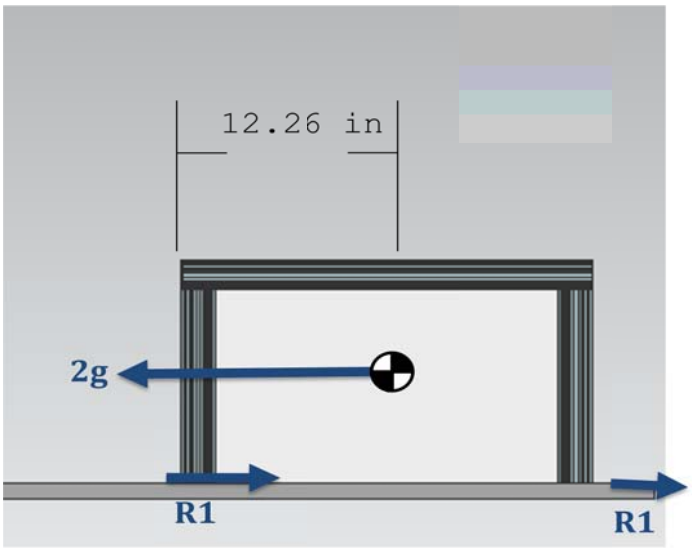


Figure A.16 Shear reaction of inner frame and power supply under 2g lateral load

$$\Sigma F = 2g - 2R = 0$$
$$\therefore R = 28.2 \text{ lbs.}$$

### *A.6.5 Margins of Safety*

Table A.7 Margins of safety for inner frame and power supply

| Configuration | Mode | Max. Load | MS |
|---|---|---|---|
| 9g-Forward | Tension | 48.12 | 21.47 |
| | Shear | 63.45 | 16.04 |
| 2g-Upward | Tension | 14.10 | 75.68 |
| 2g-Lateral | Shear | 28.20 | 18.45 |

## A.7 Outer Frame

The most critical loads on outer frame are the 9g forward force and the 2g lateral force.

### *A.7.1 Mass and allowables*

The outer frame is shown in Fig 1. The frame is attached to the aluminum bottom plate by four L-brackets (two ¼" Grade 5 steel bolts each). The power supply is supported by two L-brackets (one ¼" bolt each), one on each side for the lateral 2g load. The weight for the power supply and inner frame for this analysis (with an extra 20%) is 28.2 lbs. The center of mass was obtained using NX 6 software (x=21.5 in., y=11.5 in. ,z=14.02 in.). The allowables are shown in Table A.3.

### *A.7.2 Forward 9g Load*

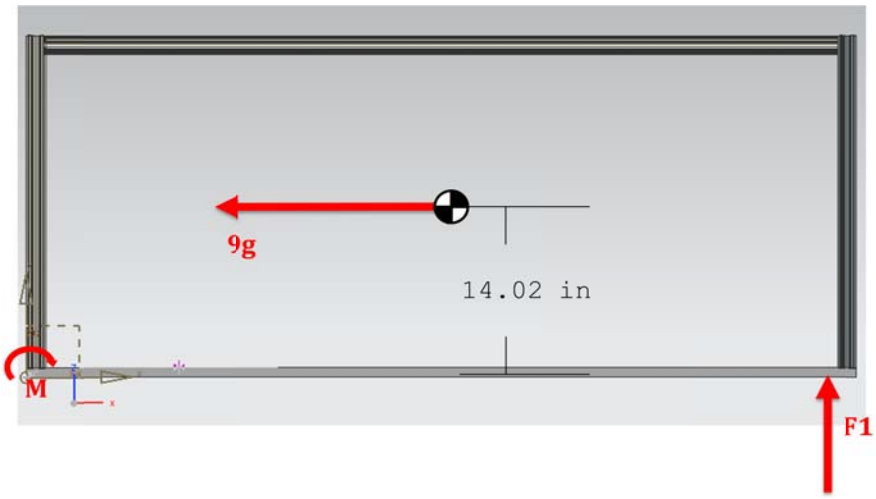


Figure A. 16 Tension reactions of outer frame under a 9g forward load

$$\Sigma M = -9g(14.02\ in) + 4F_1(43\ in) = 0$$
$$\therefore\ F_1 = 20.69\ \text{lbs.}$$

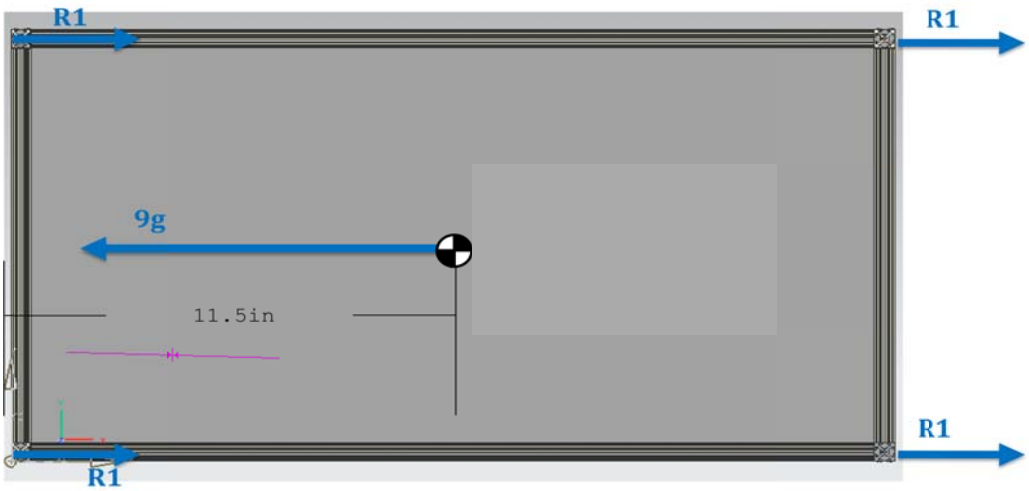


Figure A.17 Shear reactions of outer frame joint under 9g forward load

$$\Sigma F = -9g + 8R = 0 \text{ (R1=2R)}$$
$$\therefore R = 31.73 \text{ lbs.}$$

### *A.7.3 Upload 2g Load*

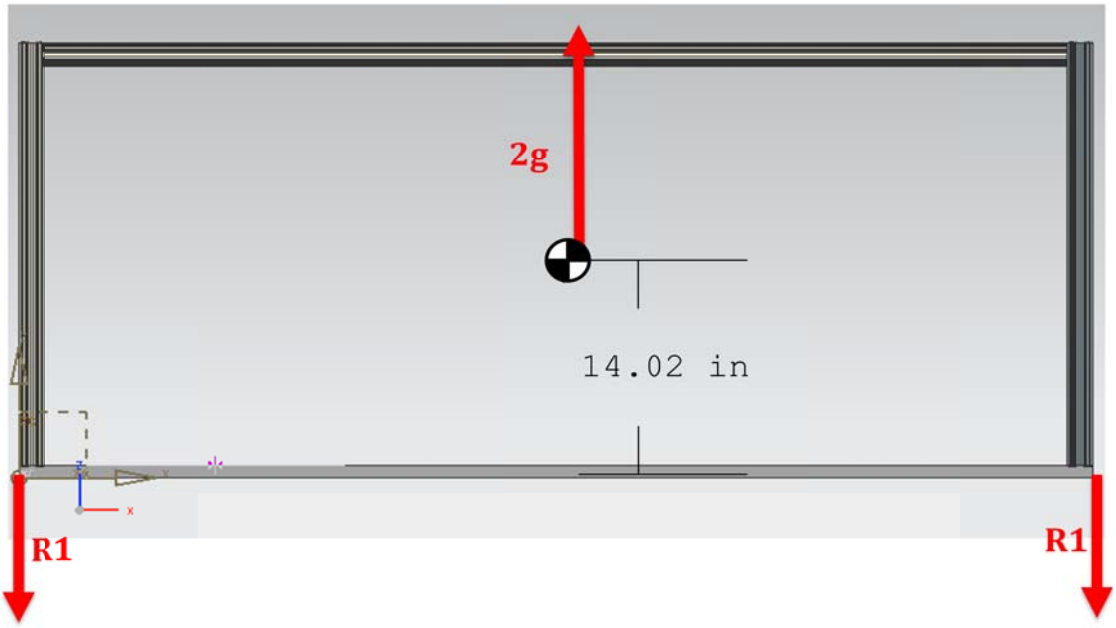


Figure A.18 Tension reactions of outer frame under a 2g upward load

$$\Sigma F = 2g - 8F1 = 0 \text{ (R1=4F1)}$$
$$\therefore F_1 = 7.05 \text{ lbs.}$$

### *A.7.4 Margins of Safety*

Table A.8 Margins of Safety for Outer Frame

| Configuration | Mode | Max. Load | MS |
|---|---|---|---|
| 9g-Forward | Tension | 20.69 | 51.26 |
| | Shear | 31.73 | 16.29 |
| 2g-Upward | Tension | 7.05 | 152.36 |

# APPENDIX B. HAZARD ANALYSIS

## B.1 Test Purpose

### *B.1.1 Purpose*

This section contains a summary of the analysis of the hazards involved with the performance of the experimental setup described in this Test Equipment Data Package. The hazards and the measures taken to mitigate them are shown in this section.

### *B.1.2 Scope*

This hazard analysis includes the hazards of operating and handling the equipment described in this document as well as during the integrated operation of the setup. Hazards involved in operation of the facility systems not directly related to the experimental setup are included in the analyses of the facility systems.

### *B.1.3 System Purpose*

The purpose of the system is to provide the conditions to perform exothermic reactions in a combustion chamber. A pressure system and an electrical system are installed to offer and manipulate the conditions necessary for combustion. The components of the system are mounted on a rig that will be installed onboard Zero-G.

This section provides a summary of the hazards present in the system.

### *B.1.4 System Functional Description*

The combustible mixtures will be produced using lunar regolith simulant JSC-1A and magnesium powder. Combustion of regolith with the two metal powders will be studied. The regolith will be ball-milled to reduce the particle size and increase the reaction rate. The milled regolith will be mixed with the metal powder using a ball mill.

The regolith/metal mixtures will then be put into quartz tubes (inner diameter 12 mm, outer diameter 14 mm, length 50 mm). The mixtures will be manually pressed. The tubes will be installed vertically at the outer edge of a cartridge with space for 15 samples (spaced every 24 degrees). Each tube will be equipped with an igniter made of Nichrome wire to ignite the mixture at the top. Upon ignition, the combustion front will travel downwards. Each combustion process will be recorded using a camcorder. The cartridge will be installed on top of a motorized rotary stage and the system will be located in a sealed steel combustion chamber.

A controller located outside the chamber will control the rotary stage and it will be programmed to rotate 24 degrees every two parabolas. This rotation is necessary to locate the

combustible mixture in front of the chamber window and allow for the video recording. The camcorder will be mounted outside of the chamber window and will record the whole experimentation process during the flight. The videos will be analyzed after the flight.

Prior to the experiments, the combustion chamber will be purged by argon from the compressed gas bottle, so that the initial atmosphere in the chamber will be argon. The combustion of regolith/metal mixtures produces mostly solid products. Some amount of liquid silicon may also form in the combustion front. The combustion may release only insignificant amounts of gases, which are present as impurities in the mixture components or constitute vapors of the involved metals. During combustion of the mixtures, these gases, as well as argon that was initially in the pores of the sample, may carry some particles through the sample top outwards, creating fumes. The rotary stage system permits running the whole set of experiments without opening the chamber so that no gases or fumes can be released to the airplane cabin. After each experiment, the chamber will be purged by argon, so that the gases and fumes will be removed through the overboard vent and the atmosphere in the chamber before the next experiment will be pure argon again. The low atmospheric pressure outside the aircraft will facilitate purging.

The ignition will be started using electrical heating. A coiled nickel-chromium wire will be installed in each quartz tube and heated up using a commercial DC power supply. All the electrical connections between the exterior and interior of the chamber will be created by means of sealed feedthroughs. The electrical current will be transmitted to the sample through a set of switches connected to the DC power supply.

The chamber (with the interior components), the power supply and the camera will be installed in the microgravity rig made of 1”x1” 80-20 beams and attached to the airplane by six bolts. The rig will have a bottom aluminum plate to bolt the chamber to it and to permit for the placing of the camera and the power supply onto the rig.

After the flights, the average combustion front velocities will be determined using obtained DVD records, while the products will be characterized using X-ray diffraction (XRD), scanning electron microscopy (SEM), and energy-dispersive X-ray spectroscopy (EDS).

## B.2 Hazard Analysis Summary

### *B.2.1 Electrical Potential*

To avoid electrical shock, the DC power supply and the experimental rack will be connected to the single-phase connection delivering 120 VAC, 20A, 60 Hz aircraft power. A kill switch will be installed to allow for the interruption of electric current if necessary. Also, a fuse rated at 20 Amps will be installed to avoid overcharging the system.

### *B.2.2 Shrapnel or Blast Wave Over-Pressurization*

To avoid damage of the chamber due to unexpected increase in pressure, the chamber will be proof tested at 20 psig and a relief valve set to 10 psig will be installed.

### *B.2.3 Fire*

The combustion process will be performed in argon atmosphere. Besides the tested mixtures, the only flammable materials in the chamber are insulation of electric wires and cables. Ignition of the insulating materials in argon atmosphere is impossible. Since the tested materials contain magnesium, a Class D fire extinguisher (for metal fires) should be onboard the plane.

### *B.2.4 High Temperatures*

Immediately after ignition, the mixture may be heated up to 1400°C (this value is the adiabatic combustion temperature while the actual temperature will be lower). This temperature will be localized within the quartz container inside the chamber.

The mass of each sample will be less than 5 g. The mass of the chamber and its volume (0.03 $m^3$) are large enough to avoid any significant increase of the chamber temperature or pressure when such small samples are burned. Chamber walls will remain much colder than the permitted touch temperature (50°C) during or after combustion of all 15 samples. This will be verified in 1-g experiments in our laboratory prior to the flights. The aluminum cartridge will also function as a heat sink to prevent overheating of the rotary stage.

After combustion of each sample, the chamber will be purged with argon, which will remove hot gases and cool the solid products. It is expected that purging after the last experiment will cool the samples to the touch temperature. The chamber will be opened after landing. By this time, the samples will be at nearly room temperature.

### *B.2.5 Low Temperatures*

No hazards are related to low temperature conditions.

### *B.2.6 Ionizing Radiation*

No hazards are related to ionizing radiation.

### *B.2.7 High Energy Electromagnetic Fields*

No hazards are related to high-energy electromagnetic fields.

### *B.2.8 Oxygen Deficient Atmospheres*

No hazards are related to oxygen deficient atmospheres.

### *B.2.9 Toxic Atmosphere*

Magnesium oxide fumes may be produced during the mixture combustion. Magnesium oxide is not toxic. Direct contact with them may result in minor irritation in skin, eyes, and throat. The fumes will be contained inside the combustion chamber and will be flushed away by the argon gas.

### *B.2.10 High Sound Levels*

No hazards are related to high sound levels.

### *B.2.11 Sharp Points or Edges*

Foam will be attached to all sharp points and edges to avoid their exposure.

### *B.2.12 Collisions*

No hazards are related to collisions.

### *B.2.13 Crushing Forces*

No forces are related to crushing forces

### *B.2.14 Environmental Pollution*

The magnesium oxide fumes will be flushed away of the chamber and will be collected in the installed filter. The fume particles will not be released to the atmosphere.

### *B.2.15 Test Article*

No hazards are related to the test article

## B.3 DOCUMENTS REVIEWED

### *B.3.1 Drawings and Component Listing*

Table B.1 shows the components used for the presented experimental setup

Table B.1 Component listing

| Item | Part Number | Material | Quantity |
|---|---|---|---|
| 1 | Bottom Aluminum Plate | 6061 Aluminum | 1 |
| 2 | 80/20 1010x17.5" | 6105 Aluminum | 4 |
| 3 | 80/20 1010x41" | 6105 Aluminum | 2 |
| 4 | 80/20 1010x21" | 6105 Aluminum | 2 |
| 5 | 80/20 1010x7.5" | 6105 Aluminum | 4 |
| 6 | 80/20 1010x12.5" | 6105 Aluminum | 2 |

| | | | |
|---|---|---|---|
| 7 | 80/20 1010x9" | 6105 Aluminum | 2 |
| 8 | Power Supply | Various | 1 |
| 9 | Steel Chamber | Steel | 1 |
| 10 | Controller | Various (electronic) | 1 |
| 11 | Cartridge | 6061 Aluminum | 1 |
| 12 | Rotary Stage | Various (electronic) | 1 |
| 13 | Igniters | Nichrome | 15 |
| 14 | Quartz Tubes | Quartz | 15 |

## B.4 SUPPORTING INFORMATION

RISK ASSESSMENT CODES (RAC's)

**Consequence**

| Class | Description |
|---|---|
| **I** | **Catastrophic** A condition that may cause death or permanently disabling injury, facility destruction on the ground, or loss of crew, major systems, or vehicle during the mission; schedule slippage causing launch window to be missed; cost overrun greater than 50% of planned cost. |
| **II** | **Critical** A condition that may cause severe injury or occupational illness, or major property damage to facilities, systems, equipment, or flight hardware; schedule slippage causing launch date to be missed; cost overrun between 15% and not exceeding 50% of planned cost. |
| **III** | **Moderate** A condition that may cause minor injury or occupational illness, or minor property damage to facilities, systems, equipment, or flight hardware; internal schedule slip that does not impact launch date; cost overrun between 2% and not exceeding 15% of planned cost. |
| **IV** | **Negligible** A condition that could cause the need for minor first-aid treatment but would not adversely affect personal safety or health; damage to facilities, equipment, or flight hardware more than normal wear and tear level; internal schedule slip that does not impact internal development milestones; cost overrun less than 2% of planned cost. |

**Likelihood Estimate**

| Letter | Description |
|---|---|
| **A** | **Likely** to occur (e.g., probability > 0.1). |
| **B** | **Probably** will occur (e.g., 0.1 ≥ probability > 0.01). |
| **C** | **May** occur (e.g., 0.01 ≥ probability > 0.001). |
| **D** | **Unlikely** to occur (e.g., 0.001 ≥ probability > 0.000001). |
| **E** | **Improbable** (e.g., 0.000001 ≥ probability). |

| Consequence Class | Likelihood Estimate | | | | |
|---|---|---|---|---|---|
| | **A** | **B** | **C** | **D** | **E** |
| **I** | 1 | 1 | 2 | 3 | 4 |
| **II** | 1 | 2 | 3 | 4 | 5 |
| **III** | 2 | 3 | 4 | 5 | 6 |
| **IV** | 3 | 4 | 5 | 6 | 7 |

| *If the RAC is…* | *Then the risk is…* |
|---|---|

| *If the RAC is…* | *Then the risk is…* |
|---|---|
| **1** | **Unacceptable** – All operations shall cease immediately until the hazard is corrected, or until temporary controls are in place and permanent controls are in work.<br>A safety or health professional shall stay at the scene at least until temporary controls are in place. RAC 1 hazards have the highest priority for hazard controls. |
| **2** | **Undesirable** – All operations shall cease immediately until the hazard is corrected or until temporary controls are in place and permanent controls are in work.<br>RAC 2 hazards are next in priority after RAC 1 hazards for control.<br>Program Manager (directorate level), Organizational Director, or equivalent management is authorized to accept the risk with adequate justification |
| **3** | **Acceptable with controls** – Division Chief or equivalent management is authorized to accept the risk with adequate justification |
| **4–7** | **Acceptable with controls** – Branch Chief or equivalent management is authorized to accept the risk with adequate justification |

DISTRIBUTION

Original AOD / Test Director
AOD / Branch Test File
AOD / Building 990
AOD Flight Safety
NS2 / Safety and Test Operations

| HAZARD | CAUSE | EFFECT | Sev/Prob RAC | CONTROLS | VERIFICATION | DISPOSITION Sev Prob RAC |
|---|---|---|---|---|---|---|
| Electrical Potential | Overcharging the electrical outlet | Overheating and fire | II/C-3 | A 20 Amps fuse is installed to avoid overcharge | Electrical test previous to the flight | II/E-5 |
| Overpressurization | Gas generation inside the chamber | Cracking of windows in combustion chamber | II/E-5 | A relief valve is installed. A pressure gauge measures the internal pressure in the chamber. | Operators will monitor pressure using the gauge and will open the outlet valve when it is necessary. | II/E-5 |
| Fire | Uncontrolled combustion inside chamber | Overheating of internal components and steel chamber | II/C-3 | Flammable materials (wire insulation) cannot burn in argon atmosphere. | Operators will maintain argon atmosphere in the chamber. | II/D-4 |
| High Temperatures | The investigated combustion process generates high temperatures in the samples | Overheating of internal components and steel chamber | III/B-3 | Purging with argon after each experiment | Operators will purge the chamber after each experiment. | III/C-4 |
| Sharp Points or Edges | The experimental rig has sharp points or edges | Injury | III/C-3 | Foam will be attached to all sharp points and edges to avoid their exposure. | Visual inspection of the foam and the sharp edges | III/E-6 |
| Environmental Pollution | Fumes may form during the investigated process | Fumes may be accumulated in the chamber | IV/B-4 | Purging with argon after each experiment removes fumes from the chamber | Operators will purge the chamber after each experiment. The particles will be collected in filter. | IV/C-5 |

# APPENDIX C. PRESSURE VESSEL VERIFICATION

## Pressure Vessel Test Report

## C.1 Vessel Description

The steel chamber (diameter 30 cm, height 40 cm) is equipped with a pressure gauge, two glass windows, one lateral plate for piping connections, and one port for the cartridge and sample installation. The top and bottom lids are made of aluminum 6061. The chamber is equipped with a pressure gauge (Omega), which measures pressure in the range from 30 mm Hg vacuum to 15 psig.

## C.2 Test Parameters

| | |
|---|---|
| Test Date: | May 20th, 2011 |
| Maximum Test Pressure: | 20.1 psig |
| Operating Pressure: | 10.0 psig |
| Test Fluid: | Argon (Ar) Gas |
| Test Fluid Temperature: | 70°F |
| Vessel Metal Temperature: | 70°F |

## C.3 Other Requirements

| | |
|---|---|
| Restricted Distance: | 0 ft |
| Cold Shock (cryo only): | 20.1 psig |

## C.4 Specific Check Points

| Test Pressure | Tester |
|---|---|
| 100 % of Maximum Test Pressure: 20.1 psig | White, Christopher |

## C.5 Signatures

| | | |
|---|---|---|
| Organization: | UTEP | Signatures |
| Cold Shock (cryo only): | Christopher White | _____ |
| Others: | Francisco Álvarez | _____ |
| | Dr. Evgeny Shafirovich | _____ |

# APPENDIX D. MATERIAL SAFETY DATA SHEETS

# CURRICULUM VITA

Francisco Alvarez was born in El Paso, Texas in 1986. He is the son of Francisco Alvarez and Monica Castrejon. He finished his high-school education in Preparatoria el Chamizal in Ciudad Juarez, Mexico, graduating in 2004. He attended The University of Texas at El Paso and received a Bachelor of Science in Mechanical Engineering degree in 2008 and a Bachelor of Science in Industrial Engineering in 2009. During the summer of 2009 he had a research internship at the Chemical Sciences and Engineering Division in Argonne National Laboratory collaborating for the production of hydrogen by means of thermochemical cycles. This research led to the publication of "Hydrolysis of CuCl2 in the Cu-Cl thermochemical cycle for hydrogen production: Experimental studies using a spray reactor with an ultrasonic atomizer" by Magali Ferrandon, Michele Lewis, Francisco Alvarez, and Evgeny Shafirovich (International Journal of Hydrogen Energy 2010, Vol. 35; Number 5, pages 1895-1904). In January of 2010, he started his studies towards a Master of Science in Mechanical Engineering working for the In-Situ Resource Utilization team at the NASA sponsored Center for Space Exploration Technology Research under the supervision of Dr. Evgeny Shafirovich. The research performed at this center led to the publication of "Combustible Mixtures of Lunar Regolith with Metals: Thermodynamic Analysis and Combustion Experiments" by Christopher White, Francisco Alvarez, and Evgeny Shafirovich (Journal of Thermophysics and Heat Transfer 2011, vol. 25, no. 4, pages 620-625).

Permanent address: 3101 Tierra Nora Dr.

El Paso, Texas, 79938

This thesis was typed by Francisco Alvarez.